Available online at www.sciencedirect.com
SCIENCE DIRECT
Progress in Particle and Nuclear Physics 57 (2006) 564–653
Progress in Particle and Nuclear Physics
www.elsevier.com/locate/ppnp

Review

Spectroscopy of Λ hypernuclei

O. Hashimoto, H. Tamura*

Department of Physics, Tohoku University, Sendai, 980-8578, Japan

Received 7 September 2004; accepted 16 May 2005

Abstract

Spectroscopy of Λ hypernuclei has recently become one of the most valuable tools for the experimental investigation of strangeness nuclear physics. Following the pioneering (π^+, K^+) reaction spectroscopy experiments at the BNL AGS in the 1970's, excitation spectra have been measured using this reaction for a wide variety of Λ hypernuclei with the superconducting kaon spectrometer (SKS) at the KEK 12 GeV PS. More recently, Λ hypernuclear spectroscopy was carried out for the first time using the $(e, e'K^+)$ reaction and the continuous electron beam at the Thomas Jefferson National Accelerator Facility (Jefferson Lab). This reaction will be further explored using a new high-resolution kaon spectrometer (HKS) installed at Jefferson Lab. At the same time, precision γ-ray spectroscopy with a germanium detector array (Hyperball) has been successfully performed for p-shell Λ hypernuclei at the KEK 12 GeV PS and at the BNL AGS. Quantitative information on Λ hypernuclear structure was obtained and the strengths of the spin-dependent Λ–nucleon interaction in the p-shell region were derived. In this review article, the progress of Λ hypernuclear spectroscopy is described and future prospects are presented.

PACS: 21.80.+a; 21.60.-n; 24.85.+p

Keywords: Λ hypernuclei; Reaction spectroscopy; γ-ray spectroscopy; (π^+, K^+) reaction; $(e, e'K^+)$ reaction

Contents

* Corresponding author.
E-mail addresses: hashimot@lambda.phys.tohoku.ac.jp (O. Hashimoto), tamura@lambda.phys.tohoku.ac.jp (H. Tamura).

0146-6410/$ - see front matter © 2005 Elsevier B.V. All rights reserved.
doi:10.1016/j.ppnp.2005.07.001

1. Introduction

Hypernuclear investigations provide invaluable information on many-body hadronic systems by utilizing a new degree of freedom "strangeness" [1–3]. Both the structure of baryons in the nuclear medium and the structure of nuclei as baryonic many-body systems can be better studied by introducing a "strangeness" degree of freedom into a nucleus. In particular, a Λ hyperon can be put deep inside a nucleus as an impurity and provides a sensitive probe of the nuclear interior.

It is not straightforward to investigate the interior of a nucleus or deeply bound nuclear states using traditional experimental techniques. Although nucleon knockout reactions such as $(e, e'p)$ and $(p, 2p)$ can reveal single-particle aspects of deeply bound states, the nuclear deeply bound states get broader for deeper bound states. For example, the spreading widths reach 5 MeV for the $1f$-shell proton states of ^{208}Pb, prohibiting precision spectroscopic investigation.

Since the Λ hyperon does not suffer from Pauli blocking by the other nucleons, it can penetrate into the nuclear interior and form deeply bound hypernuclear states. It is expected that new forms of hadronic many-body systems can be investigated using this new degree of freedom, "strangeness", and also comparing the hyperon–nucleon and nucleon–nucleon interactions. New nuclear structure, which cannot be seen in ordinary nuclei consisting only of nucleons, may manifest itself in hypernuclei, providing indispensable information on the flavor SU(3) basis for baryonic matter.

Furthermore, hyperon–nucleon (YN) and hyperon–hyperon (YY) interactions can be well studied by the spectroscopic investigation of hypernuclei. Hyperon–nucleon scattering experiments can, in principle, provide basic data on the interactions but it is quite difficult to carry out such experiments, because hyperon lifetimes are quite short (of the order

of 10^{-10} s) and hyperon beams suitable for the scattering experiments are not readily available. Spectroscopic investigations yield valuable information on the hyperon–nucleon and hyperon–hyperon interactions.

Assuming that a Λ hypernuclear wavefunction can be decomposed into a core nucleus and a Λ hyperon, the hypernuclear Hamiltonian is expressed as

$$H = H_{\text{CoreNucleus}} + t_\Lambda + \sum v_{\Lambda N}^{\text{effective}}, \tag{1}$$

where $H_{\text{CoreNucleus}}$ is the Hamiltonian for the core nucleus, t_Λ is the kinetic energy of the Λ hyperon and $v_{\Lambda N}^{\text{effective}}$ describes the effective ΛN interaction. The effective interaction can be constructed via a G-matrix calculation, starting from the two-body interactions in free space. One-boson-exchange models such as Nijmegen [4] and Jülich interactions [5] (which were constructed by extending NN interaction models on the basis of flavor SU(3) symmetry with scarce ΛN and ΣN scattering data used to adjust parameters) are widely used to describe the elementary two-body interactions.

Analytical forms of the effective potentials are often given in the form of a three-range gaussian, $V_{\Lambda N}(r) = \sum_i (a_i + b_i k_f + c_i k_f^2) \exp(-r^2/\beta_i^2)$ [6]. A wide variety of hypernuclear properties such as level structure and reaction cross sections are calculated using this potential and compared directly with experimental data. These calculations are reasonably reliable, in part, because the ΛN interaction is much weaker than the NN interaction and no anti-symmetrization against nucleons is required. It is to be noted that few-body hypernuclear systems with $A \leq 5$ can be calculated directly from free two-body interactions, in which the calculated binding energies of ground and excited states are compared precisely with experimental data. In such studies, information on Λ hypernuclear structure obtained by spectroscopic studies plays an essential role in testing and improving YN interaction models.

There is also a phenomenological approach to the effective interaction [7,8] in which the ΛN effective interaction in p-shell Λ hypernuclei is written in the form

$$V_{\Lambda N}(r) = V_0(r) + V_\sigma(r)\, \boldsymbol{s}_\Lambda\, \boldsymbol{s}_N + V_\Lambda(r)\, \boldsymbol{l}_{\Lambda N} \boldsymbol{s}_\Lambda + V_N(r)\, \boldsymbol{l}_{\Lambda N} \boldsymbol{s}_N + V_T(r) S_{12} \tag{2}$$

where $S_{12} = 3(\boldsymbol{\sigma}_\Lambda \hat{\mathbf{r}})(\boldsymbol{\sigma}_N \hat{\mathbf{r}}) - \boldsymbol{\sigma}_\Lambda \boldsymbol{\sigma}_N$. Low-lying level energies of p-shell hypernuclei can be described with radial integrals over the $s_\Lambda p_N$ wavefunction for each of the five terms in Eq. (2). These integrals, denoted as $\bar{V}$, Δ, S_Λ, S_N and T, can be determined from p-shell Λ hypernuclear data, and then compared with theoretical predictions given by free ΛN interactions through G-matrix calculation. This approach is discussed in depth below in conjunction with γ spectroscopy.

Through a quantitative understanding of YN and YY interactions we expect to be better positioned to investigate new aspects and new forms of hadronic matter. In particular, detailed information on YN and YY interactions is indispensable for our understanding of high-density nuclear matter inside neutron stars, where hyperons are possibly mixed and playing crucial roles.

Λ hypernuclear investigation has already undergone three stages of development since the first discovery of the hypernucleus in 1953 [9]. The first stage may be called the emulsion era: the binding energies of light ($A \leq 16$) Λ hypernuclei (see Fig. 1) were measured from their weak decays and the Λ potential depth was found to be about 2/3 that

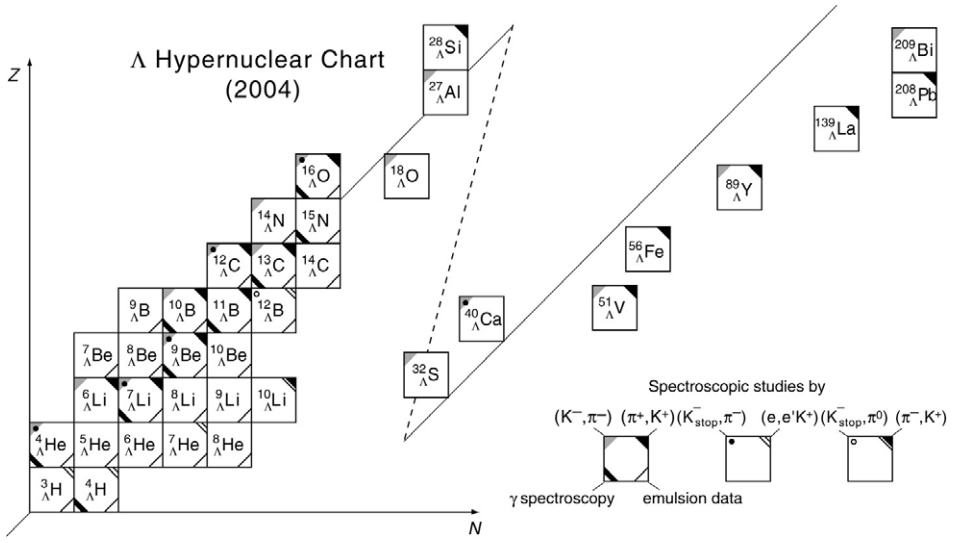

Fig. 1. Λ hypernuclear chart. The experimentally identified Λ hypernuclei and the experimental methods used to study them (reaction spectroscopies of (K^-, π^-), (π^+, K^+), $(e, e'K^+)$, etc., γ spectroscopy, and the emulsion method) are shown.

of the nucleon. However, experimental data was limited to the binding energies of ground states, and excited states could not be investigated except in a few cases.

The second stage of hypernuclear investigation began in the early 1970's with counter experiments using K^- beams at CERN and later at BNL. Spectroscopic studies including excited states of hypernuclei became possible by the (K^-, π^-) reaction. After the first experiment by the $(K^-_{\text{stop}}, \pi^-)$ reaction [10], a noble method of the in-flight (K^-, π^-) reaction in an almost recoilless condition was introduced and various hypernuclei were intensively studied [11–17]. In particular, the structure of p-shell hypernuclei was studied and it was found that the spin–orbit splittings are quite small [13,17]. Studies by the (K^-, π^-) reaction were quite powerful, particularly for light p-shell hypernuclei, but they often suffered from poor statistics due to low kaon beam intensity and from the limited energy resolution of the spectra. Moreover, because of the characteristics of the (K^-, π^-) reaction as further described in the next section, only a limited number of hypernuclear states were investigated in this era. γ-ray spectroscopy with K^- beams was also first attempted in the early 1970's [18].

The third stage, which featured the use of the (π^+, K^+) reaction, began in the mid-1980's at the alternating gradient synchrotron (AGS) of Brookhaven National Laboratory (BNL), USA [19,20] and was extended dramatically when the new experimental facilities became available at the 12 GeV proton synchrotron (PS) of the High Energy Accelerator Organization (KEK), Japan [21–25]. In particular, the superconducting kaon spectrometer (SKS) played a key role in exploring Λ hypernuclear spectroscopy by the (π^+, K^+) reaction. High-quality Λ spectra were measured for various Λ hypernuclei and hypernuclear spectroscopy was established as a broadly applicable, quantitative tool. In the

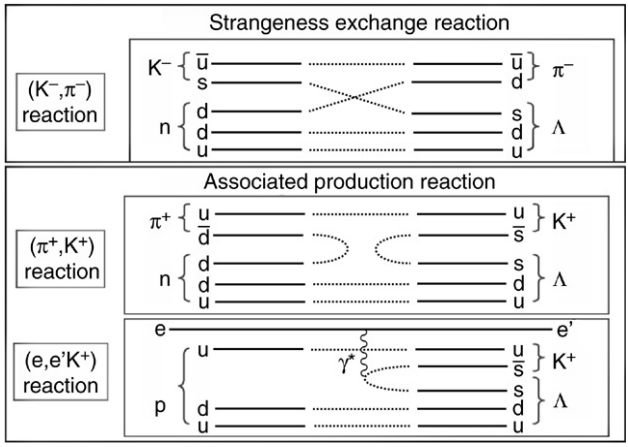

Fig. 2. A schematic presentation of three strangeness producing reactions used to study hypernuclei.

last decade, new experimental techniques have been further developed. One is hypernuclear γ-ray spectroscopy [26]. Precision spectroscopy has been carried out with unprecedented resolution of a few keV through the use of a germanium detector array called Hyperball and it has provided quantitative new information on hyperon–nucleon interactions. A second development is the use of the $(e, e'K^+)$ reaction for hypernuclear spectroscopy. The high-quality, high-intensity CW electron beams available at the Thomas Jefferson National Accelerator Facility (JLab), USA, permitted the first successful $(e, e'K^+)$ spectroscopy measurements [27]; this technique is going to be fully developed for Λ hypernuclear investigations in the near future. These developments are expected to greatly expand the possibilities for strangeness nuclear physics in the coming years.

Λ hypernuclei in the wide mass range from ${}^{3}_{\Lambda}$H up to ${}^{208}_{\Lambda}$Pb have been investigated during this three-stage period as summarized in Fig. 1.

In this paper, we will review the present status of Λ hypernuclear spectroscopy with an emphasis on good-quality reaction spectroscopy using the (π^+, K^+) and $(e, e'K^+)$ reactions and hypernuclear γ-ray spectroscopy. Experimental efforts toward the future hypernuclear spectroscopy will also be described.

2. Principles of Λ hypernuclear spectroscopy

A Λ hypernucleus is produced in a wide variety of hadronic reactions with beams of mesons, protons, and heavy ions. It can be also produced by electromagnetic interactions, a technique that became feasible only recently. In most cases of hypernuclear reactions, a hypernucleus is populated in a nucleon hole hyperon–particle state (a nucleon in the target having been converted to a Λ hyperon). The elementary processes for three typical reactions, (K^-, π^-), (π^+, K^+) and $(e, e'K^+)$, are shown schematically in Fig. 2 at the quark level. From the viewpoint of constituent quarks, an s quark in the beam kaon is exchanged with a d quark in a neutron in the case of the (K^-, π^-) reaction, while in the

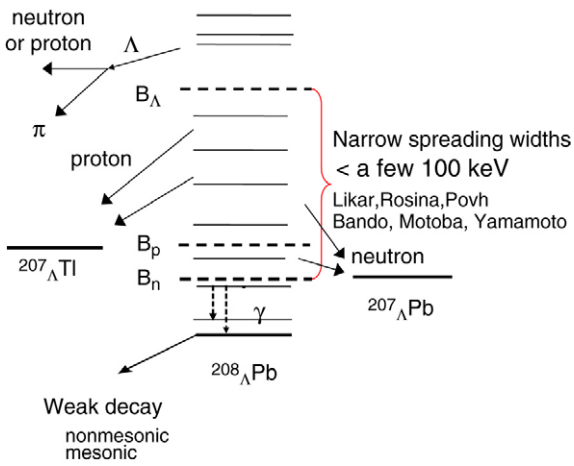

Fig. 3. Λ hypernuclear states and their decay modes.

(π^+, K^+) reaction and also in the $(e, e'K^+)$ reaction, an s–$\overline{s}$ pair is created associatively, resulting in the production of both a Λ hyperon and a kaon.

Once a Λ hypernucleus is produced in an excited state, it decays through strong, electromagnetic and weak interactions according to the nature of the states, as shown pictorially in Fig. 3.

The Λ binding energies are usually much larger than those for a proton or a neutron, and hypernuclear states in which a Λ hyperon is bound in an orbit above the p shell are often nucleon unbound and decay by emitting nucleons. Even for high-lying Λ hypernuclear states above the nucleon emission thresholds, the calculated spreading widths are narrower than a few 100 keV, in marked contrast to the case for an ordinary nucleus [28,29]. This is because (1) ΛN interaction is weaker than the nucleon–nucleon interaction, (2) ΛN spin–spin interaction is weak and therefore spin vector p_N–h_N excitation is suppressed, (3) a Λ hyperon with zero isospin can excite only isoscalar p_N–h_N modes of the core nucleus, and (4) no exchange term with nucleons is required. These characteristics make the widths of Λ hypernuclear states considerably narrower than states in an ordinary nucleus at the same excitation energy. In the case of Ca, for example, Bando et al. predicted that $\Gamma_\Lambda(1s, 0d)/\Gamma_N(0s) = 0.03$–$0.07$. The widths are expected to be much smaller than the energy spacings between the Λ major shells and, consequently, Λ hypernuclear states should be observable as reasonably narrow peaks. This provides a basis for the reaction spectroscopy of Λ hypernuclei with resolution as good as a few 100 keV for a wide range of excitation.

When Λ hypernuclear states below the particle emission threshold are populated either directly by the reaction or indirectly after de-excitation, γ transitions take place down to the hypernuclear ground state, which eventually decays through weak interaction (see Fig. 3).

Hypernuclear reactions are characterized to a good extent by the momentum transfer in the reaction, since it controls population of the hypernuclear states. In Fig. 4, typical cross sections are shown schematically versus momentum transfer for some of the reactions

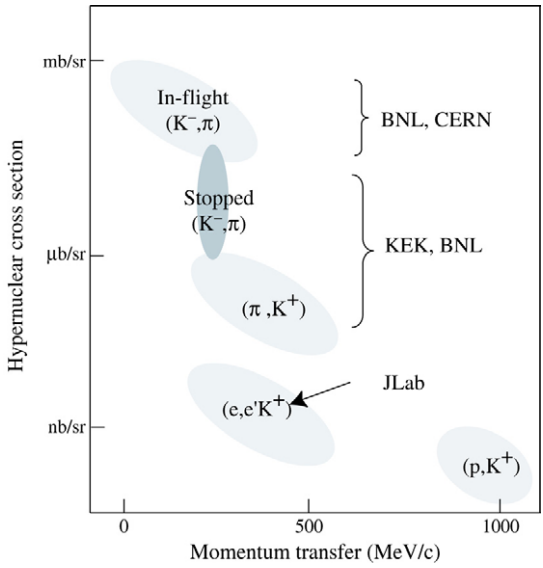

Fig. 4. Hypernuclear production cross section for typical reactions versus momentum transfer.

Table 1
Comparison of Λ hypernuclear production reactions

$\Delta Z = 0$ *Neutron to* Λ	$\Delta Z = -1$ *Proton to* Λ	Comment
(π^+, K^+)	(π^-, K^0)	Stretched, high spin
In-flight (K^-, π^-) Stopped (K^-, π^-)	In-flight (K^-, π^0) Stopped (K^-, π^0)	Substitutional
$(e, e'K^0)$ (γ, K^0)	$(e, e'K^+)$ (γ, K^+)	Spin-flip, unnatural parity

that are used for Λ hypernuclear spectroscopy. Typically, larger momentum transfers correspond to smaller hypernuclear cross sections. Characteristics of these reactions for meson and electromagnetic beams are also compared in Table 1. Each reaction has its own advantages and plays its role in a complete program of hypernuclear spectroscopy. However, only the (K^-, π^-) and (π^+, K^+) reactions have been used extensively, and the feasibility of the $(e, e'K^+)$ reaction has only been demonstrated recently, as described in Section 4.

The momentum transferred to the recoiling hypernucleus is shown in Fig. 5 as a function of incident beam momentum. The (K^-, π^-) reaction has a "magic momentum" where the recoil momentum becomes zero. It thus preferentially populates substitutional states, in which a nucleon is converted to a Λ hyperon in the same orbit with no orbital angular momentum transfer ($\Delta L = 0$). On the other hand, the (π^+, K^+) reaction and also the

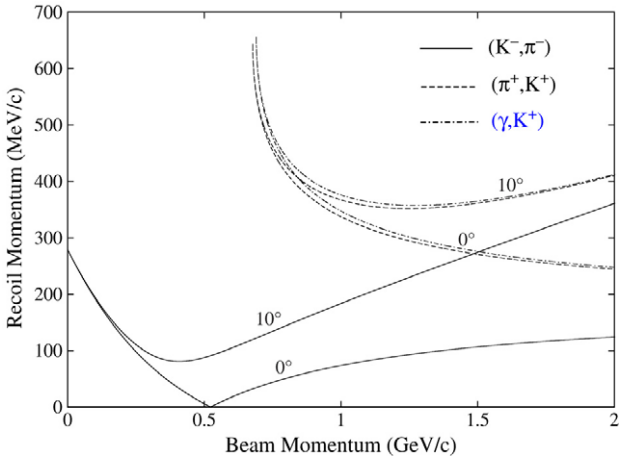

Fig. 5. Incident beam momentum dependence of hypernuclear recoil momentum for a ^{12}C target.

$(e, e'K^+)$ reaction transfer a large recoil momentum to a hypernucleus, since they are both endoergic reactions. Therefore, they can excite high-spin hypernuclear states with a nucleon hole having large angular momentum and a Λ hyperon having a small angular momentum. This is one of the advantageous features of these reactions for Λ hypernuclear spectroscopy.

As seen in Table 1, the (π^+, K^+) and (K^-, π^-) reactions convert a neutron in the target nucleus to a Λ hyperon. On the other hand, the $(e, e'K^+)$ reaction converts a proton to a Λ hyperon. In addition, since the spin-flip amplitudes in the $n(\pi^+, K^+)\Lambda$ and $n(K^-, \pi^-)\Lambda$ reactions are quite small unless appropriate kinematical conditions are selected, these reactions almost exclusively populate non-spin-flip states of hypernuclei. In contrast, the $(e, e'K^+)$ reaction can populate spin-flip hypernuclear states with unnatural parities as well.

Two types of hypernuclear spectroscopy, one reaction based and the other γ-ray based, have made considerable progress in recent years. Reaction spectroscopy, which directly populates hypernuclear states, reveals level structure in the Λ bound region and can even study excited states between the nucleon emission thresholds and the Λ emission threshold. It provides information on the Λ hypernuclear structure and ΛN interaction through the determination of hypernuclear masses, reaction cross sections, angular distributions, etc. In contrast, γ-ray spectroscopy can have access only to hypernuclear states below nucleon emission thresholds, but it achieves ultrahigh resolution (typically a few keV — almost three orders of magnitude better than that achievable with reaction spectroscopy). γ-ray spectroscopy is a powerful spectroscopic tool for the investigation, for example, of spin-dependent ΛN interactions, which requires information on the precise level structure of hypernuclei. Thus reaction spectroscopy and γ spectroscopy are highly complementary.

Table 2 lists all the hypernuclear reaction spectroscopy experiments to date. It is noted that a hypernucleus is traditionally labeled as $^{\#\ of\ baryons}_{Symbol(s)\ of\ hyperon(s)}$Z, where the number of baryons is the sum of nucleons and hyperon(s), and Z the total charge of the hypernucleus

Table 2
Experiments on Λ hypernuclear reaction spectroscopy, showing the laboratory, the year of publication, the reaction used, the hypernuclei studied and the beam line and apparatus used

Lab.	Year	Reaction p_{beam} (GeV/c)	Studied hypernuclei	Beam line/apparatus etc.	Ref.
CERN	1972	$(K^-_{\text{stop}}, \pi^-)$	${}^{12}_{\Lambda}$C		[10]
CERN	1975	(K^-, π^-) 0.90	${}^{9}_{\Lambda}$Be, ${}^{12}_{\Lambda}$C, ${}^{16}_{\Lambda}$O, ${}^{32}_{\Lambda}$S, ${}^{40}_{\Lambda}$Ca	Double Spectrometer	[11,12]
CERN	1978	(K^-, π^-) 0.79	${}^{6}_{\Lambda}$Li, ${}^{7}_{\Lambda}$Li, ${}^{9}_{\Lambda}$Be, ${}^{12}_{\Lambda}$C, ${}^{16}_{\Lambda}$O, ${}^{27}_{\Lambda}$Al,	SPESII	[13–15]
		−0.64	${}^{32}_{\Lambda}$S, ${}^{40}_{\Lambda}$Ca, ${}^{51}_{\Lambda}$V, ${}^{89}_{\Lambda}$Y, ${}^{209}_{\Lambda}$Bi		
BNL	1979	(K^-, π^-) 0.80	${}^{12}_{\Lambda}$C	LESB-I/Moby-Dick (E646)	[16]
BNL	1981	(K^-, π^-) 0.80	${}^{13}_{\Lambda}$C, ${}^{14}_{\Lambda}$N, ${}^{18}_{\Lambda}$O	LESB-I/Moby-Dick (E746)	[17]
BNL	1985	(π^+, K^+) 1.05	${}^{12}_{\Lambda}$C	LESB-I/Moby-Dick (E758)	[19]
BNL	1991	(π^+, K^+) 1.05	${}^{9}_{\Lambda}$Be, ${}^{12}_{\Lambda}$C, ${}^{16}_{\Lambda}$O, ${}^{28}_{\Lambda}$Si, ${}^{40}_{\Lambda}$Ca, ${}^{51}_{\Lambda}$V, ${}^{89}_{\Lambda}$Y	LESB-I/Moby-Dick (E798)	[20]
KEK	1990	$(K^-_{\text{stop}}, \pi^-)$	${}^{4}_{\Lambda}$He, ${}^{7}_{\Lambda}$Li, ${}^{9}_{\Lambda}$Be, ${}^{12}_{\Lambda}$C, ${}^{16}_{\Lambda}$O, ${}^{40}_{\Lambda}$Ca	K3/SKY (E117,166,167)	[30,3]
KEK	1991	(π^+, K^+) 1.05	${}^{12}_{\Lambda}$C, ${}^{56}_{\Lambda}$Fe	K2/PIK (E150)	[21]
KEK	1995	(π^+, K^+) 1.05	${}^{10}_{\Lambda}$B, ${}^{12}_{\Lambda}$C, ${}^{28}_{\Lambda}$Si, ${}^{89}_{\Lambda}$Y, ${}^{139}_{\Lambda}$La, ${}^{208}_{\Lambda}$Pb	K6/SKS (E140A)	[22,23]
KEK	1998	(π^+, K^+) 1.05	${}^{7}_{\Lambda}$Li, ${}^{9}_{\Lambda}$Be, ${}^{12}_{\Lambda}$C, ${}^{13}_{\Lambda}$C, ${}^{16}_{\Lambda}$O	K6/SKS (E336)	[24]
KEK	2001	(π^+, K^+) 1.05	${}^{12}_{\Lambda}$C, ${}^{51}_{\Lambda}$V, ${}^{89}_{\Lambda}$Y	K6/SKS (E369)	[25]
BNL	2000	$(K^-_{\text{stop}}, \pi^0)$	${}^{12}_{\Lambda}$B	LESB-II/NMS (E907)	[31]
JLab	2003	$(e, e'K^+)$ 1.8	${}^{3}_{\Lambda}$H, ${}^{4}_{\Lambda}$H	Hall-C (E91-016)	[32]
JLab	2002	$(e, e'K^+)$ 1.8	${}^{7}_{\Lambda}$He, ${}^{12}_{\Lambda}$B	Hall-C/HNSS (E89-009)	[27]
KEK	2004	(π^-, K^+) 1.20	${}^{10}_{\Lambda}$Li	K6/SKS (E519)	[33]

including hyperons. As mentioned, Λ hypernuclear reaction spectroscopy has been studied mostly by the (K^-, π^-) and (π^+, K^+) reactions so far. Reaction spectroscopy by the (π^+, K^+) reaction has attained an increasing importance recently because it can efficiently populate bound hypernuclear states. The $(e, e'K^+)$ reaction has just been applied for the first time to hypernuclear spectroscopy, but is expected to become a powerful tool for precision reaction spectroscopy in the near future. In Sections 3 and 4, we will describe the present status of Λ hypernuclear spectroscopy, emphasizing reaction spectroscopy by the (π^+, K^+) reaction and the $(e, e'K^+)$ reactions.

Table 3 lists all the γ-ray spectroscopy experiments that identified Λ hypernuclear γ rays. In most experiments, excited states of hypernuclei are produced by the (K^-, π^-) or (π^+, K^+) reactions, and γ rays are detected with NaI counters or germanium (Ge) detectors. In Section 5, we will describe the present status of γ-ray spectroscopy of hypernuclei, particularly focusing on recent experiments using a Ge detector array, Hyperball.

Table 3
Experiments that observed well-identified hypernuclear γ transitions, together with the year of publication, the γ-ray detector used, and the target and reaction used

Experiment	Year	Detector	Target/Reaction	Observed transitions	Ref.
CERN	1971	NaI	^{6}Li, ^{7}Li ($K^-_{\rm stop}, \gamma$)	$^{4}_{\Lambda}$H and/or $^{4}_{\Lambda}$He ($1^+ \to 0^+$)	[18]
CERN	1976	NaI	^{6}Li, ^{7}Li ($K^-_{\rm stop}, \gamma\pi^-$)	$^{4}_{\Lambda}$H ($1^+ \to 0^+$)	[34]
CERN	1979	NaI	^{6}Li, ^{7}Li ($K^-_{\rm stop}, \gamma\pi^0$)	$^{4}_{\Lambda}$He ($1^+ \to 0^+$)	[35]
BNL E760	1987	NaI	^{7}Li, ^{9}Be ($K^-, \pi^-\gamma$)	$^{7}_{\Lambda}$Li ($5/2^+ \to 1/2^+$), $^{9}_{\Lambda}$Be ($5/2^+, 3/2^+ \to 1/2^+$)	[36]
BNL E781	1997	NaI	^{13}C ($K^-, \pi^-\gamma$)	$^{13}_{\Lambda}$C ($1/2^- \to 1/2^+$)	[37]
KEK E419	1998	Ge(Hyperball)	^{7}Li ($\pi^+, K^+\gamma$)	$^{7}_{\Lambda}$Li ($3/2^+ \to 1/2^+$, $5/2^+ \to 1/2^+$, etc.)	[26,38]
BNL E929	2000	NaI	^{13}C ($K^-, \pi^-\gamma$)	$^{13}_{\Lambda}$C ($1/2^-, 3/2^- \to 1/2^+$, etc.)	[39]
BNL E930('98)	2002	Ge(Hyperball)	^{9}Be ($K^-, \pi^-\gamma$)	$^{9}_{\Lambda}$Be ($3/2^+ \to 1/2^+$, $5/2^+ \to 1/2^+$)	[40]
BNL E930('01)	2004	Ge(Hyperball)	^{16}O ($K^-, \pi^-\gamma$)	$^{16}_{\Lambda}$O ($1^- \to 1^-, 1^- \to 0^-$), $^{15}_{\Lambda}$N	[41]
			^{10}B ($K^-, \pi^-\gamma$)	$^{7}_{\Lambda}$Li ($7/2^+ \to 5/2^+$, etc.), $^{9}_{\Lambda}$Be ($3/2^+ \to 1/2^+$)	[42]
KEK E509	2004	Ge(Hyperball)	^{10}B, ^{11}B, ... ($K^-_{\rm stop}, \gamma$)	$^{7}_{\Lambda}$Li ($5/2^+ \to 1/2^+$) (as hyperfragments)	[43]
KEK E518	2004	Ge(Hyperball)	^{11}B ($\pi^+, K^+\gamma$)	$^{11}_{\Lambda}$B ($1/2^+ \to 5/2^+$)	[44]

3. (π^+, K^+) reaction spectroscopy

3.1. Principles of (π^+, K^+) reaction spectroscopy

As mentioned in the previous section, the (π^+, K^+) reaction selectively populates angular momentum stretched states because of the large momentum transfer to the recoil hypernucleus [45–47]. This is in contrast to the (K^-, π^-) reaction, which transfers little momentum to a hypernucleus and therefore favors the excitation of substitutional states.

The possibility of using (π^+, K^+) reaction spectroscopy for the study of Λ hypernuclei was first pointed out by Thiessen [48]. Before that, it was believed that the (π^+, K^+) reaction was not suitable for spectroscopy because of the small hypernuclear cross sections (of the order of 10 μb/sr, for example, for the ground states of light Λ hypernuclei). In contrast, cross sections for the in-flight (K^-, π^-) reaction are as large as 10 mb/sr, two to three orders of magnitude greater as shown in Fig. 4. However, pion beams are available with intensities much higher than that of kaon beams, and this can compensate the smaller cross section. It is also important to note that the (π^+, K^+) reaction for Λ hypernuclear production requires a 1 GeV region pion beam,

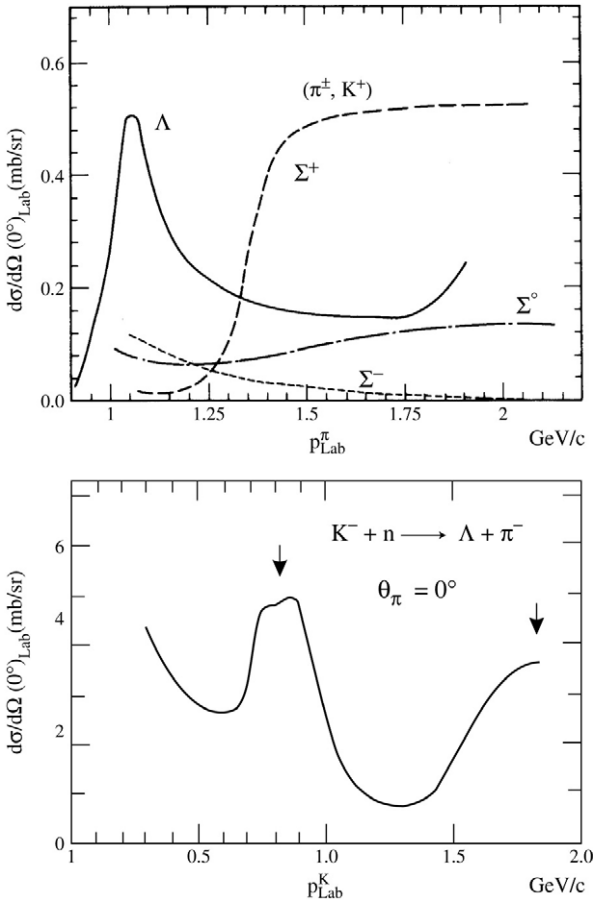

Fig. 6. The hyperon production cross section as a function of incident pion and kaon momenta for the elementary reactions $\pi^{\pm} + n \to Y + K^{+}$ and $K^{-} + n \to Y + \pi^{-}$.

since the elementary cross section for the $\pi^{+} + n \to \Lambda + K^{+}$ reaction peaks strongly at 1.05 GeV/c, while kaon beams at several 100 MeV/c have been mostly used for the (K^{-}, π^{-}) reaction as seen in Fig. 6. The 1 GeV/c pion beams are provided at proton synchrotron facilities such as the BNL AGS and the KEK 12 GeV PS but a high-resolution spectrometer system in the 1 GeV/c region is also required to conduct high-quality spectroscopy.

As explained in the previous section, the (π^{+}, K^{+}) reaction has the advantage of easily exciting deeply bound hypernuclear states, converting, for example, a neutron in a high-l orbit to a Λ hyperon in a low-l orbit. At forward angles where the spin-flip amplitude is small and the cross sections are larger, the reaction favorably populates hypernuclear states with stretched angular momentum and a natural parity as

$$[(j_{>}^{-1})_N (J_{<})_\Lambda] J_{\max} \qquad \text{or} \qquad [(j_{<}^{-1})_N (J_{>})_\Lambda] J_{\max},$$

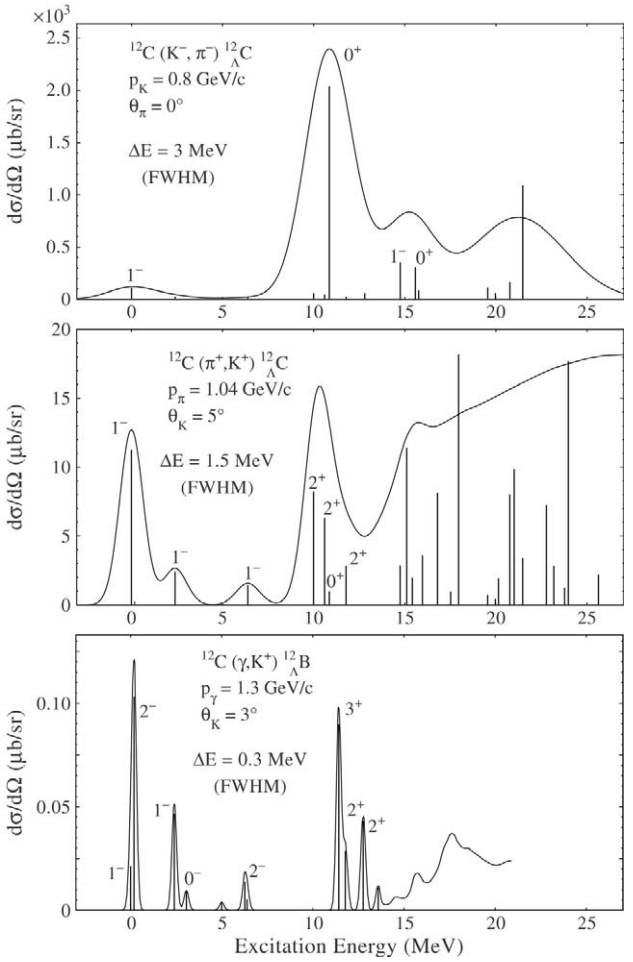

Fig. 7. Comparison of the excitation functions to be observed in the (K^-, π^-), (π^+, K^+) and $(e, e'K^+)$ reactions on a ^{12}C target.

with j and J are the total spins of a nucleon and a Λ hyperon, and $J_> = l + 1/2$, $J_< = l - 1/2$, giving $J_{\max} = l_N + l_\Lambda$.

In Fig. 7 excitation spectra for the three hypernuclear production reactions on a ^{12}C target are compared schematically. As seen in the figure, the in-flight (K^-, π^-) reaction preferentially populates substitutional hypernuclear states with small total angular momenta near the nucleon emission threshold. On the other hand, the (π^+, K^+) reaction and the $(e, e'K^+)$ reaction, equivalently the (γ, K^+) reaction, efficiently populate bound hypernuclear states. The $(e, e'K^+)$ reaction has the additional feature that it can excite spin-flip states as is explained later in detail.

For the meson induced reactions, it is necessary to measure the beam energy, particle by particle, since the secondary beam has a wide momentum spread of more than a

few % at the experimental target. Because of this requirement, the beam intensity must be kept below a few MHz; otherwise it becomes difficult to measure the momentum of a beam particle by tracking its trajectory due to accidental coincidence even when the beam duty factor is 100%.

Kaons with momenta about 0.72 GeV/c are emitted in the hypernuclear production reaction using a 1.05 GeV/c pion beam. Therefore, a kaon spectrometer with a momentum resolution better than 10^{-3} is required to achieve a hypernuclear mass resolution of a few MeV, which is necessary to resolve the major shell spacings of Λ orbits in heavy hypernuclei.

Reaction spectroscopy using the (π^+, K^+) reaction was first applied to a carbon target at the BNL AGS [19], and was further developed and then extended to heavier systems both at BNL and KEK [20–25]. In recent years, the SKS spectrometer at the KEK 12 GeV PS has played a substantial role, taking advantage of its considerably upgraded performance to explore (π^+, K^+) reaction hypernuclear spectroscopy. From high-quality (π^+, K^+) spectra with a resolution better than 2 MeV FWHM, it became possible to study the unique structure of Λ hypernuclei and the nature of the ΛN interaction quantitatively. On the basis of these series of experiments it is now recognized that the (π^+, K^+) reaction is one of the best reactions for hypernuclear spectroscopy. In the subsections below, the experimental aspects of the SKS spectrometer and the measured spectra are described.

3.2. The SKS spectrometer and (π^+, K^+) reaction spectroscopy

The superconducting kaon spectrometer (SKS) system was designed specifically for spectroscopy using the (π^+, K^+) reaction [49], and was installed at the KEK 12 GeV PS K6 beam line. The spectrometer system consists of the beam particle spectrometer and the scattered kaon spectrometer shown schematically in Fig. 8 [50]. The basic parameters of the beam line spectrometer, the SKS spectrometer (the scattered kaon spectrometer) and the SKS dipole magnet are summarized in Table 4.

In order to fully take advantage of the (π^+, K^+) reaction for hypernuclear spectroscopy, it is of vital importance to have a kaon spectrometer with both a high detection efficiency and the required momentum resolution. The SKS spectrometer provides a good momentum resolution and a large solid angle for kaons at the central momentum of 0.72 GeV/c. The combination of a large acceptance (100 msr) and a good momentum resolution (0.1% FWHM) is achieved by using a superconducting dipole magnet with a pole gap of 0.5 m and a maximum magnetic field of 3 T. The magnet has a fan shape and bends the central trajectory by 100 degrees with momentum dispersion of 3.2 cm/%. Even for the large geometrical acceptance, a first-order focusing is realized as seen in Fig. 8. This focus is important not only for the momentum reconstruction but also for particle identification with threshold type Čerenkov counters. The spectrometer is equipped with aerogel Čerenkov counter arrays ($n = 1.055$) and an acrylic Čerenkov counter hodoscope ($n = 1.33$) together with a TOF wall for particle identification. Particle trajectories are analyzed by the four sets of drift chambers, two installed upstream (SDC1,2) and two installed downstream of the dipole magnet (SDC3,4). Although the SKS magnet can be rotated around the target pivot with four compressed air pads, the spectrometer is positioned at

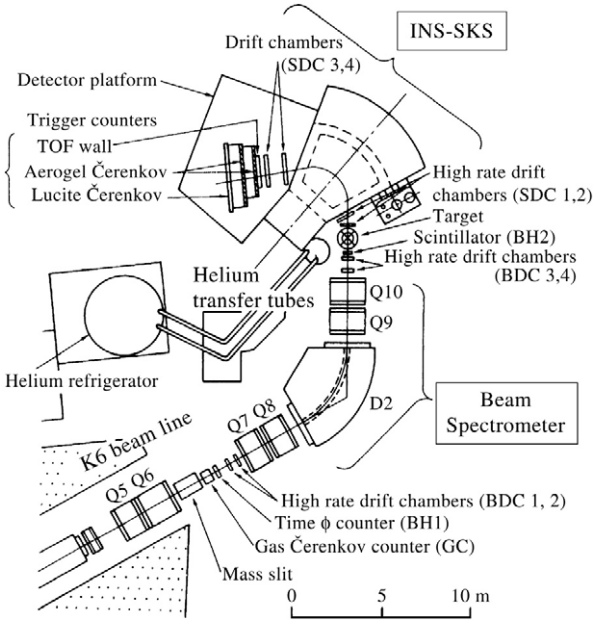

Fig. 8. Schematic drawing of the SKS spectrometer system with the beam line spectrometer.

Table 4
Parameters of the SKS spectrometer system and its dipole magnet

Beam line spectrometer	
Momentum resolution	1×10^{-3} (FWHM) at 1 GeV/c
Max. momentum	1.2 GeV/c
Momentum bite	±3%
Typical π^+ intensity	6.5×10^6 per 10^{12} protons
Channel length	30 m
SKS spectrometer	
Momentum resolution	1×10^{-3} (FWHM) at 0.72 GeV/c
Max. momentum	1.1 GeV/c
Momentum bite	±10%
Bending angle	100 degrees
Solid angle	100 msr
Flight length	∼5 m for central trajectory
Dipole magnet	
Maximum magnetic field	3 T
Stored energy	10.6 MJ
Pole gap	0.4975 m
Conductor	NbTi/Cu
Total weight	280 ton
Heat leak at 4 K	5 W
Volume of liquid He	156 *l*

zero degrees for hypernuclear spectroscopy, covering up to ±15 degrees. With this large angular acceptance, the SKS spectrometer captures most of the hypernuclei produced (∼60%–70%).

The (π^+, K^+) hypernuclear spectrometer system includes much more than the SKS spectrometer. The pion beam of about 1 GeV/c has to be momentum analyzed particle by particle with resolution comparable to that of the SKS spectrometer, $\Delta p/p \sim 10^{-3}$. The downstream portion of the K6 separated beam line of KEK 12 GeV PS was modified and used as a QQDQQ beam spectrometer, as shown in Fig. 8. This configuration allows us to adjust the $\langle x \mid \theta \rangle$ term of the transfer matrix almost to zero, so that the effect of multiple scattering from materials along the beam line on the momentum resolution of the beam line spectrometer is minimized. Altogether 24 layers of drift chamber planes are installed in the beam line. These drift chambers (BDC1,2,3,4), each with the drift length of 2.5 mm, are capable of tracking beam particles at rates as high as several MHz. A detailed description of the SKS spectrometer system can be found in Ref. [50].

As shown in Fig. 9, the performance of the SKS spectrometer system is demonstrated by the excitation spectrum of ${}^{12}_{\Lambda}$C observed in the E369 experiment for the ^{12}C(π^+, K^+) reaction at $p_\pi = 1.06\,\mathrm{GeV/c}$; it achieved 1.45 MeV FWHM resolution [25]. Also shown is the spectrum obtained with the Moby-Dick spectrometer at the BNL AGS, it achieved 3 MeV FWHM resolution. In these spectra, two prominent peaks are immediately identified. These two peaks correspond to the ${}^{12}_{\Lambda}$C states with Λ hyperons in the s and p orbits. Since it is known that the width of the ground state is much less than a few keV, the observed width tells us that the spectrometer resolution, including the effect of energy loss fluctuation in the target, is 1.45 MeV FWHM. This is the best resolution ever obtained in hypernuclear reaction spectroscopy with meson beams. Comparing the SKS spectrum of 1.45 MeV FWHM resolution with the BNL spectrum of 3 MeV FWHM resolution, the improvement of the spectrum in the region between the two prominent peaks is evident. Excited states corresponding to core excitations are now visible between the two prominent peaks in the spectrum.

Before presenting in detail the hypernuclear mass spectra obtained using the (π^+, K^+) reaction, a few key principles of the analysis are explained below.

The mass of the hypernucleus (M_{HYP}) is derived from the measured momentum vectors of the incident pion (p_{π^+}) and the outgoing kaon (p_{K^+}) as follows:

$$M_{\mathrm{HYP}} = \sqrt{(E_{\pi^+} + M_A - E_{K^+})^2 - (p_{\pi^+}^2 + p_{K^+}^2 - 2p_{\pi^+}p_{K^+}\cos\theta)}, \tag{3}$$

where E_{π^+} and E_{K^+} are total energies of the pion and the kaon respectively, θ is the kaon scattering angle, and M_A is the target mass.

The binding energy of a Λ hyperon is then deduced, by assuming the core nucleus is in its ground state as

$$B_\Lambda = M_{\mathrm{core}} + M_\Lambda - M_{\mathrm{HYP}}. \tag{4}$$

Here M_{core} is the mass of the core nucleus and M_Λ is the mass of the Λ hyperon. The spectra in Fig. 9 are shown as a function of the Λ binding energy, B_Λ.

Next, the absolute mass scales of the hypernuclear spectra presented below have been adjusted using as a reference the ${}^{12}_{\Lambda}$C ground-state peak, whose binding energy is well

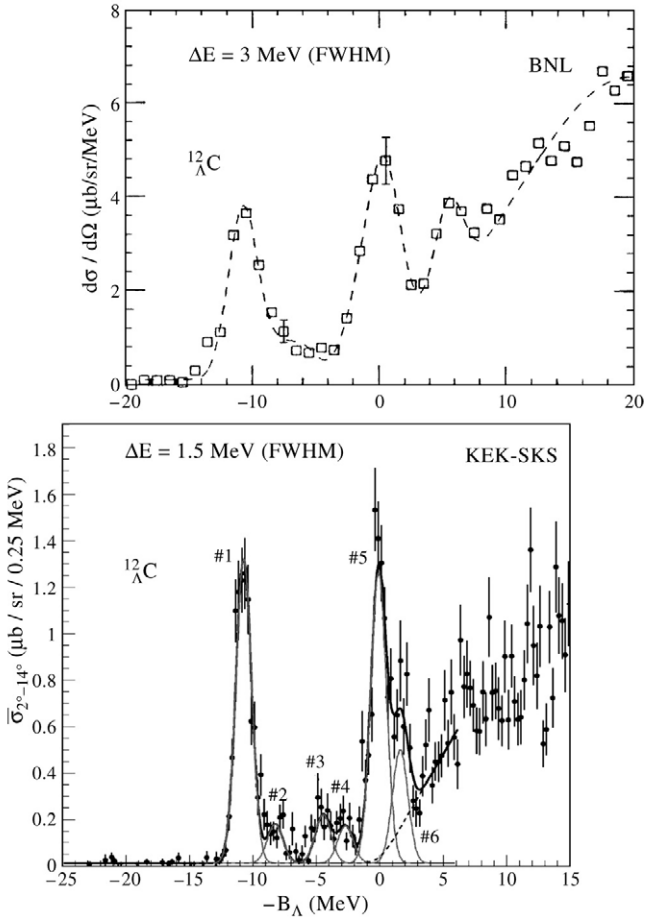

Fig. 9. Missing mass spectra of the $^{12}C(\pi^+, K^+)^{12}_{\Lambda}C$ reaction measured at the BNL AGS with 3 MeV FWHM resolution [20] (top) and at the KEK 12 GeV PS using the SKS spectrometer with 1.45 MeV FWHM resolution [25] (bottom).

determined from emulsion experiments to be $B_{\Lambda} = 10.76$ MeV [51]. The systematic errors associated with this mass scale have been evaluated to be at most ± 0.5 MeV for the spectra presented in the next subsection.

The linearity of the mass scale was also examined by letting the beam particles pass through the SKS spectrometer and varying their momenta; it was found to be smaller than the other systematic errors.

Finally, it is noted in advance that the vertical scales of the SKS spectrometer spectra are presented differently for the E336, E369 and E140 experiments. This is due to the fact that the acceptance of the SKS spectrometer is quite large and the cross section varies by more than a factor of three within its angular acceptance.

Table 5
The (π^+, K^+) experiments with the SKS spectrometer

E140a	Systematic spectroscopy of Λ hypernuclei	${}^{10}_{\Lambda}$B, ${}^{12}_{\Lambda}$C, ${}^{28}_{\Lambda}$Si, ${}^{89}_{\Lambda}$Y, ${}^{139}_{\Lambda}$La, ${}^{208}_{\Lambda}$Pb
E336	Light Λ hypernuclear spectroscopy	${}^{7}_{\Lambda}$Li, ${}^{9}_{\Lambda}$Be, ${}^{12}_{\Lambda}$C, ${}^{13}_{\Lambda}$C, ${}^{16}_{\Lambda}$O
E369	Spectroscopy of medium-heavy hypernuclei	${}^{12}_{\Lambda}$C, ${}^{51}_{\Lambda}$V, ${}^{89}_{\Lambda}$Y

For E336, which is the source of many of the (π^+, K^+) reaction spectra discussed in this article, the vertical axis of the spectra is presented as the cross sections integrated over the given angular range with a correction for the SKS acceptance of 0.183 msr:

$$\sigma_{2^\circ-14^\circ} = \int_{\theta=2^\circ}^{\theta=14^\circ} \left(\frac{\mathrm{d}\sigma}{\mathrm{d}\Omega}\right) \mathrm{d}\Omega. \tag{5}$$

For the E369 spectra, the cross section was divided by the SKS acceptance:

$$\overline{\sigma_{2^\circ-14^\circ}} = \int_{\theta=2^\circ}^{\theta=14^\circ} \left(\frac{\mathrm{d}\sigma}{\mathrm{d}\Omega}\right) \mathrm{d}\Omega \Bigg/ \int_{\theta=2^\circ}^{\theta=14^\circ} \mathrm{d}\Omega = \sigma_{2^\circ-14^\circ}/0.183 \text{ msr}. \tag{6}$$

Finally, for the E140a spectra, yields were integrated over the SKS acceptance without correction for the angular acceptance:

$$Y_{2^\circ-14^\circ} = \int_{\theta=2^\circ}^{\theta=14^\circ} \left(\frac{\mathrm{d}\sigma}{\mathrm{d}\Omega}\eta(\Omega)\right) \mathrm{d}\Omega, \tag{7}$$

where $\eta(\Omega)$ is the SKS acceptance function.

With the present configuration of the SKS spectrometer, the hypernuclear yield rate for the ${}^{12}_{\Lambda}$C ground state using the $\pi^+ + {}^{12}$C reaction is approximately 5–8 events/$(10^9\pi^+)$/(g/cm^2). This rate is equivalent to about 1000 events/day for a 2 g/cm^2 thick ^{12}C target. This high detection efficiency of the SKS spectrometer makes it an efficient "strangeness tagger" for the (π^+, K^+) reaction hypernuclear γ-ray spectroscopy, which is the subject of Section 5. This efficiency also made experiments on hypernuclear weak decay feasible, though they are beyond the scope of this article.

The (π^+, K^+) reaction spectroscopy experiments that have been carried out with the SKS spectrometer are listed in Table 5. In the following two subsections, the high-statistics ${}^{12}_{\Lambda}$C spectrum is presented first as a reference spectrum, then the other spectra are described in the order of hypernuclear mass number.

3.3. Light Λ hypernuclear spectroscopy

3.3.1. ${}^{12}_{\Lambda}$C hypernucleus

A carbon target is widely used as a reference for Λ hypernuclear spectra, since it clearly demonstrates distinct peaks corresponding to the s and p Λ major shells and it is easy to prepare the target. Although the high-resolution ${}^{12}_{\Lambda}$C spectrum measured in the E369 experiment with a thin target (0.86 g/cm^2) was already presented in Fig. 9, a higher-statistics ${}^{12}_{\Lambda}$C spectrum, which was obtained in E336 with a thicker target (1.86 g/cm^2), is shown in Fig. 10. The spectrum is given as a function of $M_{\mathrm{HYP}} - M_A$,

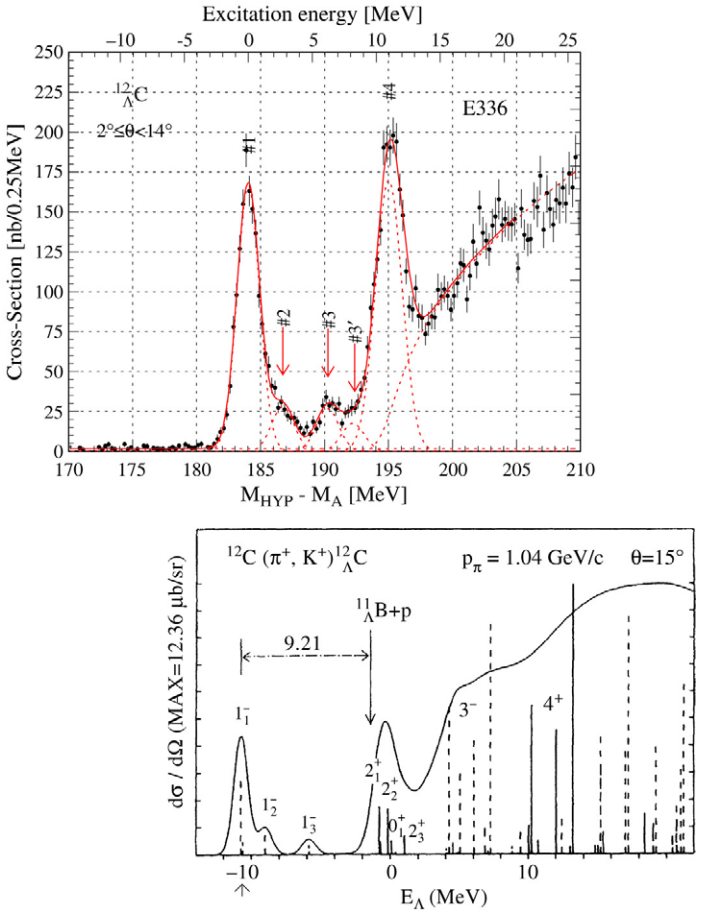

Fig. 10. High-statistics excitation spectrum of $^{12}_{\Lambda}$C from E336 (top) and the spectrum calculated in the DWIA using a configuration-mixing shell model [52] (bottom) for the ^{12}C$(\pi^+, K^+)^{12}_{\Lambda}$C reaction.

where M_{HYP} and M_A correspond to the masses of $^{12}_{\Lambda}$C and ^{12}C. It is also presented as a function of the excitation energy.

The spectrum was fitted assuming five gaussians, two for the major peaks and three for the small ones, and a quasifree contribution. The result is listed in Table 6. As already mentioned, the two major peaks, #1 and #4, at $E_X = 0$ and 11 MeV arise from the coupling of a Λ hyperon in the $l = 0$ and $l = 1$ orbits to the ground state of a core nucleus of ^{11}C. They have configurations of $\nu p^{-1}_{3/2} \otimes \Lambda s_{1/2}$ and $\nu p^{-1}_{3/2} \otimes \Lambda p_{1/2,3/2}$. The width of the ground-state peak corresponds to the mass resolution of the present spectrum and is 2 MeV FWHM, broader than the 1.45 MeV FWHM obtained with a thin target (0.86 g/cm^2) that was shown in Fig. 9. The second major peak (#4) seems to be wider than the ground-state peak. This may indicate that the peak is composed of more than two states, as was also suggested by the 1.45 MeV high-resolution spectrum.

Table 6
Excitation energies and cross sections of $^{12}_{\Lambda}$C in the (π^+, K^+) reaction

Peaks	B_Λ or E_X (MeV)	FWHM (MeV)	Cross sections $\sigma_{2^\circ-14^\circ}$ (μb)
# 1	$B_\Lambda = 10.80$ (fixed)	1.97 ± 0.03	1.44 ± 0.03
# 2	$E_X = 2.63 \pm 0.06$	1.97 ± 0.03	0.24 ± 0.02
# 3	$E_X = 6.09 \pm 0.08$	1.97 ± 0.03	0.23 ± 0.02
# 3′	$E_X = 8.12 \pm 0.17$	1.97 ± 0.03	0.18 ± 0.02
# 4	$E_X = 11.00 \pm 0.03$	2.39 ± 0.06	1.81 ± 0.05

The fitting procedure assumed that the four peaks from #1 to #3′ have a common width.

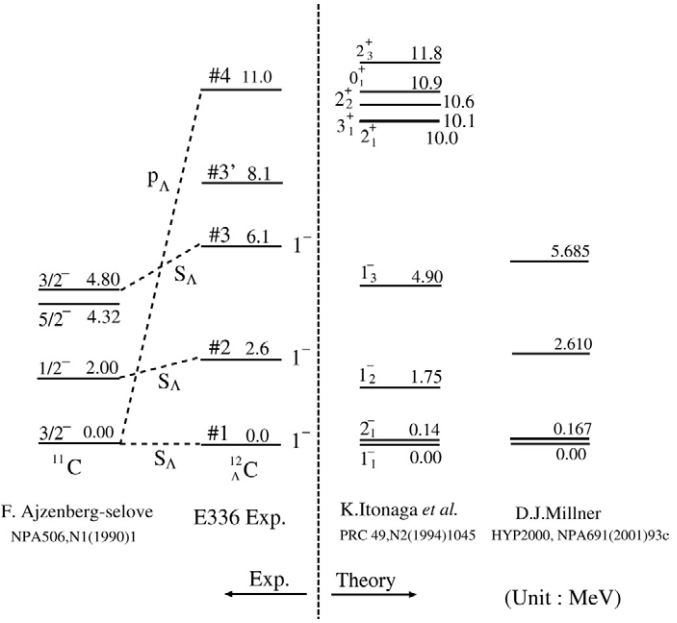

Fig. 11. Comparison of the experimental energy levels and the theoretical calculations for the $^{12}_{\Lambda}$C.

In the present high-statistics $^{12}_{\Lambda}$C spectrum, at least three satellite peaks were identified between the two prominent peaks (#1 and #4). These satellite peaks were first observed by the E140a experiment [22,23]. They have about 1/10 the cross sections of the major peaks and were interpreted as an $s_{1/2}$ Λ hyperon coupled to excited states of the ^{11}C core. Since the spectroscopic factors of the $p_{3/2}$ neutron for the corresponding excited states of the ^{11}C core are about 10% of the ground state, the cross section ratios of the excited states to the ground state are expected to be 1/10 to first order. In Fig. 10, a $^{12}_{\Lambda}$C spectrum calculated based on DWIA and configuration-mixing shell model wavefunctions is shown [52]. The calculated spectrum shows spectral structure similar to the experimental data, including the satellite peaks at excitation energies from 6 to 9 MeV.

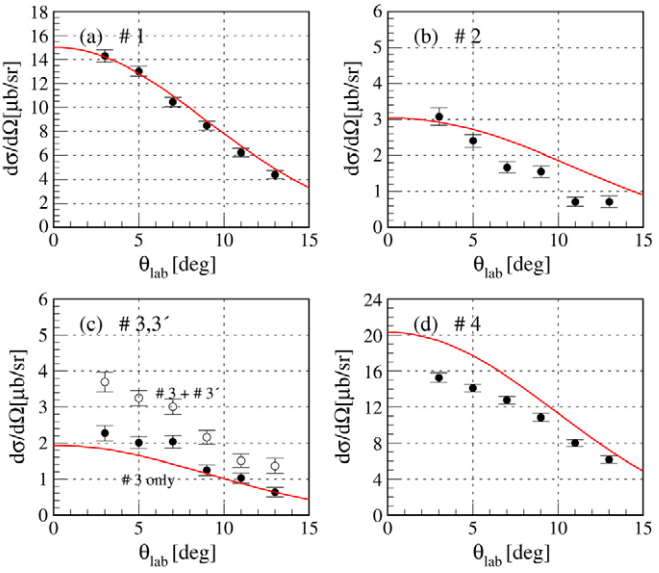

Fig. 12. Angular distribution of kaons in the ^{12}C(π^+, K^+) $^{12}_{\Lambda}$C reaction measured in E336.

The experimental excitation energies of $^{12}_{\Lambda}$C and the ^{11}C core are compared in Fig. 11 with those calculated for $^{12}_{\Lambda}$C by Itonaga [52] and Millener [53]. Because a Λ hyperon weakly couples to the core, the level spacings of Λ hypernucleus are expected to be similar to those of the core nucleus. In the present spectrum, the excitation energy of the #3 peak, which is considerably higher than the corresponding core excitation energy of 4.8 MeV, is of particular interest, as first pointed out in Ref. [22]. The excitation energy and the cross section of the state at 6.1 MeV (#3) are less well understood. Although these were discussed in conjunction with a spin-dependent part of the ΛN interaction [22], the excitation energy appears to be too high to be explained in the present theoretical framework.

Kaon angular distributions were measured simultaneously in E336, taking an advantage of the large SKS solid angle, which spans an angular range from 0 to 15 degrees. The angular distributions are shown in Fig. 12 for peaks #1 to #4. The calculated angular distributions [54], which are also shown in the figure agree well with the data for both the shapes and the absolute cross sections. The comparison of the angular distributions and the cross sections of peaks #3 and #3′ supports the conjecture that there are at least two peaks in that excitation energy region, and the peak #3 can be assigned to the 1^-_3 states. There are arguments that the #3 peak at 6.1 MeV is simply due to a ^{11}C(4.8 MeV) $\otimes$ s_{Λ} configuration but could have some contribution from inter-shell configuration mixing in which positive parity core excited states with a Λ in the p orbit mix with the dominant ^{11}C(4.8 MeV) $\otimes$ s_{Λ} configuration [55,56].

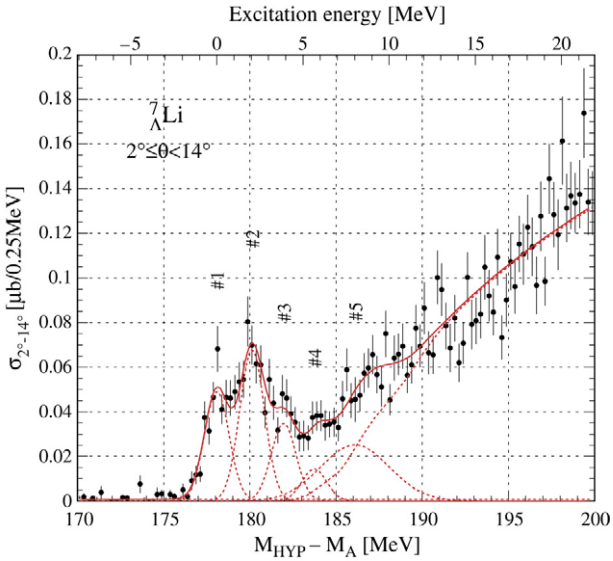

Fig. 13. Excitation spectrum of $^{7}_{\Lambda}$Li measured in E336 by the (π^+, K^+) reaction with the SKS spectrometer system.

Table 7
Excitation energies and cross sections of $^{7}_{\Lambda}$Li obtained in the (π^+, K^+) reaction by the E336 experiment

Peaks	B_Λ or E_X (MeV)	FWHM (MeV)	Cross sections $\sigma_{2°-14°}$ (μb)
# 1	$B_\Lambda = 5.22 \pm 0.08$	1.81 (fixed)	0.345 ± 0.032
# 2	$E_X = 2.05$ (fixed)	1.81 (fixed)	0.486 ± 0.032
# 3	$E_X = 3.88$ (fixed)	1.81 (fixed)	0.241 ± 0.033
# 4	$E_X = 5.61 \pm 0.24$	1.81 (fixed)	0.136 ± 0.050
# 5	$E_X = 7.99 \pm 0.37$	3.81 ± 0.81	0.398 ± 0.078

3.3.2. $^{7}_{\Lambda}$Li, $^{9}_{\Lambda}$Be *and* $^{10}_{\Lambda}$B *hypernuclei*

$^{7}_{\Lambda}$Li

The $^{7}_{\Lambda}$Li excitation spectrum has been studied using both the in-flight and stopped (K^-, π^-) reactions. The ^{7}Li(π^+, K^+) $^{7}_{\Lambda}$Li spectrum was first measured in E336 as shown in Fig. 13. The $^{7}_{\Lambda}$Li spectrum was fitted with five gaussians and a quasifree contribution. The mass resolution of the first four peaks was fixed to 1.81 MeV FWHM, which was determined from the $^{12}_{\Lambda}$C spectra taken during the experiment, correcting for the difference of energy loss straggling in the ^{7}Li and ^{12}C targets. The excitation energies and the cross sections are listed in Table 7. The observed Λ binding energy, $B_\Lambda = 5.22 \pm 0.08$(stat) $\pm$ 0.36(syst) MeV, agrees well with the emulsion data, $B_\Lambda = 5.58 \pm 0.03$ MeV [63].

The energy difference between the first and the second peaks was found to be 2.0 MeV, which is consistent with the measured γ-ray energy assigned to the $E2$ transition between the $5/2^+$ and $1/2^+$ states [36]. The transition from peak #3 to the ground state was also identified in a recent γ-ray experiment [26]. The excitation energies of these states were fixed to the γ-ray values.

The ${}^{7}_{\Lambda}$Li hypernucleus has been investigated theoretically in the framework of both the cluster and the shell model. In the cluster model, the ${}^{7}_{\Lambda}$Li hypernucleus was treated as $\alpha + d + \Lambda$. A ^{3}He$+t + \Lambda$ configuration was also included to explain highly excited states [46]. More recently the ${}^{5}_{\Lambda}$He$+p + n$ configuration was also studied [57].

Reactions leading to ${}^{7}_{\Lambda}$Li have also been compared to calculations, using large scale shell model wavefunctions [58]. The ground state and the first excited state, which have configurations of $[{}^{6}\mathrm{Li}(1^+) \otimes \Lambda s_{1/2}]1/2^+, T = 0$ and $[{}^{6}\mathrm{Li}(3^+) \otimes \Lambda s_{1/2}]5/2^+, T = 0$ respectively, are populated by the (π^+, K^+) reaction. In addition, extra strength was seen just below the Λ binding threshold. It was operationally represented by two additional gaussian peaks as shown in the spectrum. Although the decomposition of this strength into two peaks is somewhat arbitrary, the $T = 1$ states that have been predicted at this excitation energy by both the shell model and cluster model calculations are considered excellent candidates for this strength. As a result of recent advances in the cluster model treatment of light Λ hypernuclei [59], one can expect detailed information on excitation energies and cross sections to provide unique data for further understanding Λ hypernuclear structure and the ΛN interaction.

The ${}^{7}_{\Lambda}$Li is the first Λ hypernucleus thoroughly studied with high-precision γ-ray spectroscopy using a germanium detector array and will be described in detail in Section 5.

${}^{9}_{\Lambda}$Be

The ${}^{9}_{\Lambda}$Be hypernucleus has a highly symmetric configuration with a ^{8}Be core, and its structure is expected to exhibit unique features. It was first pointed out by Dalitz and Gal, who used a shell model basis, that unique Λ hypernuclear states should appear as "supersymmetric states" [60,61]. Such states were later investigated by Bandō et al. in the framework of a cluster model and referred to as "genuine hypernuclear states" [46]. To first order, the ${}^{9}_{\Lambda}$Be hypernucleus is treated as having the cluster configuration of $2\alpha + \Lambda$, the 2α forming the ^{8}Be core. Three series of band structures are expected as is shown pictorially in Fig. 14; A: $[(\alpha\alpha) \otimes \Lambda s_{1/2}]_{K=0^+}$, B: $[(\alpha\alpha) \otimes p^{\parallel}_{\Lambda}]_{K=0^-}$, C: $[(\alpha\alpha) \otimes p^{\perp}_{\Lambda}]_{K=1^-}$. Among these, the B-series represents the genuine hypernuclear states in which a Λ hyperon sits in the p orbit parallel to the α–α axis. Such states cannot be formed in an ordinary ^{9}Be nucleus, which would have the $(\alpha + \alpha + n)$ configuration, because of the Pauli exclusion principle.

The ${}^{9}_{\Lambda}$Be spectrum measured in E336 is shown in Fig. 15. It clearly shows structure in both the bound and unbound regions. The spectrum was fitted assuming eight peaks and a quasifree continuum contribution; the result is summarized in Table 8.

The ground and the first excited states at $E_X = 0$ and 2.93 MeV are observed as distinct peaks. According to theoretical calculations, these states have configurations of a Λ hyperon in the s orbit coupled to ${}^{8}\mathrm{Be}(0^+)$ and ${}^{8}\mathrm{Be}(2^+)$. The strengths at $\sim$6 and 10 MeV excitation (#3 and #4) were interpreted as the "genuine hypernuclear" states based on comparison with the calculated spectrum. These states can be generated by coupling a

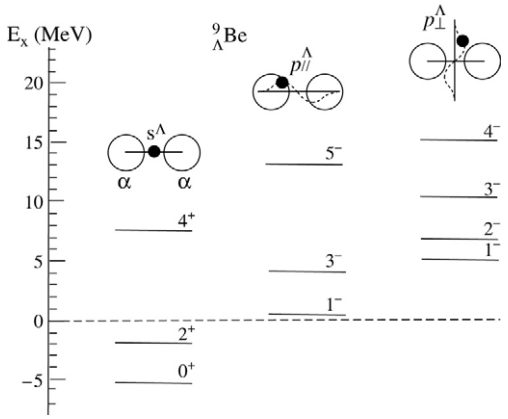

Fig. 14. Calculated energy levels of ${}^{9}_{\Lambda}$Be for three cluster configurations. A band corresponding to genuine hypernuclear states appears as an $\alpha - \alpha - \Lambda(p_\Lambda)$ configuration. The ${}^{9}_{\Lambda}$Be spins before the Λ spin is coupled are shown [3].

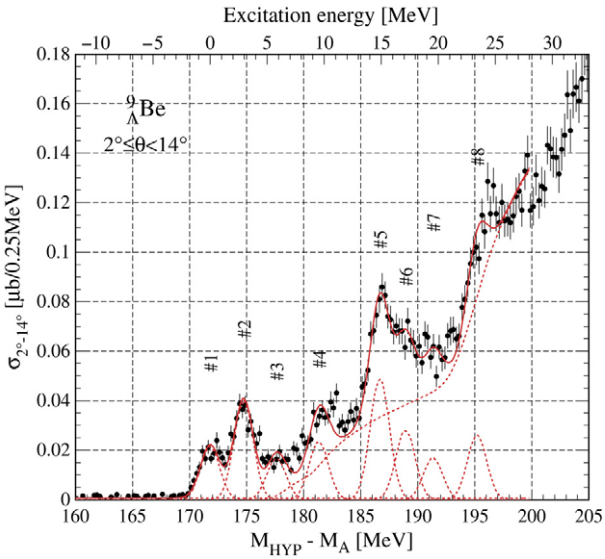

Fig. 15. Excitation spectrum of ${}^{9}_{\Lambda}$Be measured using the (π^+, K^+) reaction with the SKS spectrometer system.

$p^{\parallel}_{\Lambda}$ hyperon to the core of ^{8}Be 1^- and 3^-. Previously, the BNL exploratory ${}^{9}_{\Lambda}$Be spectrum suggested the excitation of the predicted genuine hypernuclear states [20]. The present spectrum confirms and clearly establishes the existence of these states.

In addition, structure is observed at about $E_X = 15$ MeV. It can be considered as an α cluster excitation of the core nucleus, as was predicted in the recent cluster calculations of

Table 8
Excitation energies and cross sections of ${}^{9}_{\Lambda}$Be in the (π^+, K^+) reaction measured in the KEK E336 experiment

Peaks	B_Λ or E_X (MeV)	FWHM (MeV)	Cross sections $\sigma_{2^\circ-14^\circ}$ (μb)
# 1	$B_\Lambda = 5.99 \pm 0.07$	1.99 (fixed)	0.181 ± 0.009
# 2	$E_X = 2.93 \pm 0.07$	1.99 (fixed)	0.340 ± 0.012
# 3	$E_X = 5.80 \pm 0.13$	1.99 (fixed)	0.141 ± 0.009
# 4	$E_X = 9.52 \pm 0.13$	1.99 (fixed)	0.198 ± 0.013
# 5	$E_X = 14.88 \pm 0.10$	1.99 (fixed)	0.412 ± 0.024
# 6	$E_X = 17.13 \pm 0.20$	1.99 (fixed)	0.238 ± 0.022
# 7	$E_X = 19.54 \pm 0.32$	1.99 (fixed)	0.143 ± 0.021
# 8	$E_X = 23.40 \pm 0.21$	1.99 (fixed)	0.220 ± 0.027

Yamada [62]. However, the excitation energy of this state is considerably lower than the calculated value. Improved treatment of the core nucleus of ^{8}Be will be required to resolve the disagreement.

It is noted here that the binding energy of ${}^{9}_{\Lambda}$Be was found to be 5.99 ± 0.07(stat) ± 0.36(syst) MeV, which should be compared with the value from emulsion data: $B_\Lambda = 6.71 \pm 0.03$ MeV [63]. Considering the fact that the binding energies of ${}^{7}_{\Lambda}$Li and ${}^{13}_{\Lambda}$C agree with the emulsion data within the errors of the E336 experiment, the difference in the case of ${}^{9}_{\Lambda}$Be is significant even if we include the systematic error. The reason for this disagreement is not known and further investigation is needed.

${}^{10}_{\Lambda}$B

The ${}^{10}_{\Lambda}$B hypernucleus was previously studied both by emulsion and counter experiments [63,94]. A higher quality spectrum was measured in the E140a experiment and is shown in Fig. 16. This spectrum exhibits three peaks in the bound region and a broader one in the unbound region ($-B_\Lambda \approx 2$ MeV). These peak structures are resolved with the 2.2 MeV resolution of the present spectrum. All of these peaks are regarded to have configurations of a Λ hyperon in the s orbit coupled to the ^{9}B core nucleus. The three excited-state peaks are interpreted as corresponding to the excited states of the ^{9}B core at 2.4 ($5/2^-$), 7.1 ($7/2^-$) and 11.5 ($7/2^-$) MeV. The spectrum was fitted with four gaussians and a second-order polynomial function that described the continuum region. The width of the gaussians was fixed to the estimated experimental energy resolution of 2.2 MeV except for the fourth peak, which is clearly wider than the experimental energy resolution. The results are listed in Table 9. The excitation energies obtained from this fit (2.5, 6.2 and 9.5 MeV) deviated from the calculated excitation energies of the three corresponding ^{9}B core states.

In Fig. 16, a ${}^{10}_{\Lambda}$B spectrum that was calculated by a configuration-mixing shell model [52] is also shown. It has a four-peak structure (2^-_1, 3^-_1, 3^-_2 and 3^-_4) similar to that of the observed spectrum. It was pointed out that the level spacings of these four states were sensitive to the choice of the ΛN residual interaction and therefore ${}^{10}_{\Lambda}$B is a good Λ hypernucleus for studying the ΛN residual interaction, as is the case for ${}^{12}_{\Lambda}$C [64].

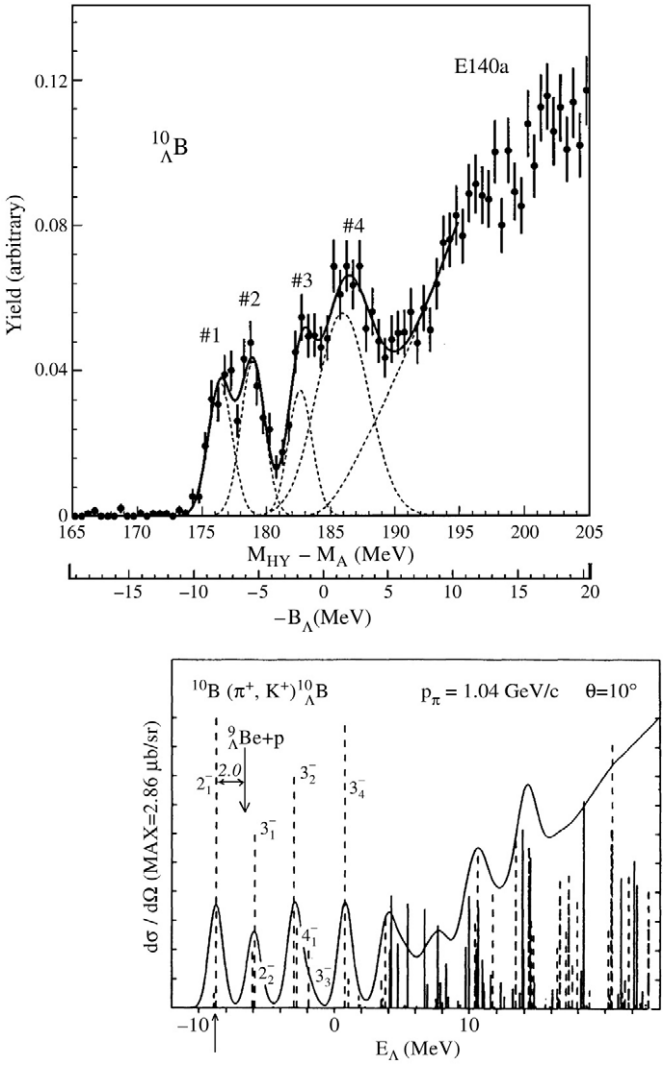

Fig. 16. Excitation spectrum of $^{10}_{\Lambda}$B (top) measured in the E140a experiment using the ^{10}B(π^+, K^+)$^{10}_{\Lambda}$B reaction [23] and (bottom) calculated using DWIA and a configuration-mixing shell model [52].

3.3.3. $^{13}_{\Lambda}$C *and* $^{16}_{\Lambda}$O *hypernuclei*

$^{13}_{\Lambda}$C

The $^{13}_{\Lambda}$C spectrum observed in the E336 experiment is presented in Fig. 17 and the angular distributions of kaons leading to particular states in this spectrum are shown in Fig. 18. The spectrum is composed of: (1) distinct peaks in the excitation region below 5 MeV, (2) a large peak at $E_X = 15$ MeV with a shoulder toward lower excitation energy, (3) bump structure at $E_X = 24$–28 MeV, and (4) a quasifree contribution

Table 9
Excitation energies and relative hypernuclear yields of $^{10}_{\Lambda}$B measured in the KEK E140a experiment [23]

Peaks	B_Λ or E_X (MeV)	FWHM (MeV)	Relative yield (arbitrary)
# 1	$B_\Lambda = 8.1 \pm 0.1$	2.2 (fixed)	0.17 ± 0.02
# 2	$E_X = 2.5 \pm 0.2$	2.2 (fixed)	0.20 ± 0.02
# 3	$E_X = 6.2 \pm 0.3$	2.2 (fixed)	0.16 ± 0.05
# 4	$E_X = 9.5 \pm 0.3$	4.8 ± 0.8	0.57 ± 0.14

The quoted errors are statistical.

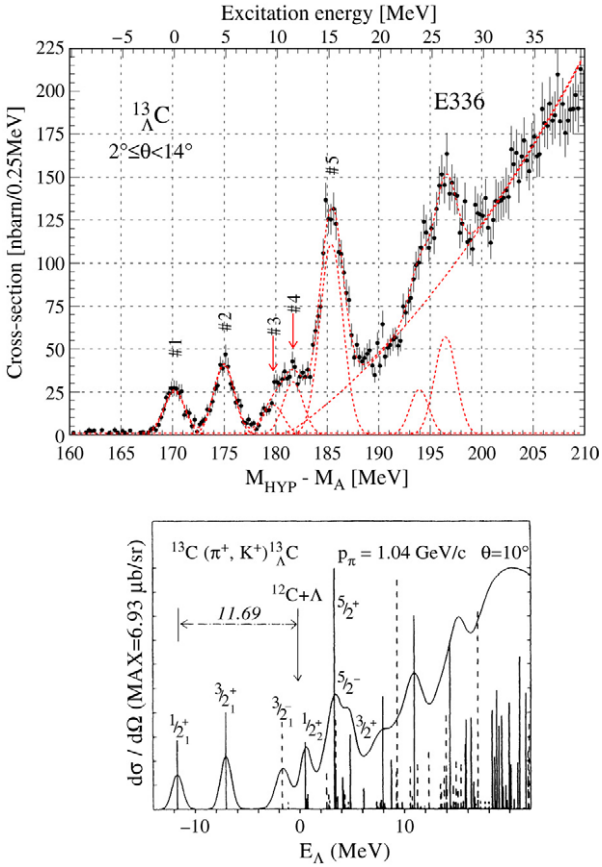

Fig. 17. High-statistics excitation spectrum of $^{13}_{\Lambda}$C obtained by E336 using the ^{13}C(π^+, K^+) $^{13}_{\Lambda}$C reaction (top), and the calculated spectrum [52] (bottom).

above the threshold. The spectrum was fitted assuming seven gaussian peaks and a quasifree contribution, and the results are summarized in Table 10. The binding energy was determined as $B_\Lambda = 11.38 \pm 0.05(\text{stat}) \pm 0.36(\text{syst})$ MeV, which agrees well with the

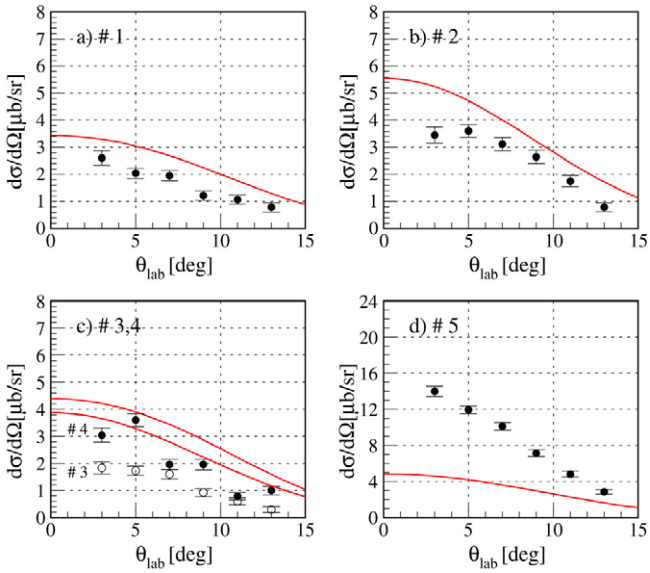

Fig. 18. Angular distributions of kaons in the $^{13}C(\pi^+, K^+)\,^{13}_{\Lambda}C$ reaction.

Table 10
Excitation energies and cross sections of $^{13}_{\Lambda}C$ states as populated by the (π^+, K^+) reaction

Peaks	B_Λ or E_X (MeV)	FWHM (MeV)	Cross sections $\sigma_{2^\circ-14^\circ}$ (μb)
# 1	$B_\Lambda = 11.38 \pm 0.05$	2.23 ± 0.06	0.25 ± 0.02
# 2	$E_X = 4.85 \pm 0.07$	2.23 ± 0.06	0.42 ± 0.02
# 3	$E_X = 9.73 \pm 0.14$	2.23 ± 0.06	0.22 ± 0.02
# 4	$E_X = 11.75 \pm 0.15$	2.23 ± 0.06	0.30 ± 0.02
# 5	$E_X = 15.31 \pm 0.06$	2.46 ± 0.08	1.29 ± 0.04
# 6	$E_X = 23.68 \pm 0.16$	2.20 ± 0.29	0.33 ± 0.04
# 7	$E_X = 26.37 \pm 0.11$	2.41 ± 0.17	0.76 ± 0.06

emulsion data value, $B_\Lambda = 11.69 \pm 0.12$ MeV. As seen in Fig. 17 (bottom), the general features of the spectrum are well reproduced by the DWIA calculation.

A simple configuration of a Λ hyperon coupled to a ^{12}C core can be assumed for the $^{13}_{\Lambda}C$ hypernucleus. The lowest two peaks, #1 and #2, are interpreted as having configurations of $1/2^+_1[^{12}C(0^+_1; g.s.) \otimes \Lambda s_{1/2}]$ and $3/2^+_1[^{12}C(2^+_1; 4.4\ \text{MeV}) \otimes \Lambda s_{1/2}]$. The excitation energy of peak #2 is consistent with the γ-ray energy recently measured with NaI [39]. The shoulder peaks in the $E_X = 10$ MeV region were assigned to $[^{12}C(0^+) \otimes \Lambda p_{3/2}]3/2^-$ and $[^{12}C(1^+) \otimes \Lambda s_{1/2}]1/2^+$ as predicted by the DWIA calculation of Itonaga [65]. Peak #5 is regarded as formed dominantly by a Λ hyperon in the p orbit, but positive parity states may also contribute. The summed cross section for peaks #1 through #5 is found to

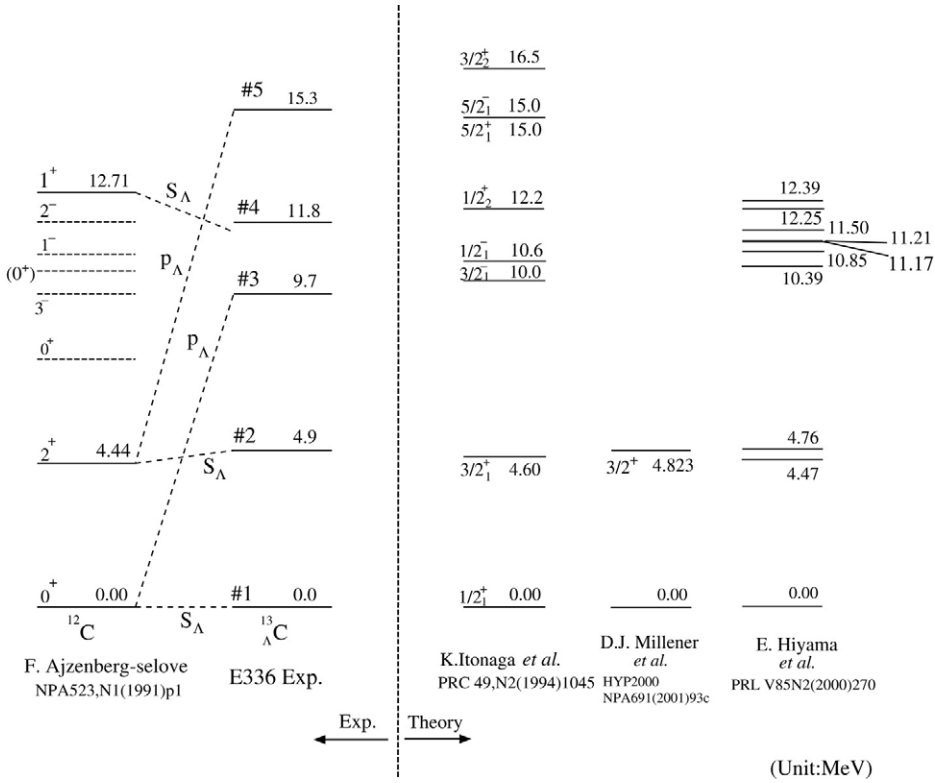

Fig. 19. Comparison of the measured energy levels and the theoretical calculations for $^{13}_{\Lambda}$C.

be $\sigma_{2^\circ-14^\circ} = 1.25 \pm 0.04 \pm 0.10$ μb, which agrees reasonably well with the calculated summed cross section of 1.47 μb [52].

The peak at about $E_X = 25$ MeV is also predicted by the calculation; $T = 1$ ^{12}C excitations are thought to be most responsible to the structure, although the expected peak position is about 1 MeV below the measured position. Comparison of the $^{13}_{\Lambda}$C level structure with that of the core nucleus, ^{12}C, and recent theoretical calculations is summarized in Fig. 19.

$^{16}_{\Lambda}$O

The $^{16}_{\Lambda}$O hypernucleus has a relatively solid core of ^{15}O as the excitation energy of the first state in ^{15}O is 5.2 MeV. Since this energy is much larger than the resolution of the spectrometer, the core excited $^{16}_{\Lambda}$O states are expected to be well separated from each other in the hypernuclear excitation spectrum. The spectrum of $^{16}_{\Lambda}$O measured in E336 is shown in Fig. 20, in which four distinct peaks are clearly seen.

In the $^{16}_{\Lambda}$O hypernuclei, both $p_{1/2}$ and $p_{3/2}$ neutron hole states are responsible for exciting low-lying hypernuclear states; this is in contrast to the $^{12}_{\Lambda}$C case in which the $p_{3/2}$ neutron hole plays a major role. Accordingly, we expect to observe four peaks in the bound

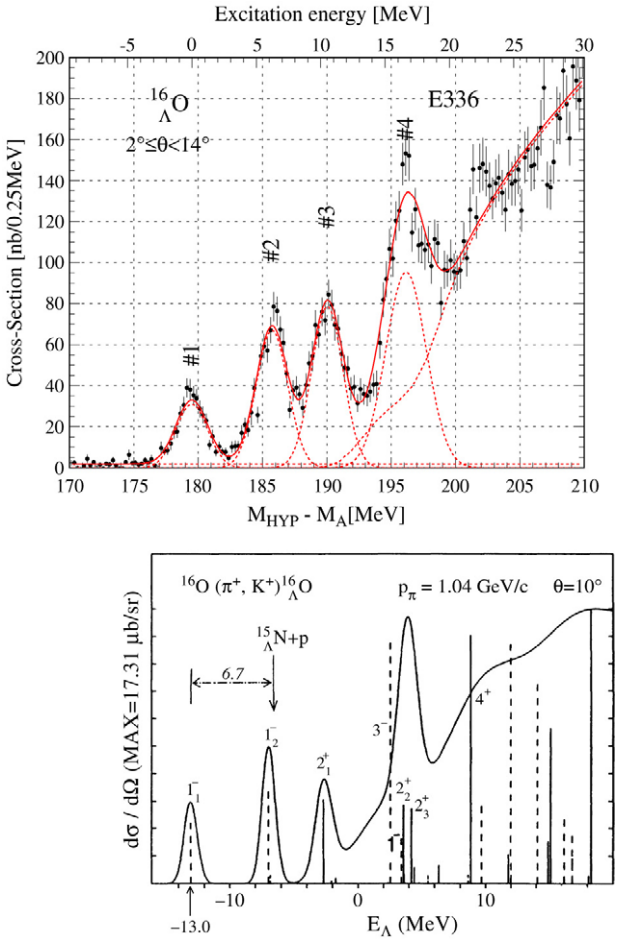

Fig. 20. High-statistics excitation spectrum of $^{16}_{\Lambda}$O from E336 (top) and the calculated spectrum [52] for the ^{16}O(π^+, K^+) $^{16}_{\Lambda}$O reaction (bottom).

region of the excitation spectra measured using the (π^+, K^+) and (K^-, π^-) reactions. These states are expected to have configurations of $[\nu p^{-1}_{1/2} \otimes \Lambda s_{1/2}]1^-_1$, $[\nu p^{-1}_{3/2} \otimes \Lambda s_{1/2}]1^-_2$, $[\nu p^{-1}_{1/2} \otimes \Lambda p_{3/2,1/2}]2^+_1, 0^+_1$ and $[\nu p^{-1}_{3/2} \otimes \Lambda p_{3/2,1/2}]2^+_2, 0^+_2$. The $^{16}_{\Lambda}$O spectrum was fitted using the same procedure as was applied to the other (π^+, K^+) spectra and the results are summarized in Table 11. The binding energy was determined as $B_\Lambda = 12.42 \pm 0.05(\text{stat}) \pm 0.36(\text{syst})$ MeV. The angular distributions of the four peaks measured in the (π^+, K^+) reaction are also presented in Fig. 21 and compared with the DWIA calculation. The close agreement between the measured and calculated spectra supports the choice of major configurations used in the calculations. The level structure of $^{16}_{\Lambda}$O is compared with that of the core nucleus, ^{15}O, and the recent theoretical calculations in Fig. 22.

Table 11
Excitation energies and cross sections of ${}^{16}_{\Lambda}$O in the (π^+, K^+) reaction

Peaks	B_Λ or E_X (MeV)	FWHM (MeV)	Cross sections $\sigma_{2^\circ-14^\circ}$ (μb)
# 1	$B_\Lambda = 12.42 \pm 0.05$	2.75 ± 0.05	0.41 ± 0.02
# 2	$E_X = 6.23 \pm 0.06$	2.75 ± 0.05	0.91 ± 0.03
# 3	$E_X = 10.57 \pm 0.06$	2.75 ± 0.05	1.05 ± 0.03
# 4	$E_X = 16.59 \pm 0.07$	3.13 ± 0.11	1.38 ± 0.06

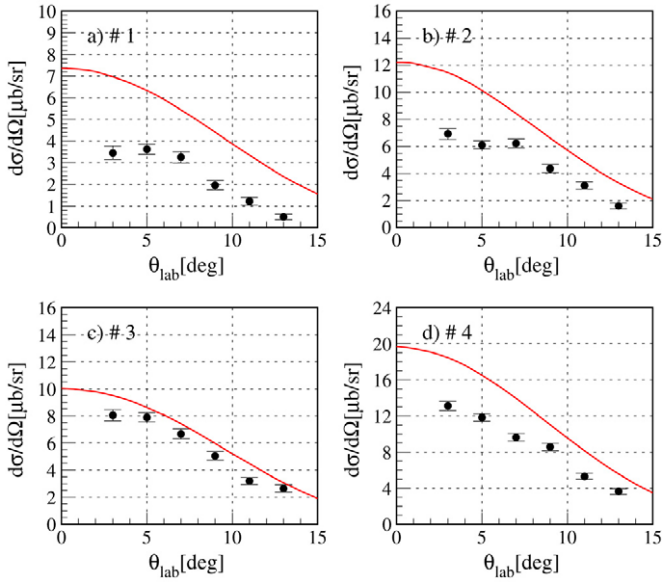

Fig. 21. Angular distributions of kaons in the ${}^{16}\mathrm{O}(\pi^+, K^+)\,{}^{16}_{\Lambda}$O reaction.

It has been widely believed that the spin–orbit splitting in p-shell Λ hypernuclei is quite small. The CERN ${}^{12}_{\Lambda}$C and ${}^{16}_{\Lambda}$O [13,66], and BNL ${}^{13}_{\Lambda}$C data [17] gave very small values for the splitting. However, a recent reanalysis of the emulsion ${}^{16}_{\Lambda}$O data claimed that the splitting of the spin–orbit partner (2^+_1 and 0^+_1) is 1.56 ± 0.12 MeV, which is much larger than the above small splitting [67]. A possible large ls splitting is also suggested in the analysis of the ${}^{89}_{\Lambda}$Y spectrum as described in this section.

To address this apparent discrepancy, the present high-quality ${}^{16}_{\Lambda}$O spectrum measured using the (π^+, K^+) reaction has been carefully analyzed and compared with the spectrum by the (K^-, π^-) reaction. In the ${}^{16}_{\Lambda}$O spectrum, the 2^+_1 state can be excited favorably by the (π^+, K^+) reaction because of the large momentum transfer in that reaction, while the 0^+_1 state is preferentially excited by the recoilless (K^-, π^-) reaction [47,65]. The excitation energy of the 2^+_1 state can be determined with a good precision from the present (π^+, K^+) spectrum of ${}^{16}_{\Lambda}$O to be $10.57 \pm 0.06 \pm 0.14$ MeV. The excitation energy of the

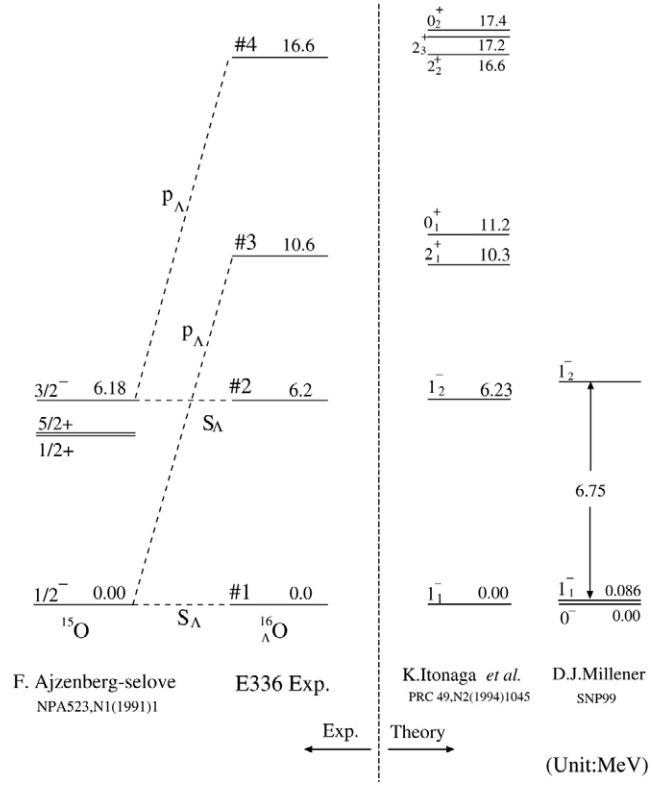

Fig. 22. A comparison of the experimental energy levels and theoretical calculations for ${}^{16}_{\Lambda}$O.

ls partner 0^+_1 state was determined from a fit to the CERN (K^-, π^-) in-flight spectrum of ${}^{16}_{\Lambda}$O [13] to be 10.61 ± 0.28 MeV [68]. Thus, the energy difference between the 2^+_1 and 0^+_1 is obtained to be 0.04 ± 0.32 MeV.

To further investigate the *ls* splitting, the energy splitting of these two states, 2^+_1 and 0^+_1, was calculated as a function of $\delta_\Lambda \equiv \epsilon_\Lambda(1p^{-1}_{1/2}) - \epsilon_\Lambda(1p^{-1}_{3/2})$ taking into account both the particle–hole interaction and a different ΛN interaction. As shown in Fig. 23 [55], the splitting is not sensitive to the choice of the ΛN interaction, but is sensitive to the strength of the spin–orbit interaction. Therefore, we can safely conclude that the spin–orbit splitting of the p orbit is quite small, -0.8 MeV $\leq \delta \leq 0.2$ MeV. The present analysis agrees with the long-held belief that the *ls* splitting of a Λ hyperon is small. This conclusion is also consistent with recent γ-ray results [39,40], which will be discussed in detail in Section 5.7.

3.4. (π^+, K^+) reaction spectroscopy beyond the p-shell region

Hypernuclear spectra beyond the p-shell region have also been measured taking advantage of the good resolution and high detection efficiency of the SKS spectrometer. In

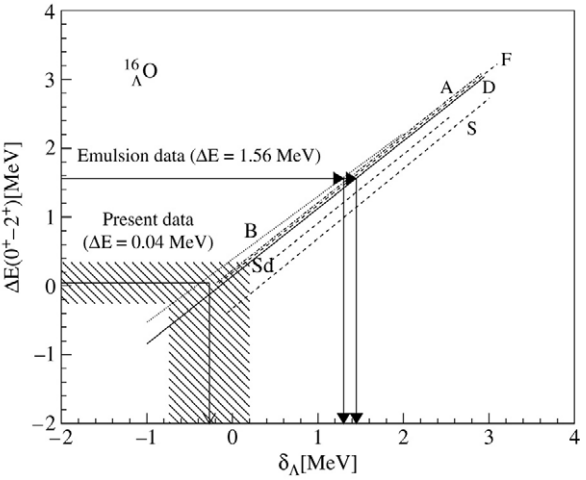

Fig. 23. The excitation energy difference between the 0^+_1 and 2^+_1 states of $^{16}_{\Lambda}$O as a function of $\delta_\Lambda \equiv \epsilon_\Lambda(1p^{-1}_{1/2}) - \epsilon_\Lambda(1p^{-1}_{3/2})$. The differences were calculated assuming the Jülich potentials A and B (denoted as A, B) and the Nijmegen potentials D, F and soft core (denoted here as D, F, S and S_d) [55].

Table 12
Excitation energies and relative hypernuclear yields of $^{28}_{\Lambda}$Si measured in the KEK E140a experiment [23]

Peaks	B_Λ or E_X (MeV)	FWHM (MeV)	Relative yield (arbitrary)
# 1	$B_\Lambda = 16.6 \pm 0.2$	2.2 (fixed)	0.09 ± 0.01
# 2	$E_X = 4.7 \pm 0.4$	4.4 ± 1.0	0.10 ± 0.04
# 3	$E_X = 9.6 \pm 0.2$	2.7 ± 0.3	0.27 ± 0.05
# 4	$E_X = 12.4 \pm 0.2$	1.4 ± 0.4	0.07 ± 0.04
# 5	$E_X = 17.7 \pm 0.8$	6.5 ± 1.1	0.51 ± 0.16

The errors quoted are statistical.

the E140a experiment, which was the first in the series of the SKS experiments, four targets beyond the p-shell region [$^{\text{natural}}$Si(2.37 g/cm^2), $^{89}_{39}Y_{50}$(3.13 g/cm^2), $^{139}_{57}La_{82}$(3.66 g/cm^2) and $^{208}_{82}Pb_{126}$(3.41 g/cm^2, 99% enriched)] were employed together with the light p-shell targets of ^{10}B and ^{12}C. The $^{89}_{39}Y_{50}$, $^{139}_{57}La_{82}$ and $^{208}_{82}Pb_{126}$ were chosen as targets since they have neutron closed shells of $\nu g_{9/2}$, $\nu h_{11/2}$ and $\nu i_{13/2}$ and, in addition, isotopically pure targets are available. It was expected that excitation energy spectra of $^{89}_{\Lambda}$Y, $^{139}_{\Lambda}$La and $^{208}_{\Lambda}$Pb reflecting the Λ major shell structure would be observed because of the simple configurations of the core neutron shells. The narrowness of the hypernuclear bound states, which was emphasized in Section 2, should make it possible to determine binding energies of a Λ hyperon orbiting with various angular momenta in a nuclear potential. More recently, intensive data taking for the ^{89}Y(2.22 g/cm^2) and ^{51}V(2.82 g/cm^2) targets was conducted with much higher statistics and better resolution at KEK E369 with SKS [25].

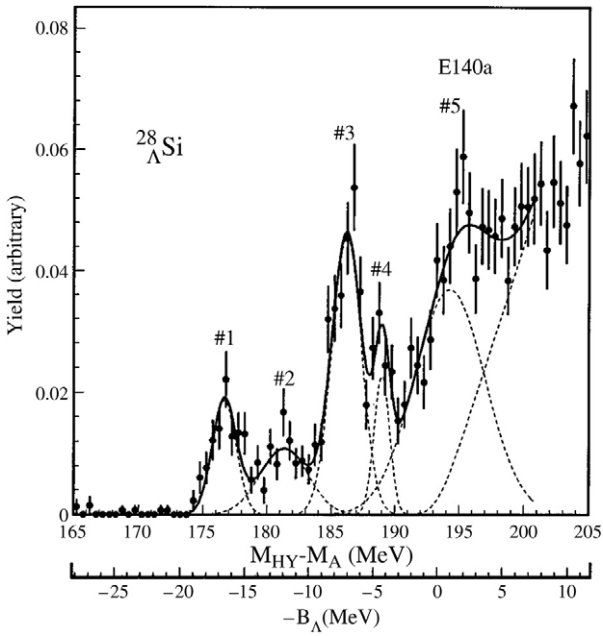

Fig. 24. Excitation spectrum of $^{28}_{\Lambda}$Si measured in E140a by the (π^+, K^+) reaction [23].

For these hypernuclear spectra, the energy resolutions were experimentally determined to be 2.2 MeV FWHM for $^{28}_{\Lambda}$Si, 1.65 MeV FWHM for $^{89}_{\Lambda}$Y, 1.95 MeV FWHM for $^{51}_{\Lambda}$V, 2.3 MeV FWHM for $^{139}_{\Lambda}$La and 2.2 MeV FWHM for $^{208}_{\Lambda}$Pb. These resolutions were assumed in the analysis of the spectra presented below.

3.4.1. $^{28}_{\Lambda}$Si

The $^{28}_{\Lambda}$Si spectrum measured with a natural silicon target (^{28}Si:92%) in E140a is shown in Fig. 24. Four peaks at around B_Λ= 17, 12, 8 and 5 MeV and a broad bump structure in the quasifree region were observed. The spectrum was fitted with five gaussians and a second-order polynomial. The gaussian width of the ground-state peak was set to the estimated energy resolution of 2.2 MeV, while the widths of the other peaks were allowed to vary in the fit. The strength at about B_Λ = 6–3 MeV (#4) was represented by a gaussian. The excitation energies and relative yields obtained from the fit are summarized in Table 12. As discussed in the BNL experiment [20], the three peaks at B_Λ = 17, 7 and −1 MeV (#1, #3 and #5) were interpreted as having the configurations of $[0d^{-1}_{5/2}, \Lambda s_{1/2}]$, $[0d^{-1}_{5/2}, \Lambda p_{1/2,3/2}]$ and $[0d^{-1}_{5/2}, \Lambda d_{3/2,5/2}]$, respectively.

A calculation with a "full" $[0d^{-1}_{5/2}, 1s^{-1}_{1/2}, 0d^{-1}_{3/2}]$ model space was recently carried out for $^{28}_{\Lambda}$Si [69]. The three major peaks observed experimentally are well accounted for by the calculation, but the strength of peak #2 is not well explained. Although strength was observed at the similar excitation energy in the BNL $^{28}_{\Lambda}$Si spectrum [20], the origin of the

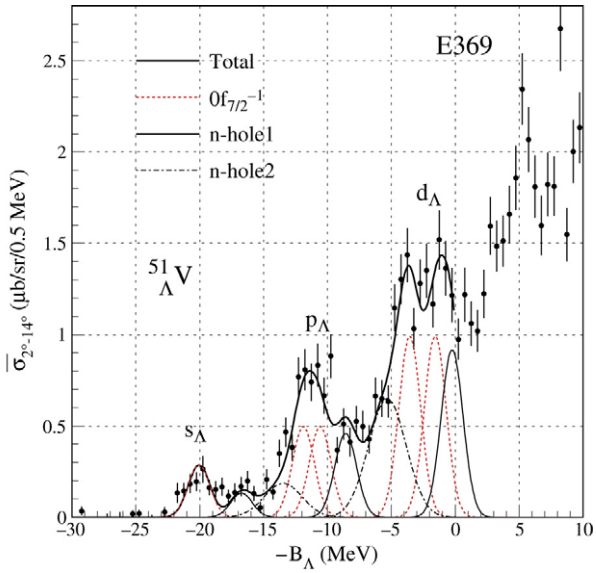

Fig. 25. Missing mass spectrum of ${}^{51}_{\Lambda}$V (KEK E369) [25].

strength at such a low excitation energy is not known. This situation should be clarified in a future high-precision spectroscopy measurement with a ^{28}Si enriched target.

3.4.2. ${}^{51}_{\Lambda}$V *and* ${}^{89}_{\Lambda}$Y

The first measurement of the ${}^{89}_{\Lambda}$Y hypernuclear spectrum by the (π^+, K^+) reaction was carried out at the BNL AGS and the major shell structure of a Λ hyperon was clearly observed [20]. Higher-quality spectra of heavy hypernuclei up to ${}^{208}_{\Lambda}$Pb were subsequently measured in the KEK E140a experiment with the SKS spectrometer [23]. High-statistics good-resolution spectra have also been obtained for ${}^{89}_{\Lambda}$Y and ${}^{51}_{\Lambda}$V in KEK E369 [25], which aimed to resolve the detailed structure of the major shell peaks. The measured spectra of ${}^{51}_{\Lambda}$V and ${}^{89}_{\Lambda}$Y are shown in Figs. 25 and 26.

For ${}^{89}_{\Lambda}$Y, the series of bumps observed in the spectrum reflects the coupling of a Λ hyperon in the major orbits to the $0g_{9/2}^{-1}$ neutron hole state of the ^{88}Y core. As noted above, the widths of the states corresponding to the p, d, and f orbits were significantly broader than the experimental resolution of the ${}^{89}_{\Lambda}$Y spectrum as estimated from the resolution of the ${}^{12}_{\Lambda}$C spectrum and energy loss straggling of pions and kaons in the target. Assuming that each bump corresponding to a major shell is actually composed of two peaks, the spectra were fitted with the fixed width determined from the ground-state peak. Excitation of the f hole states was taken into account in addition to excitation of the g neutron hole states. This described the intensity in the valley regions between the major bump structures. Assuming the experimental resolution of 1.65 MeV FWHM for all peaks, the energy difference between the two peaks in the broad bumps was found to be 1.37, 1.63 and 1.70 MeV for the p, d, f orbits, respectively, and the intensity ratios were determined as

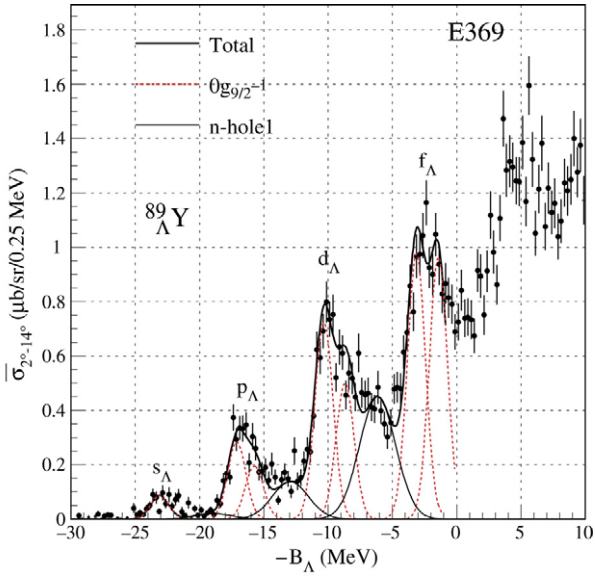

Fig. 26. Missing mass spectrum of $^{89}_{\Lambda}$Y (KEK E369) [25].

1.37, 1.63 and 1.70 for $l = 1, 2$ and 3, respectively. There are two possible explanations for the apparent splitting of the major shell bumps. One is the interplay of core excited states due to different holes for the neutron orbits, and the second is ls splitting of the high-l Λ orbits [25]. If the observed splitting is attributed solely to the ls splitting, the ls interaction in $^{89}_{\Lambda}$Y is much larger than that observed in light Λ hypernuclear data, particularly the recent γ-ray measurements [39,40]. Motoba pointed out the intensity ratios between the two split peaks should be 0.69, 0.69 and 0.98, if the two peaks are ls partners; these ratios are simply determined by kinematical considerations. However, the experimental ratios are greater than unity in contrast to the theoretical expectation. An intensive calculation taking into account the configurations of $0g_{9/2}$, $2p_{1/2}$, $2p_{3/2}$, $0f_{5/2}$, $0f_{7/2}$ and sd neutron hole states was recently carried out. It was reported that the calculated spectrum accounted for the experimental spectrum without assuming large ls splitting [70]. This result implies that the explanation of spectral shapes for the heavy Λ hypernuclei requires proper consideration of core excitation and mixing of different parity states, since it becomes easier to excite the various states of the core nucleus in heavy hypernuclei.

3.4.3. $^{139}_{\Lambda}$La *and* $^{208}_{\Lambda}$Pb

The (π^+, K^+) reaction spectroscopy of $^{139}_{\Lambda}$La and $^{208}_{\Lambda}$Pb was carried out in E140a. The hypernuclear spectra obtained are shown in Fig. 27. They both show characteristic bump structures starting from the binding energies B_Λ around 25 MeV that can be explained as due to a Λ hyperon in the major shells. The (π^+, K^+) reaction spectra for $^{139}_{\Lambda}$La and $^{208}_{\Lambda}$Pb were calculated using the DWIA [3] and the one for $^{208}_{\Lambda}$Pb is shown in Fig. 28. As can be seen from the figure, not only are the hole states of the outermost neutron excited, but a series of sub-major hole states are excited as well. For $^{139}_{\Lambda}$La, the three

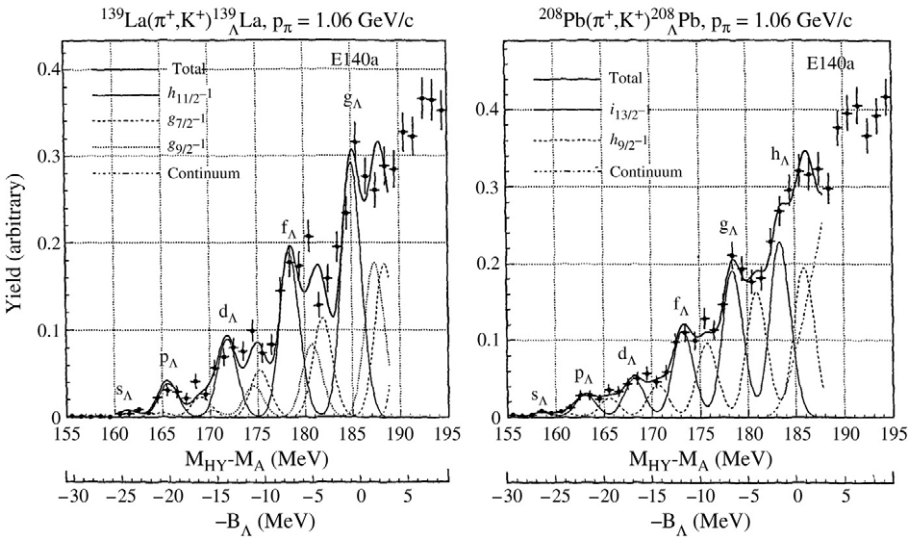

Fig. 27. Missing mass spectrum of $^{139}_{\Lambda}$La and $^{208}_{\Lambda}$Pb measured in E140a [23].

neutron hole configurations, $h_{11/2}^{-1}$, $g_{7/2}^{-1}$, $g_{5/2}^{-1}$, are expected to contribute to the excitation spectrum with considerable strength and for $^{208}_{\Lambda}$Pb, two configurations, $i_{13/2}^{-1}$ and $g_{9/2}^{-1}$, are important. The spectra were fitted taking into account these neutron hole excitations as labeled in Fig. 27. For simplicity of analysis, the spectral shapes for each series of neutron hole excitations were fixed but the relative strengths were allowed to vary. The energy difference between the major and sub-major hole series were also fixed to averaged experimental values. $E_{g_{9/2^-}} - E_{h_{11/2^-}} = 3.44$ MeV and $E_{g_{7/2^-}} - E_{h_{11/2^-}} = 8.92$ MeV for $^{139}_{\Lambda}$La and $E_{h_{9/2^-}} - E_{i_{13/2^-}} = 2.48$ MeV for $^{208}_{\Lambda}$Pb. The fits to the spectra based on these assumptions are presented in Fig. 27. The binding energies of a Λ hyperon in $^{139}_{\Lambda}$La and $^{208}_{\Lambda}$Pb were then inferred assuming they correspond to the peak centroids of the bumps. Although the binding energies may depend on details of the bump structures that are not known experimentally and theoretically, the centroid values can be reasonably well deduced from the fitting. The results are listed in Table 13. Values of binding energies for $^{28}_{\Lambda}$Si and $^{89}_{\Lambda}$Y are also given in the table, assuming the weighted center of the doublets seen for each l represents the Λ orbits.

The observed spectra are significantly smoother than those expected from the DWIA calculation and the experimental energy resolution. Possible sources of this smoothness are: (1) larger spreading widths of high-l neutron hole states of the core nucleus, (2) greater contributions from various deeper neutron hole states and core excited states, and (3) other reaction mechanisms not taken into account in the shell model + DWIA calculation.

Therefore, it is of vital importance to perform precision spectroscopy of medium-heavy Λ hypernuclei with mass resolution comparable to or better than the energy differences of core excited states, in order to further investigate the structure of the Λ hyperon deeply

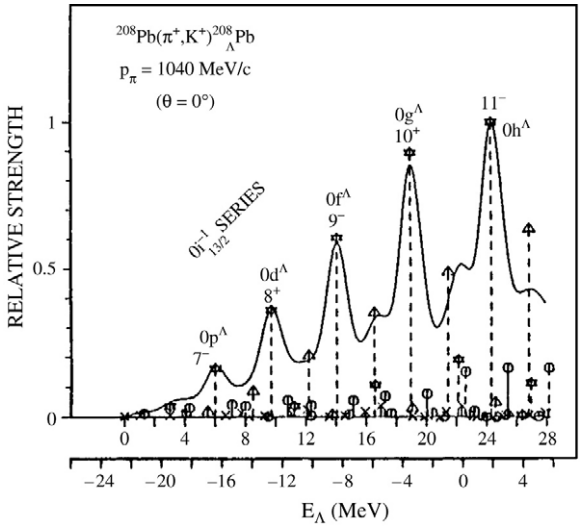

Fig. 28. The theoretical ^{208}Pb(π^+, K^+)$^{208}_{\Lambda}$Pb spectrum based on a DWIA calculation. Both the $i_{13/2}$ neutron hole series and the $h_{9/2}$ neutron hole series have strength [3].

Table 13
Binding energies of a Λ hyperon in heavy Λ hypernuclei derived by fitting $^{139}_{\Lambda}$La and $^{208}_{\Lambda}$Pb spectra (in MeV)

Hypernucleus	*s* orbit	*p* orbit	*d* orbit	*f* orbit	*g* orbit
$^{28}_{\Lambda}$Si	16.6 ± 0.2	7.0 ± 0.2			
$^{89}_{\Lambda}$Y	23.1 ± 0.5	16.5 ± 4.1	9.1 ± 1.3	2.3 ± 1.2	
$^{139}_{\Lambda}$La	24.5 ± 1.2	20.4 ± 0.6	14.3 ± 0.6	8.0 ± 0.6	1.5 ± 0.6
$^{208}_{\Lambda}$Pb	26.3 ± 0.8	21.9 ± 0.6	16.8 ± 0.7	11.7 ± 0.6	6.6 ± 0.6

The quoted errors for $^{139}_{\Lambda}$La and $^{208}_{\Lambda}$Pb are quadratic sums of the statistical error and the systematic error (assumed to be 0.5 MeV).

bound states in heavier nuclei. $(e, e'K^+)$ spectroscopy, which is the subject of the next section, is a promising approach to this problem.

3.5. Mass dependence of hypernuclear binding energies

Binding energies of light Λ hypernuclei in the *p*-shell region were well determined by early emulsion experiments [51] and the hypernuclear potential depth was determined as about 2/3 the depth of the nuclear potential for a nucleon by extrapolating the binding energies to nuclear matter. In the present series of spectroscopy experiments that include heavier hypernuclei up to $^{208}_{\Lambda}$Pb, binding energies of a Λ single-particle orbit for a given *l* were derived experimentally as a function of hypernuclear mass number for the wide mass range as described in the previous sections. These experimental data are summarized in Table 13 and the hypernuclear mass dependences are shown in Fig. 29.

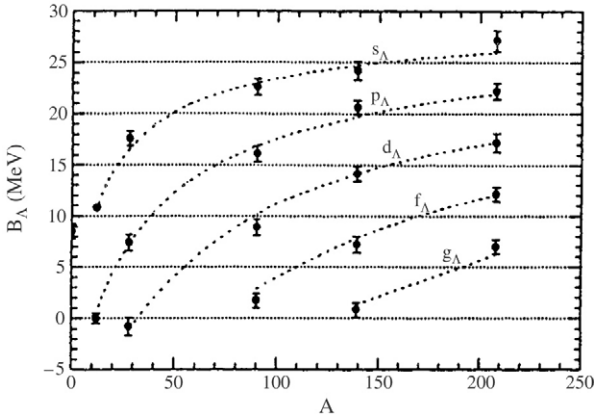

Fig. 29. Hypernuclear mass dependence of a Λ hyperon binding energy in various orbits.

In general, a Λ hypernuclear potential can be expressed using the Woods–Saxon form as

$$U_\Lambda = V_0^\Lambda f(r) + V_{LS}^\Lambda \left(\frac{\hbar}{m_\pi c}\right)^2 \frac{1}{r}\frac{\mathrm{d}f(r)}{\mathrm{d}r}\boldsymbol{ls} \tag{8}$$

$$f(r) = [1 + \exp((r - R)/a)]^{-1}. \tag{9}$$

Assuming the Woods–Saxon functional form of the Λ hypernuclear potential, the depth and diffuseness were obtained by fitting the binding energy data for ${}^{12}_{\Lambda}\mathrm{C}$, ${}^{89}_{\Lambda}\mathrm{Y}$, ${}^{139}_{\Lambda}\mathrm{La}$ and ${}^{208}_{\Lambda}\mathrm{Pb}$ with no spin–orbit splitting. The fitted values for this particular data set are $V_0^\Lambda = -31$ MeV and $a_\Lambda = 0.84$ fm, with the radius of the potential $R = R_0(A-1)^{1/3}$ ($R_0 = 1.1$ fm). If we take standard parameters for the Woods–Saxon potential as $V_0^\Lambda = -30$ MeV, $a_\Lambda = 0.6$ fm and $V_{LS}^\Lambda = 2$ MeV [47], the result also explains the A dependence satisfactorily. Since a single potential with the above mass dependence describes the binding energies consistently in the wide mass region, it can be said that the single-particle nature of a Λ hyperon persists to first order even for deeply bound orbits of Λ hypernuclei as heavy as $A = 208$ [23].

There have been a number of theoretical discussions on the Λ single-particle potentials. Millener et al. discussed the density dependence and non-locality of the potential [71] and Yamamoto et al. studied three-body ΛNN forces and Λ effective mass in the Skyrme Hartree–Fock approach [72] using the data up to ${}^{89}_{\Lambda}\mathrm{Y}$. Later, the Skyrme–Hartree–Fock treatment was extended taking into account both the published and unpublished data up to ${}^{208}_{\Lambda}\mathrm{Pb}$ presented here [73].

An interesting question was raised by Dover about the distinguishability of a Λ hyperon as a hyperon in a nucleus [74]. It was suggested that the mass number dependence of the binding energies could differ depending on whether a hyperon keeps its identity as a baryon in a nucleus or not. In other words, the quark picture and the baryon picture of Λ hypernuclear states would yield different hypernuclear mass dependences of the Λ binding energies. Although it may be claimed that the argument is too simplified, precision

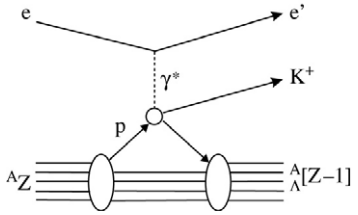

Fig. 30. Schematic diagram of the $(e, e'K^+)$ reaction.

measurements of binding energies in heavy Λ hypernuclei may provide clues for further discussion about the nature of a baryon in a nucleus. In this regard, the high-quality spectroscopic investigation of heavy Λ hypernuclei has unique importance.

Through the series of SKS experiments, (π^+, K^+) reaction spectroscopy has been established as a powerful tool for the investigation of Λ hypernuclei in a broad mass range and for wide excitation energies including deeply bound hypernuclear states of heavy systems. However, it is also clear that the resolution of these spectra is not sufficient to resolve important details connected with the nuclear structure and/or ΛN interaction. It is certainly essential to further explore high-quality hypernuclear spectroscopy further to address these issues properly.

4. $(e, e'K^+)$ hypernuclear spectroscopy

4.1. Principles of $(e, e'K^+)$ hypernuclear spectroscopy

The $(e, e'K^+)$ reaction provides unique opportunities for strangeness nuclear physics, particularly for $S = -1$ hypernuclear spectroscopy. This is true despite the fact that $(e, e'K^+)$ hypernuclear cross sections are small compared to those of hadron induced reactions. The reaction is depicted schematically in Fig. 30. It has characteristics complementary to those of hadronic reactions and is indispensable for hypernuclear spectroscopy as described in Section 2.

Although the elementary processes of strangeness production by photon and electron beams have been studied for a wide variety of reaction channels, there have been only a few experimental investigations with nuclear targets. One example is the investigation of quasifree Λ production on ^{12}C by the tagged photon beam at INS-ES [75]. The data suggested formation of hypernuclear states, in addition to the quasifree Λ production processes. Another is a JLab experiment on ^{3}He and ^{4}He which observed Λ bound-state peaks [32]. However, there were no experiments that clearly observed hypernuclear states in heavier systems via the $(e, e'K^+)$ reactions until recently. Hypernuclei and their characteristic states accessible by spectroscopic studies will be greatly expanded through the use of this reaction. Experimentally, as emphasized in Sections 1 and 2, it is important that $(e, e'K^+)$ reaction spectroscopy be carried out with the highest possible resolution for the hypernuclear excitation energy spectra. In this section, the basic features of hypernuclear spectroscopy using the $(e, e'K^+)$ reaction are explained, recent experimental data are presented, and the short-term prospects for $(e, e'K^+)$ spectroscopy are described.

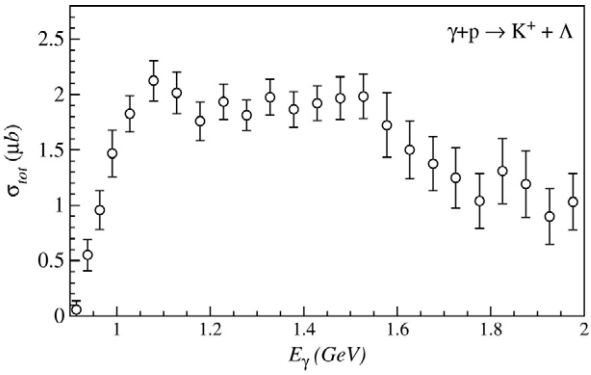

Fig. 31. Energy dependence of total cross section for the $\gamma + p \to \Lambda + K^+$ reaction [82].

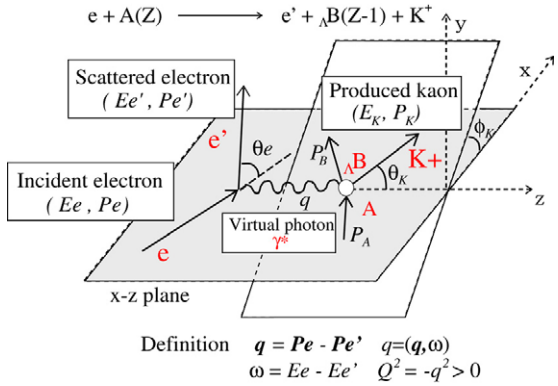

Fig. 32. Kinematics of the $(e, e' K^+)$ reaction and definition of the kinematical variables.

4.1.1. Elementary electro-photo-strangeness production

Experimental investigations of strangeness photo-production have been carried out recently at ELSA SAPHIR, INS-ES, JLab Hall B, SPring-8 and GRAAL. In most of these experiments positive kaons and/or recoil hyperons were detected (see for example Ref. [76]). On the basis of these data, a number of phenomenological models have been constructed for the elementary amplitudes of strangeness production. Coupling constants were adjusted, and the production form factors and number of various resonance states to be included were studied [77,78]. In particular, high-quality data on photo-production of kaons at SAPHIR and more recently at JLab and SPring-8 provide the basis for the phenomenological models. There has also been an effort to investigate photo-production of neutral kaons on the neutron, which is unique in the sense that no charge is involved in this reaction. Comparison of the process with those of positive kaons is expected to provide valuable information on photo-strangeness production [79]. Electro-production of strangeness has also been studied intensively at JLab, where experiments even untangled the longitudinal and transverse amplitudes for kaon production [80].

The elementary amplitudes for the real photon reaction, $\gamma p \to \Lambda K^+$ in $E_\gamma = 1$–2 GeV, are most relevant to the $(e, e'K^+)$ reaction. This is because scattered electrons are detected at very forward angles (in order to have larger hypernuclear yield rates) and so the virtual photons associated with the hypernuclear production reaction can be regarded as almost real. The transition matrix of the elementary photo-strangeness production can be expressed using the four amplitudes, the spin-independent (f_0) and spin-dependent, spin-flip and non-spin-flip (g_0, g_1 and g_{-1}) terms [81] as

$$\begin{aligned} T_{if}^{lab} &= |\langle k - p, p \mid t \mid k, 0\rangle_L|^2 \\ &= \varepsilon_0(f_0 + g_0\sigma_0) + \varepsilon_x(g_1\sigma_1 + g_{-1}\sigma_{-1}). \end{aligned} \tag{10}$$

where the kinematical variables are defined in Fig. 32. The differential cross section for the elementary process is given in terms of these amplitudes as

$$\left.\frac{\mathrm{d}\sigma}{\mathrm{d}\Omega}\right|_{lab} = \frac{(2\pi)^4 p^2 E_K E_\gamma E_\Lambda}{k(p(E_\Lambda + E_K) - kE_K\cos\theta_L)}(|f_0|^2 + |g_0|^2 + |g_1|^2 + |g_{-1}|^2). \tag{11}$$

The $|f_0|^2$ term is quite small but $|g_{0,1,-1}|^2$ is comparable in ordinary kinematical conditions.

The photon energy dependence of the elementary cross section is shown in Fig. 31. The cross section rises sharply at the threshold energy of $E_\gamma = 0.911$ GeV and stays almost constant from 1.1 to 1.6 GeV [82]. The total cross section for K^+ production in the energy range from threshold to 2 GeV is reasonably well explained by phenomenological models that are the basis for further theoretical calculations of hypernuclear production processes.

4.1.2. Hypernuclear production by the $(e, e'K^+)$ reaction

Spectroscopy using electromagnetic probes is practical only by using the $(e, e'K^+)$ reaction since the yield rates and mass resolution necessary for spectroscopy cannot be achieved with real photon beams. Hypernuclear production using the $(e, e'K^+)$ reaction is diagrammatically depicted in Fig. 30. An electron interacts with a target nucleus, emitting a virtual photon that hits a proton in the target and a hyperon and a kaon are associatively produced. A Λ hypernucleus is formed when the Λ hyperon is bound to the residual nuclear core with charge $(Z - 1)$. In order to determine the hypernuclear mass experimentally, it is necessary to know the incident beam energy and to measure momenta of both the scattered electron and the kaon in coincidence.

The hypernuclear production cross section for the $(e, e'K^+)$ reaction can be expressed in terms of the elementary photo production process and the virtual photon flux. The triple differential cross section in the laboratory system is given by

$$\frac{\mathrm{d}^3\sigma}{\mathrm{d}\omega\mathrm{d}\Omega'_e\mathrm{d}\Omega_K} = \Gamma\frac{\mathrm{d}\sigma^*_\gamma}{\mathrm{d}\Omega_K}, \tag{12}$$

where Γ is the virtual photon flux defined for the reaction of interest in the laboratory frame and ε is the virtual photon polarization. These quantities are given by

$$\Gamma = \frac{\alpha}{2\pi^2 Q^2}\frac{E_\gamma}{1-\varepsilon}\frac{E'_e}{E_e}, \qquad E_\gamma = \omega + \frac{q^2}{2m_p}, \tag{13}$$

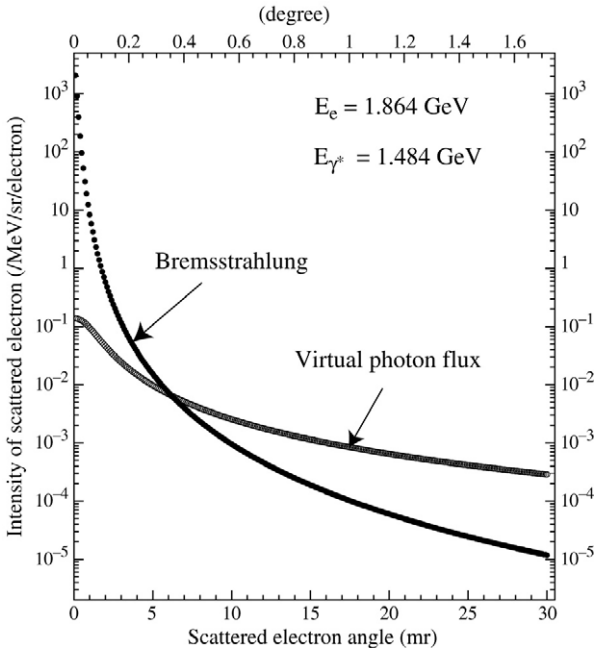

Fig. 33. Angular distributions of electrons associated with the bremsstrahlung process and virtual photons of hypernuclear production.

and

$$\varepsilon = 1 \Big/ \left(1 + \frac{2|q|^2}{Q^2} \tan^2\left(\frac{\theta_e}{2}\right)\right). \tag{14}$$

The angular distributions of virtual photons and their associated electrons are very forward peaked, and the angular distribution of bremsstrahlung electrons is even more peaked at zero degrees; the two are compared in Fig. 33. Keeping this angular distribution in mind, it is clear that the scattered electrons should be measured at very forward angles to make the hypernuclear yield as large as possible. Under this condition, the virtual photons can be regarded as almost real.

Hypernuclear cross sections to given states by the $(e, e'K^+)$ reaction are calculated using DWIA [83,84] in a manner similar to calculations of the (π^+, K^+) reaction. A typical angular distribution of K^+ for the $\gamma + {}^{12}\mathrm{C} \to {}^{12}_{\Lambda}\mathrm{B} + K^+$ reaction at $E_\gamma = 1.4$ GeV is shown in Fig. 34. It peaks at zero degrees, and the cross section drops to half its zero-degree value at ten degrees in this particular kinematical condition. It is evident from Fig. 34 that kaons should be also detected at angles as forward as possible to maximize the hypernuclear yield rates.

The characteristics of the $(e, e'K^+)$ reaction for Λ hypernuclear spectroscopy can be summarized in the following three points:

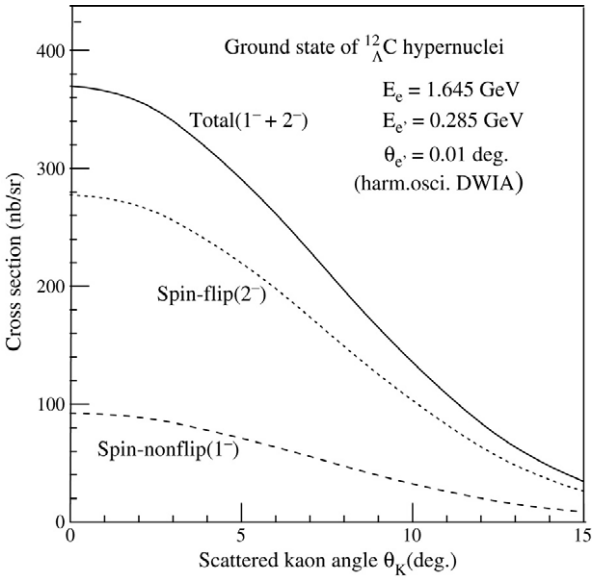

Fig. 34. Kaon angular distribution for the $^{12}\mathrm{C}(e, e'K^+)^{12}_{\Lambda}\mathrm{B}$ reaction populating the ground-state doublet calculated using the DWIA code of Sotona [85].

- A large momentum (∼320 MeV/c at zero degrees) is transferred to a recoil hypernucleus because the reaction is endothermic, which is similar to the case of the (π^+, K^+) reaction. It thus populates high-spin states and is suitable for investigating deeply bound states of a Λ hyperon.
- Sizable spin-flip amplitudes are present even at zero degrees as described for the elementary processes because the photon has spin 1. This feature persists in hypernuclear production and thus both spin-flip and non-spin-flip hypernuclear states are excited with significant cross sections. This is in contrast to the case for (π^+, K^+) and (K^-, π^-) reactions.
- A proton in the target nucleus is converted to a Λ hyperon. Therefore, Λ hypernuclei that are not accessible by reactions such as the (π^+, K^+) and (K^-, π^-) are populated. Neutron-rich Λ hypernuclei are produced, particularly in the light mass region. For example, $^{7}_{\Lambda}$He from the ^{7}Li target, which is predicted to be a neutron halo Λ hypernucleus, can be investigated. In addition, a comparison of the spectra obtained using the $(e, e'K^+)$ reaction with those from the (K^-, π^-) and (π^+, K^+) reaction allows us to study charge symmetry in Λ hypernuclei.

From the experimental point of view, an important advantage of the $(e, e'K^+)$ reaction is that it has the potential to carry out hypernuclear reaction spectroscopy with sub-MeV mass resolution. A resolution of a few 100 keV can be achieved and will have great impact on hypernuclear reaction spectroscopy. The expected 3–400 keV resolution is comparable to spreading widths of hypernuclear states excited above the nucleon emission thresholds and to the excitation energies of many core excited states. Therefore, it becomes possible to identify a hyperon single-particle orbit more clearly, untangling core excited states

even in heavier Λ hypernuclei. Through the mass dependence of Λ binding energies, for example, characteristics of a Λ hyperon in a nucleus can be investigated based on more reliable precision data. Studies of hypernuclear structure and ΛN interaction can also be further deepened, since somewhat ambiguous interpretation of the excitation spectra due to unresolved peaks can be greatly improved.

Spectroscopy with this high resolution becomes possible because primary electron beams are now available with excellent beam emittance of a few nm rad and with energy resolution better than 10^{-4}. For example, the intensity of the electron beams at JLab can be as high as 100 μA and the beam spot size at the target is as small as 0.1 mmϕ. With such beams, small and thin targets can be used and even experiments using enriched isotope targets, which open new possibilities for hypernuclear investigations, are feasible.

4.2. $(e, e'K^+)$ hypernuclear reaction spectroscopy

It has been known for some time that the $(e, e'K^+)$ reaction would be invaluable for the study of Λ hypernuclei. However, it has been impractical to perform hypernuclear spectroscopy experiments with electron beams because of experimental difficulties until recently. Hypernuclear spectroscopy requires a high-quality GeV electron beam with a 100% duty factor. It also requires high-resolution spectrometers that can measure scattered electrons and kaons in a high-background environment.

The conditions required to the electron beams can be summarized as:

1. Beam energy above 1.6 GeV in order to get virtual photons above the kaon production threshold.
2. High duty factor for coincidence measurements of an electron and a K^+.
3. Low beam emittance with a beam spot size as small as a few 100 μm at the target, and beam energy spread better than $\Delta E/E \leq 10^{-4}$.

At present, electron beams that satisfy these conditions are available only at the CEBAF accelerator(Continuous Electron Beam Accelerator Facility) of the Thomas Jefferson National Accelerator Facility (JLab), Virginia, USA, though MAMI-C at Mintz will accelerate such a high-quality electron beam soon.

At JLab, there have been two parallel experimental efforts for hypernuclear spectroscopy, one in Hall A and the other in Hall C. This article describes the first successful JLab hypernuclear experiment which was carried out using the HyperNuclear Spectrometer System (HNSS) in Hall C as JLab E89-009. Sub-MeV resolution, the best resolution achieved in hypernuclear reaction spectroscopy as of spring of 2004, was demonstrated in the experiment by the $^{12}\mathrm{C}(e, e'K^+)\,^{12}_{\Lambda}\mathrm{B}$ reaction [27].

The experimental set-up of E89-009 is shown schematically in Fig. 35. It was designed to use the "zero-degree tagging" configuration, in which the zero-degree electrons associated with the most intense portion of the virtual photon fluxes were detected. Thus a large fraction of virtual photon flux was captured in this configuration.

Electron beams of 1.7 and 1.8 GeV bombarded the target in the E89-009 experiment. The beam specification relevant to the $(e, e'K^+)$ reaction is listed in Table 14.

In order to measure electrons and kaons at very forward angles, a splitter magnet was installed immediately downstream of the target. Scattered electrons and positive kaons

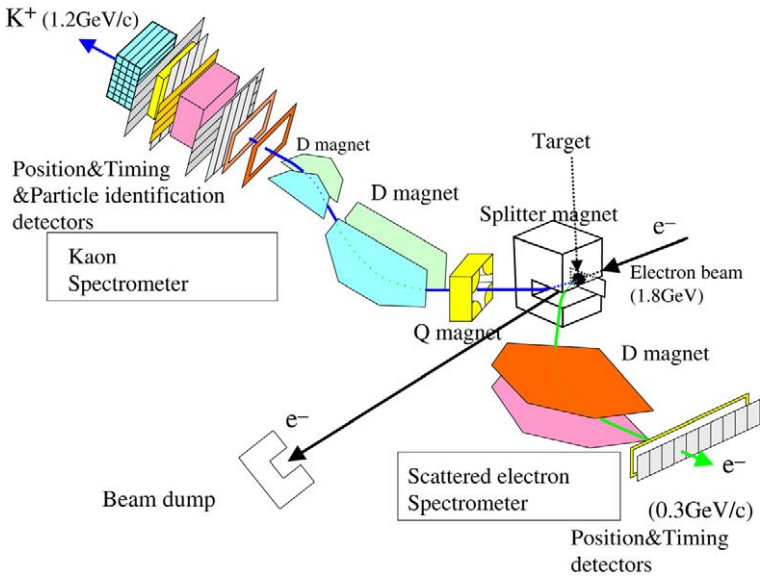

Fig. 35. Hypernuclear Spectrometer system in JLab Hall C for E89-009.

Table 14
Basic parameters of CEBAF electron beams

Beam energy	Up to 6 GeV
Beam intensity	Up to 200 μA in each Hall (A, B, C)
Typical beam emittance	2×10^{-9} m rad
Typical energy spread	$<1 \times 10^{-4}$
Beam microstructure in the Hall	Every 2 ns (499 MHz)

emerging from the target at zero degrees were bent in opposite direction by this magnet. The emerging particles were momentum analyzed by a pair of spectrometers, one for electrons and the other for kaons.

The electron momentum was measured using an Enge split-pole-type spectrometer that had a large momentum acceptance from 200 to 400 MeV. It has a long focal plane (about 70 cm) and maintains superb optical characteristics of the original ENGE spectrometer despite some slight deterioration due to the splitter magnet. Momentum analysis of the electron was carried out by simply measuring the horizontal position of the electron at the position of the focal plane. This position information was obtained using 10 silicon strip detectors (SSD), each of which covered 7 cm with 144 channels of 0.5 mm strips. In order to cope with high count rates, only digital information was recorded using TEKZ preamplifier/discriminator chips [86]. A hodoscope consisting of 25 scintillators backed up the SSD's and served as timing counters as well. With the current set-up of the electron spectrometer, 30% of the virtual photon flux was detected.

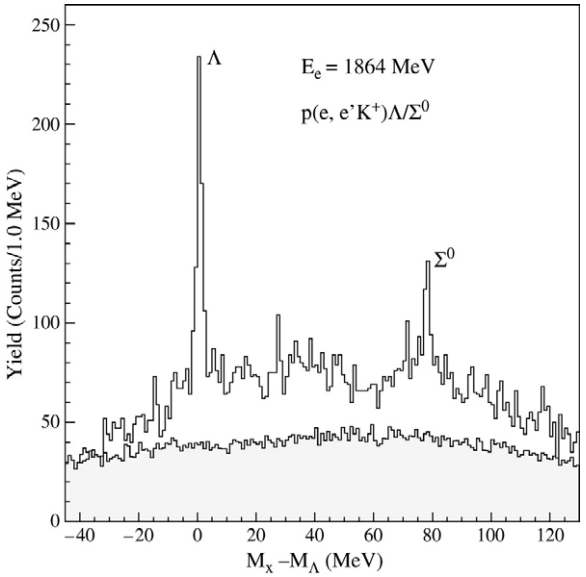

Fig. 36. Missing mass spectrum of the $(e, e'K^+)$ reaction on a CH_x target. The two peaks correspond to production of Λ and Σ hyperons. The shaded area represents the background which comes from quasifree hyperon production reactions on carbons. Note that the resolution is dominated by the kinematical broadening due to experimental angular resolution but not by the spectrometer resolution [27].

The kaon momentum is measured using the Short Orbit Spectrometer (SOS), a standard part of the equipment in Hall C. This spectrometer has a wide momentum acceptance ($\pm 12.5\%$) in the 1 GeV/c region, and has reasonably good momentum resolution (5×10^{-4}). The kaon spectrometer covered a solid angle of 6 msr and scattering angles from zero to six degrees. The spectrometer optics was calibrated initially using data obtained with a sieve slit installed between the splitter and the first quadrupole magnet of the SOS spectrometer and then by using the missing mass spectra iteratively.

The experiment was carried out using three targets, CH_x, ^{12}C and ^{7}Li. The CH_x target was employed for calibration of the hypernuclear mass scale using the peak positions of the Λ and Σ hyperons in the missing mass spectrum (see Fig. 36).

The experimental parameters are summarized in Table 15 together with those of the E01-011 experiment, which is under preparation as the second-generation $(e, e'K^+)$ spectroscopy experiment, and is described in the following subsection.

The first Λ hypernuclear spectroscopy experiment using the $^{12}C(e, e'K^+)\,^{12}_{\Lambda}B$ reaction was carried out with a relatively low beam current of 0.66 μA and a target thickness of 20 mg/cm^2. The luminosity was limited by the singles rate of the electron arm, which amounted to a few $\times 10^8$ Hz.

Fig. 37 shows a missing mass spectrum for the $^{12}C(e, e'K^+)\,^{12}_{\Lambda}B$ reaction. The horizontal axis is given in units of both excitation energy and Λ binding energy, B_Λ, assuming the ^{11}B core nucleus is in its ground state. Two prominent peaks are visible in the spectrum, similar to the case of the (π^+, K^+) reaction on the ^{12}C target. These peaks are

Table 15
Experimental conditions and specifications of the previous and proposed hypernuclear spectrometer systems

	E89-009	**E01-011**
Beam condition		
Beam energy	1.8 GeV	Same
Beam momentum stability	1×10^{-4}	Same
General configuration	Splitter + Kaon spectrometer + Electron spectrometer	Same
Kaon spectrometer		
Spectrometer	SOS spectrometer	HKS spectrometer
Configuration	QDD (vertical bend)	QQD (horizontal bend)
Central momentum	1.2 GeV/c	1.2 GeV/c
Momentum acceptance	±10%	12.5%
Resolution ($\Delta p/p$)	5×10^{-4} (beam spot size 0.1 mm assumed)	2×10^{-4}
Solid angle (with splitter)	5 msr	20 msr
Solid angle (without splitter)	9 msr	30 msr
Kaon detection angle	0–7 degrees	1–14 degrees
Flight length	8 m	10 m
Scattered electron spectrometer		
Enge split-pole spectrometer		
Central momentum	0.3 GeV/c	
Momentum acceptance	±20%	
Momentum resolution ($\delta p/p$)	2×10^{-4}	Same
Tilt angle	0 degrees	4.5 degrees
Electron detection angle		
Horizontal	0 degrees	Same
Vertical	2.25 degrees	3.7–5.7 degrees

interpreted as having the configurations with the outermost proton–hole in the p orbit and a Λ hyperon in the s_Λ orbit coupled as $[(p_{3/2})_p^{-1} \otimes (s_{1/2})_\Lambda]$ and $[(p_{3/2})_p^{-1} \otimes (p_{1/2}, p_{3/2})_\Lambda]$.

The energy resolution was determined from the width of the ground-state peak to be 0.9 MeV FWHM, which is considerably better than the best one (1.45 MeV) obtained in the SKS hypernuclear experiments. Both of the s_Λ and p_Λ doublets, $(1^-, 2^-)$ and $(2^+, 3^+)$, are not resolved. It is believed that the splittings are smaller than tens of keV.

The Λ binding energy of the ${}^{12}_{\Lambda}$B ground state was determined as 11.4 ± 0.5 MeV by fitting the spectrum. This value is consistent with that determined from an emulsion experiment, 11.37 MeV [63].

The curve in Fig. 37 is not the one originally fit to the data but the one calculated assuming 0.9 MeV FWHM resolution, in which the cross sections for the hypernuclear states were taken from the DWIA calculation of Motoba at an angle of 3° and a photon energy of 1.3 GeV [84,87]. The excitation function used was the one calculated by Millener based on effective p-shell ΛN interactions adjusted to the spectroscopic data of the (π^+, K^+) excitation spectra and γ-ray spectra [88]. The agreement for the two prominent peaks is remarkably good.

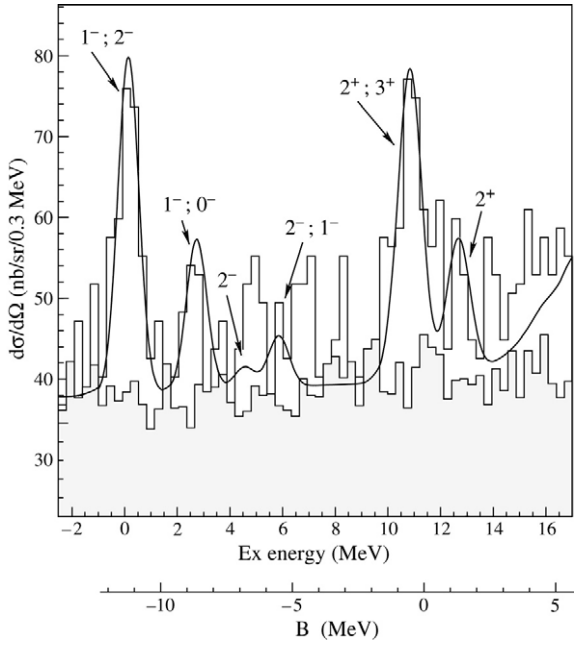

Fig. 37. Missing mass spectrum for the $^{12}\mathrm{C}/\mathrm{CH}_X(e, e'K^+)$ reaction. The shaded histogram is the accidental background, which was determined experimentally [27].

The cross section was derived from the experimental yields, the geometrical and momentum acceptances of both spectrometers, the detector efficiencies and the number of virtual photons which was obtained by integrating over the momentum acceptance of the electron spectrometer. The cross section of the $^{12}_{\Lambda}\mathrm{B}$ ground state was determined as $147 \pm 17(\mathrm{stat}) \pm 18(\mathrm{syst})$ nb/sr. The theoretical prediction by Motoba of 152 nb/sr for this cross section agrees well with this result [89]. As can be seen from Fig. 37, the DWIA calculation using a phenomenological potential for the ΛN interaction describes both the hypernuclear spectrum and the absolute cross sections for the $(e, e'K^+)$ reaction reasonably well, as was the case for the (π^+, K^+) reaction. The effective proton number, which is the ratio of the quasifree cross section to the elementary one, was determined from this spectrum to be 4.2, a value consistent with that obtained from previous $^{12}\mathrm{C}(\gamma, K^+)^{12}_{\Lambda}\mathrm{C}$ quasifree data [75].

4.3. *Upgrading* $(e, e'K^+)$ *spectroscopy*

Although the first $(e, e'K^+)$ experiment, E89-009, was successful, there were two major obstacles that had to be overcome before Λ hypernuclear spectroscopy using high-intensity electron beams could reach its full potential: the hypernuclear yield rates were too low and the resolution, although much better than that obtained by previous techniques, had to be further improved to address many issues of interest. It took a full month to obtain the $^{12}_{\Lambda}\mathrm{B}$ spectrum shown in Fig. 37. The "zero-degree tagging method" adopted in the E89-009 experiment has an advantage that allows one to run using a low-intensity electron beam and

a thin target. However, in this method, the electron beam intensity must be kept quite low in order to suppress the singles rate of scattered electrons and the accidental background. The main source of the background is mainly the electrons that produced bremsstrahlung in the target. With the beam intensity of 0.6 μA, the yield rate for the ${}^{12}_{\Lambda}\mathrm{B}$ ground state was as low as 0.9 event/h with the E89-009 experimental configuration. The signal-to-accidental ratio was small for the experimental conditions listed in Table 15. The background from bremsstrahlung processes will become even more serious when heavier targets are used, since it is expected to be proportional to Z^2. It was concluded that it would be difficult to investigate medium-heavy to heavy hypernuclei using electron beams if the "zero-degree tagging method" was used.

Electrons incident on the focal plane of the electron spectrometer are associated with: (1) the bremsstrahlung process, (2) Møller scattering, and (3) a wide variety of nuclear reactions including hypernuclear production. Since the Møller scattering is a binary process, the scattered electrons are emitted to a well-defined cone whose opening angle is determined by the beam electron energy. Examining the E89-009 data, a new experimental configuration (the "tilt method") was proposed. With this configuration one can use much higher beam intensity and thicker targets, and thereby increase hypernuclear yields considerably, compared with those obtained during the E89-009 experiment [90]. The tilt method takes advantage of the fact that the angular distribution of the electrons associated with the virtual photons is less forward peaked than that of electrons associated with the bremsstrahlung process, as can be seen in Fig. 33. The electron spectrometer can be positioned at very forward angles, guaranteeing higher rates of virtual photons.

The SOS spectrometer that analyzed kaon momenta in E89-009 has insufficient momentum resolution and, as a consequence, the hypernuclear mass resolution was limited. By replacing the SOS with a new high-resolution kaon spectrometer (the HKS), which will have a momentum resolution as high as 1×10^{-4}, we will improve on the kaon momentum resolution by a factor of two, resulting in hypernuclear mass resolution of 300–400 keV FWHM. Furthermore, the HKS has a larger geometrical acceptance that will triple hypernuclear yield rates.

A plan view of the new experimental set-up is shown schematically in Fig. 38. A schematic layout of the new spectrometer system installed in Hall C is also shown in Fig. 39 (the apparatus could be installed in either Hall A and Hall C at JLab). The characteristics of the new experimental configuration are summarized in Table 15 of Section 4 along with those of the apparatus used for E89-009.

In the new configuration [90], scattered electrons and kaons are bent by a splitter magnet in opposite directions from each other as was the case for the E89-009 experiment. However, the electron spectrometer is tilted by a small angle vertically (perpendicular to the dispersive plane of the splitter). This tilt angle must be optimized for the operating conditions of the apparatus. The angular distributions of bremsstrahlung and Møller electrons are dependent on the beam energy, peaking more and more forward with the increasing beam energy, but with different beam energy dependences. For the E01-011 set-up, which uses an 1.8 GeV electron beam, the angular distribution of the Møller electrons extends to larger angles than that of the bremsstrahlung electrons. Thus, it is necessary to set the acceptance of the electron spectrometer outside the Møller ring. With higher beam energy, the Møller ring becomes smaller and the bremsstrahlung electrons become

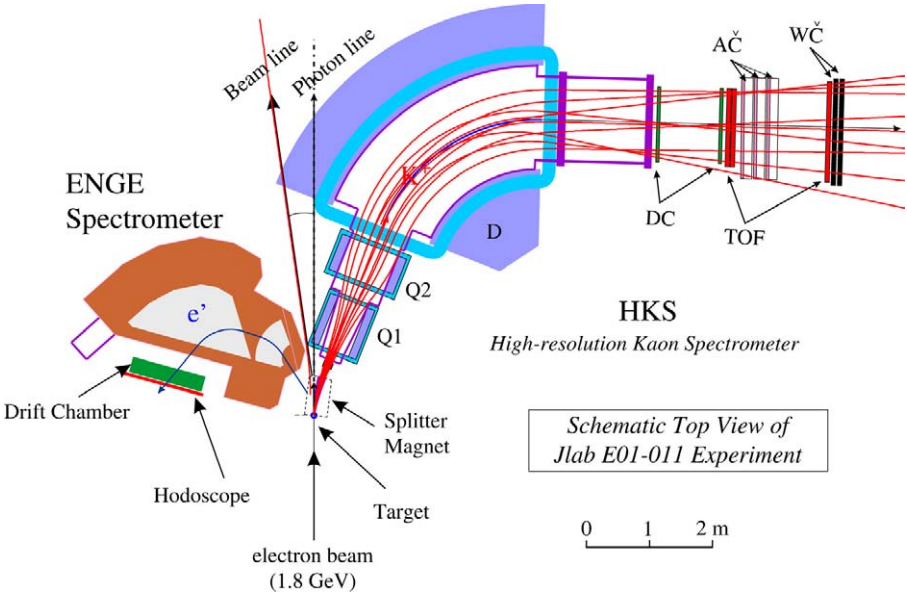

Fig. 38. Schematic drawing of the HKS spectrometer system that has been built and is now being installed at JLab to carry out a broad program of $(e, e' K^+)$ hypernuclear spectroscopy.

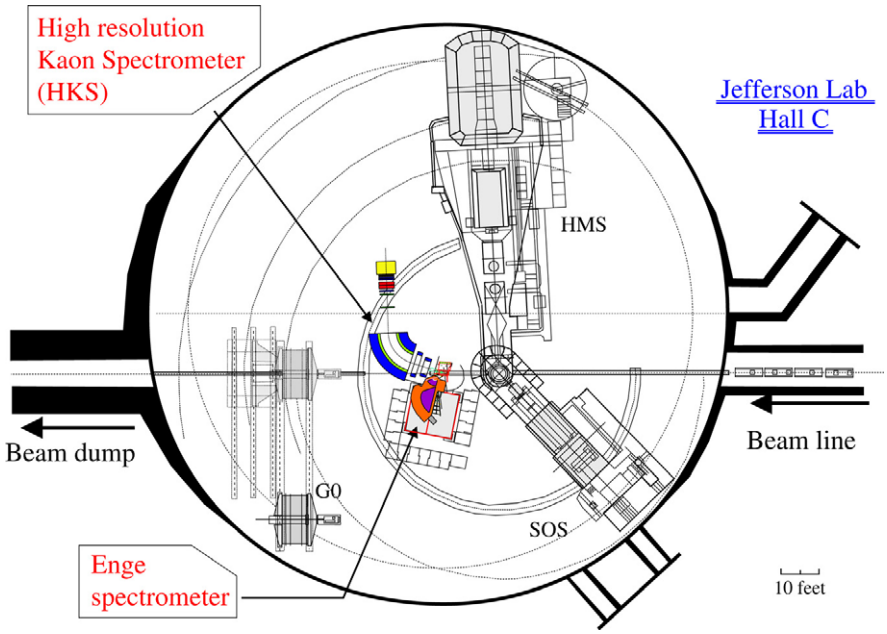

Fig. 39. General layout of the planned installation of the HKS spectrometer system in Hall C.

Table 16
Expected singles rates for the E01-011 experimental configuration with a beam intensity of 30 μA and a target thickness of 100 mg/cm^2

Target	Kaon spectrometer (HKS)			e' spectrometer (Enge)	
	π^+ rate (kHz)	K^+ rate (kHz)	p rate (kHz)	e^- rate (MHz)	π^- rate (kHz)
^{12}C	800	0.34	280	2.6	2.8
^{28}Si	800	0.29	240	5.1	2.8
^{51}V	770	0.26	230	6.9	3.0

the dominant contribution to the background at a given scattering angle. The optimized tilt angle depends on the experimental conditions. For the beam energies planned for the new HKS based experiment, design studies found the optimized tilt angle to be 8.5 degrees, corresponding to an electron scattering angle of 4.5 degrees. With this "tilted" configuration, an electron beam of 30 μA can be accepted even with a 100 mg/cm^2 ^{12}C target. Under these conditions, the singles rate at the focal plane of the Enge spectrometer is estimated to be of the order of 1 MHz as shown in Table 16; this is two orders of magnitude lower than the rates measured in E89-009. At the same time, the hadronic rates in the kaon spectrometer will become much higher than those of E89-009. Therefore, a good particle identification system capable of suppressing pion and proton backgrounds is important. In the E01-011 set-up, two layers of water Cherenkov counter arrays with a wavelength shifter ($n = 1.33$) and three layers of aerogel Cherenkov counters ($n = 1.05$) will be installed, rejecting protons with an efficiency of 2×10^{-4} and pions by 1×10^{-4} (see Fig. 38). The expected singles rates in the kaon and electron spectrometers are listed for three targets, ^{12}C, ^{28}Si and ^{51}V. They were calculated by extrapolating measured values.

It is also important to have a momentum acceptance as large as possible to maximize hypernuclear yields. Fig. 40 presents the correlations between the electron and kaon momenta for the production of Λs, Σs and hypernuclear states. The momentum acceptances of the two spectrometers that will be used for the E01-011 experiment are indicated as a box.

The estimated hypernuclear mass resolutions for ^{12}C, ^{28}Si and ^{51}V targets are listed together with a breakdown of the contributions of the spectrometer resolutions and beam energy spread to the resolution in Table 17. The overall mass resolution is expected to be 300–400 keV FWHM for the proposed E01-011 experiment, in contrast to the 750–800 keV FWHM which was expected for E89-009 where the relatively poor resolution of the SOS spectrometer dominated.

The yield rate for the $^{12}_{\Lambda}$B ground state was evaluated by extrapolating the E89-009 result for the ^{12}C$(e, e'K^+)^{12}_{\Lambda}$B reaction. It is estimated to be more than 50 times higher, and to have a signal-to-accidental ratio improved by almost a factor of 10 relative to the E89-009. This hypernuclear production rate is comparable to that of the (π^+, K^+) reaction with 1–2 g/cm^2 thick targets, and the mass resolution almost 5 times better. The hypernuclear spectra expected for a ^{28}Si target as well as for a ^{12}C target are shown in Fig. 41. The E01-011 experiment is scheduled to take data in 2005 for a ^{12}C and ^{28}Si targets.

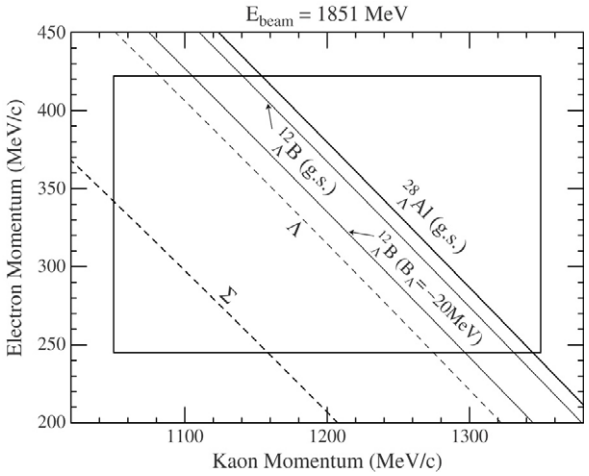

Fig. 40. The momentum correlation between the kaon and electron arms for hyperon and hypernuclear production reactions.

Table 17
The energy resolution of the HKS system

Item	Contribution to the resolution (keV, FWHM)		
Target	C	Si	V
HKS momentum (2×10^{-4})		216	
Beam momentum ($\leq 1 \times 10^{-4}$)		$\leq$180	
Enge momentum (5×10^{-4})		150	
K^+ angle resolution	152	64	36
Target (100 mg/cm^2)	$\leq$18	$\leq$171	$\leq$148
Overall	$\leq$400	$\leq$370	$\leq$350

With the large hypernuclear yields expected, the HKS spectrometer can be regarded as an efficient "strangeness tagger" for the $(e, e'K^+)$ reaction and it may even be possible to use it for hypernuclear coincidence experiments. A hypernuclear fission experiment is also under preparation; it aims to measure lifetimes of heavy Λ hypernuclei by detecting fission fragments in coincidence [91]. It should also be mentioned that a new electron spectrometer that matches the HKS spectrometer and can analyze electron momentum up to 1 GeV/c is under design. It will greatly enhance the opportunities for the hypernuclear program by the $(e, e'K^+)$ reaction at JLab.

The present facility has a rather narrow range of electron beam energies that are compatible with the spectrometer pair's limitations. With a new, higher-momentum electron spectrometer it will be possible to use the facility with a wide range of electron beam energies consistent with all operating conditions for beams at JLab both with the present 6 GeV accelerator and the planned 12 GeV Upgrade.

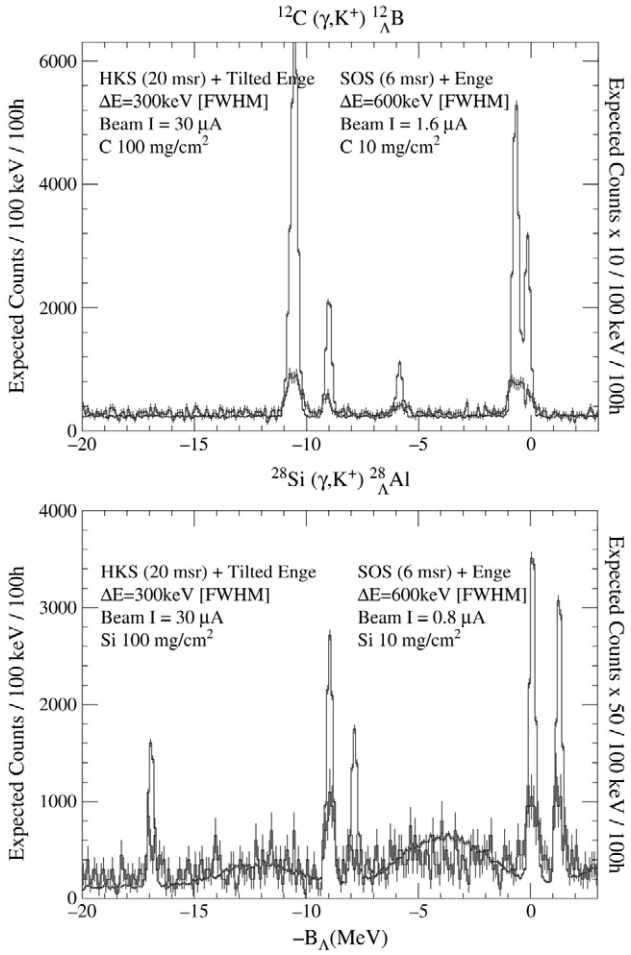

Fig. 41. Expected mass spectra of $^{12}_{\Lambda}$B (top) and $^{28}_{\Lambda}$Al (bottom) for 100 h beam time with the HKS spectrometer system [90].

A parallel effort in hypernuclear spectroscopy is under way as E94-107 [92] using the existing Hall A spectrometer pair, supplemented with a septum magnet (permitting the spectrometers to reach smaller angles relative to the beam) and a ring imaging Cherenkov counter (providing better kaon identification). Although the kinematical conditions are different from those of the HKS spectrometer, the set-up is expected to achieve a mass resolution as good as a few 100 keV with reasonable hypernuclear yields for light Λ hypernuclei (∼several tens/day for $^{12}_{\Lambda}$B ground state). The yield rate is expected to be between those of E89-009 and E01-011.

Even though $(e, e'K^+)$ spectroscopy becomes increasingly difficult for higher-Z targets due to the increasing rates for the unwanted bremsstrahlung and Møller electrons, it is thought that a target as heavy as ^{89}Y can be studied utilizing the E01-011 set-up with

the HKS spectrometer. With a superb mass resolution of a few 100 keV and yield rates comparable to or higher than those obtained via (π^+, K^+) spectroscopy using the SKS spectrometer, this next generation spectrometer system for $(e, e'K^+)$ spectroscopy will be an indispensable facility for strangeness nuclear physics.

5. Hypernuclear γ-ray spectroscopy

5.1. Historical background

The observation of hypernuclear γ rays was first reported in 1971 [18] as shown in Table 3. This experiment is the first counter experiment for hypernuclei, and was carried out even before hypernuclear reaction spectroscopy with magnetic spectrometers began. The inclusive γ-ray spectrum from stopped K^- absorption on a ^{7}Li target exhibited an unknown γ-ray peak at 1.09 MeV. It was assigned to the γ rays from the $1^+ \rightarrow 0^+$ transitions of $A = 4$ hypernuclei ($^4_\Lambda$H and $^4_\Lambda$He), since these are the only γ transitions expected from hyperfragments with mass numbers smaller than 6. Later, by measuring coincidences between these γ rays and pions (π^- and π^0) that have energies corresponding to the weak decay of $^4_\Lambda\mathrm{H} \rightarrow {}^4\mathrm{He} + \pi^-$ and $^4_\Lambda\mathrm{He} \rightarrow {}^4\mathrm{He} + \pi^0$, the $1^+ \rightarrow 0^+$ transitions of $^4_\Lambda$H and $^4_\Lambda$He were separately identified [34,35]. The level ordering and the spacing of the ground-state doublet $(1^+, 0^+)$ in $^4_\Lambda$H and $^4_\Lambda$He provided unique data for understanding the ΛN spin–spin interaction.

In 1985, the observation of γ transitions from well-identified Λ hypernuclei produced by the (K^-, π^-) direct reaction was first reported. An experiment performed at the BNL-AGS observed the $^7_\Lambda$Li $E2(5/2^+ \rightarrow 1/2^+)$ transition and the $^9_\Lambda$Be $E2(5/2^+, 3/2^+ \rightarrow 1/2^+)$ transitions [36] (see Fig. 47(c), (d)) when the bound-state regions for $^7_\Lambda$Li and $^9_\Lambda$Be were selected in the ^{7}Li, ^{9}Be (K^-, π^-) missing mass spectra. In the latter case, the two $E2$ transitions in $^9_\Lambda$Be were not resolved due to the limited energy resolution of the NaI(Tl) detectors. This measurement suggested a very small magnitude of the Λ-spin-dependent spin–orbit interaction (see Section 5.7).

Later, in a similar method, another BNL experiment observed the 11 MeV $E1(1/2^- \rightarrow 1/2^+)$ transition of $^{13}_\Lambda$C which corresponds to the $p_\Lambda \rightarrow s_\Lambda$ inter-shell transition of the $1\hbar\omega$ energy [37]. Then a subsequent experiment succeeded in observing both $E1(1/2^- \rightarrow 1/2^+$ and $3/2^- \rightarrow 1/2^+)$ transitions of $^{13}_\Lambda$C, and detected the small spin–orbit splitting of Λ single-particle states ($p_{1/2}$ and $p_{3/2}$) described in Section 5.7 [39].

In all of the experiments described above, NaI(Tl) crystals were employed as γ-ray detectors, which limited the energy resolution to ~0.1 MeV (FWHM) at 1 MeV. Although high-precision γ-ray spectroscopy using germanium (Ge) detectors with a few keV resolution has played a remarkably important role in the development of nuclear physics, use of Ge detectors for hypernuclei has been quite difficult because of small experimental yields, huge backgrounds and, in particular, technical problems in operating Ge detectors under conditions of very high count rates. Hypernuclear experiments using Ge detectors were first attempted in 1979 [93] and then in 1990 [94] at the BNL-AGS. The latter experiment searched for a hypernuclear γ transition from $^{10}_\Lambda$B; this transition was not

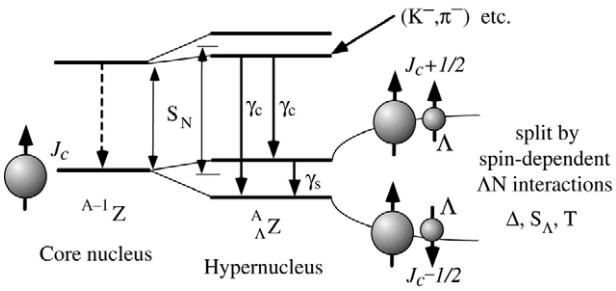

Fig. 42. Schematic scheme of low-lying levels of a Λ hypernucleus and their γ transitions. γ_c and γ_s are referred to as the "core transition" and "Λ spin-flip transition", respectively. The excellent resolution achieved using Ge detectors is essential for resolving each member of the doublet which is split by the ΛN spin-dependent interactions (called "hypernuclear fine structure"). See the text for details.

identified, but the observation of a candidate for an unassigned hypernuclear γ ray was reported [94].

In 1998, a large-acceptance Ge detector array dedicated to hypernuclear γ-ray spectroscopy (Hyperball) was constructed. The experimental problems due to high counting rates and huge backgrounds were solved by special readout electronics and background suppression counters as described in Section 5.4. Hyperball established a new technique for hypernuclear study, "high-precision hypernuclear γ spectroscopy", and a series of experiments have been performed systematically using Hyperball, which have revealed detailed level schemes of various p-shell hypernuclei. In the following sections of this paper, we focus mainly on the description of the Hyperball experiments.

Theoretically, γ transitions in p-shell hypernuclei were first investigated in Refs. [7, 95] together with both the production of these nuclei and their structure. Then, as more and more experimental information became available, p-shell hypernuclear γ transitions were studied by many authors using both shell models and cluster models (for example, see Refs. [96,97,8,98–100,53,101]).

5.2. Hypernuclear γ transitions

In the weak-coupling picture for a Λ hyperon and a core nucleus, γ transitions in hypernuclei are classified into three types: (1) core transitions, (2) Λ spin-flip transitions, and (3) Λ inter-shell transitions. Fig. 42 illustrates the low-lying levels of a hypernucleus schematically. Each state of the core nucleus with non-zero spin (J_C) is split into a doublet ($J_C + 1/2$, $J_C - 1/2$) by the spin coupling between the Λ hyperon and the core nucleus.

A transition connecting different doublets (γ_c in Fig. 42) is called a "core transition". It is induced by a transition in the core nucleus itself (shown with a dashed arrow in Fig. 42) and is described using the matrix element for this transition in the weak-coupling limit. This type of transition was first observed for $^{7}_{\Lambda}\mathrm{Li}(5/2^+ \rightarrow 1/2^+)$ and $^{9}_{\Lambda}\mathrm{Be}(5/2^+, 3/2^+ \rightarrow 1/2^+)$.

A transition from the upper to the lower member of the same doublet (γ_s in Fig. 42) is an $M1$ transition caused by a flip of the Λ spin. It is called a "Λ spin-flip transition". The 1.1 MeV ${}^{4}_{\Lambda}$H and ${}^{4}_{\Lambda}$He ($1^+ \rightarrow 0^+$) transitions are the oldest examples of this type. When the doublet spacing energy is less than ~100 keV, the Λ spin-flip transition rate is generally smaller than the weak decay transition rate, and the γ transition is not expected to be observed.

The other type of hypernuclear γ transition is an $E1$ transition in which the Λ hyperon changes the major shell orbit from p_Λ to s_Λ ("Λ inter-shell transition"). The 11 MeV ${}^{13}_{\Lambda}$C($1/2^-, 3/2^- \rightarrow 1/2^-$) γ transitions are the only example of a Λ inter-shell transition observed to date. This type of transition is not expected to be seen often in light (p-shell) hypernuclei because the transition energy is usually higher than nucleon separation energies. On the other hand, Λ inter-shell transitions are expected to be observed in medium and heavy hypernuclei.

5.3. Physics subjects in hypernuclear γ spectroscopy

The excellent energy resolution achieved in γ-ray spectroscopy opens new physics possibilities described in this section.

5.3.1. ΛN interaction

The precision with which the structure of Λ hypernuclei can be investigated by γ spectroscopy allows us to study the ΛN interaction in much greater detail. In particular, the spin-dependent interactions (spin–spin, spin–orbit, and tensor interactions), the ΛN–ΣN coupling interaction, and charge symmetry breaking in the ΛN interaction can be investigated.

The excellent energy resolution of a few keV (FWHM) achieved by Ge detectors is most useful in resolving the spin doublet in hypernuclei that is called "hypernuclear fine structure" because this structure has a small energy spacing (of the order of 10–100 keV). Even if the spacing is so small (<100 keV) that the Λ spin-flip transition is overwhelmed by weak decay, the spacing can be obtained by separately observing the two core transitions going to the two members of the doublet as illustrated in Fig. 42. The spacing of such a doublet provides us with valuable information on the spin-dependent components of the ΛN interaction, which can barely be studied by ΛN scattering experiments.

In the $p^{A-5}s_\Lambda$ shell model description, the low-lying level energies of p-shell hypernuclei can be described using five radial integrals for the $s_\Lambda p_N$ wavefunction based on the five terms in Eq. (2). The four integrals of the spin-dependent terms are denoted as Δ, S_Λ, S_N, and T for the spin–spin term V_σ, the Λ-spin-dependent spin–orbit term V_Λ, the nucleon-spin-dependent spin–orbit term V_N, and the tensor term V_T, respectively [7,8]. By comparing the measured level energies with the shell model predictions, these integrals (parameters) can be determined experimentally. The values of Δ, S_Λ and T are derived from the spacing of the doublet, while S_N is given by the change of the excitation energy of the core nucleus. The three parameters (Δ, S_Λ and T) can be determined from a combined analysis of three doublet spacings, where it is desirable that each doublet spacing has a particularly large contribution of each parameter. As described later, the ${}^{7}_{\Lambda}$Li($3/2^+, 1/2^+$), ${}^{9}_{\Lambda}$Be($3/2^+, 5/2^+$), and ${}^{16}_{\Lambda}$O($1^-, 0^-$) spacings have played important roles in determination

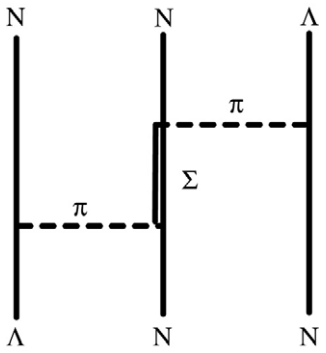

Fig. 43. The three-body force caused by ΛN–ΣN coupling. It is not incorporated in the effective two-body ΛN interaction and must be studied for each hypernucleus.

of Δ, S_Λ, and T, respectively, and the core excitation energy in ${}^{7}_{\Lambda}$Li has been used to determine S_N.

In addition, the three-body ΛNN interaction that arises from ΛN–ΣN coupling (Fig. 43) [102,103] (and which cannot be incorporated in the two-body ΛN effective interaction) can be investigated by measuring the energies of various hypernuclear levels.

The large difference of the binding energies between ${}^{4}_{\Lambda}$H and ${}^{4}_{\Lambda}$He suggests a large charge symmetry breaking (CSB) in the ΛN interaction. Detailed level data for mirror hypernuclear pairs will allow us to investigate the origin of the CSB in the ΛN interaction [104].

5.3.2. Impurity effects induced by a Λ hyperon

When a Λ hyperon is added to a nucleus, nuclear properties such as size, shape, symmetry, cluster and shell structure, collective motions may be modified. Such effects induced by "impurity" of a Λ hyperon can be investigated experimentally by measuring $B(E2)$ values and detailed level schemes. See Ref. [105] for details.

For example, loosely bound nuclei and neutron-rich nuclei with neutron halos are expected to be modified drastically by a Λ hyperon. Since a Λ hyperon is free from Pauli blocking by nucleons, it occupies the $0s$ orbit and attracts surrounding nucleons, which results in shrinkage of the nucleus. The nuclear shrinkage is predicted for ${}^{7}_{\Lambda}$Li, ${}^{8}_{\Lambda}$Be, ${}^{9}_{\Lambda}$Be, etc. [96]. The ground state of ${}^{20}_{\Lambda}$Ne is expected to have a negative parity due to a difference in shrinking effect between positive parity levels and negative parity levels [106]. In ${}^{7}_{\Lambda}$He, a neutron halo in ^{6}He is expected to disappear [59].

As described in Section 5.4, transition probabilities such as $B(E2)$ can be derived from the lifetimes of the excited states of hypernuclei which are measured using the Doppler shift attenuation method.

5.3.3. Nuclear medium effects of baryons

Since a Λ hyperon is free from Pauli blocking in a nucleus, it can be used as a probe to investigate the possible modifications of baryon properties in nuclear matter that are expected to occur due to a partial restoration of chiral symmetry. By measuring a $B(M1)$

value of the spin-flip $M1$ transition between the hypernuclear doublet members, the g-factor of a Λ hyperon in a nucleus can be derived.

In the weak-coupling limit between a Λ hyperon and a core nucleus, the reduced transition probability $B(M1)$ for a Λ spin-flip $M1$ transition in a hypernucleus is given by [7]

$$\begin{aligned} B(M1) &= (2J_{\rm up}+1)^{-1}|\langle\psi_{\rm low}\|\boldsymbol{\mu}\|\psi_{\rm up}\rangle|^2 \\ &= (2J_{\rm up}+1)^{-1}|\langle\psi_{\rm low}\|[g_c\boldsymbol{J_c}+g_\Lambda\boldsymbol{J_\Lambda}]\|\psi_{\rm up}\rangle|^2 \\ &= (2J_{\rm up}+1)^{-1}|\langle\psi_{\rm low}\|[g_c\boldsymbol{J}+(g_\Lambda-g_c)\boldsymbol{J_\Lambda}]\|\psi_{\rm up}\rangle|^2 \\ &= \frac{3}{4\pi}\frac{3}{2}(2J_{\rm low}+1)\begin{Bmatrix} 1/2 & J_{\rm low} & J_c \\ J_{\rm up} & 1/2 & 1 \end{Bmatrix}^2 (g_c-g_\Lambda)^2 \\ &= \frac{3}{8\pi}\frac{2J_{\rm low}+1}{2J_c+1}(g_c-g_\Lambda)^2, \end{aligned} \tag{15}$$

where g_c, g_Λ, $\boldsymbol{J_c}$ and $\boldsymbol{J}_\Lambda$ denote the effective g-factors of the core nucleus and the Λ hyperon, and their spins, respectively. Here the spatial components of the wavefunctions for the lower state of the doublet, $\psi_{\rm low}$ and $\psi_{\rm up}$ (with spin $J_{\rm low}$ and $J_{\rm up}$), are assumed to be identical.

$B(M1)$ values can be measured with the Doppler shift attenuation method and the γ–weak coincidence method as described in Section 5.4.

5.4. Experimental method and apparatus

5.4.1. Direct reaction method

The direct reactions ${}^A{\rm Z}(\pi^+, K^+){}^A_\Lambda{\rm Z}$ and ${}^A{\rm Z}(K^-, \pi^-){}^A_\Lambda{\rm Z}$ are usually used for γ spectroscopy of hypernuclei. Excited bound states of ${}^A_\Lambda{\rm Z}$ hypernuclei are selected by gating a bound-state region (or a particular part of the bound-state region) in the missing mass spectrum of the ${}^A{\rm Z}(\pi^+, K^+){}^A_\Lambda{\rm Z}$ and ${}^A{\rm Z}(K^-, \pi^-){}^A_\Lambda{\rm Z}$ reactions, and γ rays emitted from the hypernuclei are measured with γ-ray detectors in coincidence with the reaction. By selecting unbound excited states of the hypernucleus ${}^A_\Lambda{\rm Z}^*$ in the mass spectrum, we can investigate γ transitions in lighter hypernuclei that are produced by particle decays of ${}^A_\Lambda{\rm Z}^*$. Since the (K^-, π^-) and (π^+, K^+) reactions convert a neutron into a Λ hyperon, a hypernucleus produced from a $T = 0$ $(Z = N)$ target nucleus has a particularly low proton emission threshold compared with other particle decay thresholds. Therefore, excited states of such a hypernucleus often decay into excited states of ${}^{(A-1)}_\Lambda[Z-1]$ by proton emission and γ rays from this daughter hypernucleus can be also investigated.

Using this method, hypernuclear states can be selected by taking advantage of the selectivity of the reaction (spin-flip or non-spin-flip states, substitutional states with $\Delta L = 0$ or stretched states with a large ΔL) and the measured hypernuclear mass. Therefore, the background level in the γ-ray spectrum is generally low, particularly when magnetic spectrometers with a good mass resolution are used.

Since the recoil momentum vector of the excited hypernucleus and the direction of the γ ray are known for each event, the Doppler shift effect can be corrected for on

event-by-event basis using the equation

$$E_\gamma^{\text{corrected}} = E_\gamma^{\text{measured}} \frac{1}{\sqrt{1-\beta^2}}(1-\beta\cos\theta), \tag{16}$$

where β and θ denote the velocity of the recoiling hypernucleus and the γ-ray emission angle with respect to the recoil direction of the hypernucleus. This correction works well if the γ ray is emitted before the recoiling hypernucleus slows down in the target material. The accuracy of the Doppler shift correction is usually limited by the γ-ray detector size and the spatial resolution of the determination of the reaction point; it is generally much worse than the intrinsic energy resolution of Ge detectors (about 2 keV (FWHM) at 1 MeV).

When the stopping time of the recoiling excited hypernucleus in the target material is of the same order as the lifetime of the excited hypernuclear state, the lifetime can be measured using the Doppler shift attenuation method. The lifetime sensitively affects the γ-ray peak shape due to partial Doppler broadening if γ rays are emitted as the recoiling hypernucleus slows down in the target. In particular, the ratio of counts between a narrow peak (which is due to γ-ray emission at rest) and broad tails (which are due to γ-ray emission in flight) gives a good measure of the lifetime. The excellent energy resolution of Ge detectors is indispensable for the use of this method.

Lifetimes of the excited states and their decay branching ratios give transition probabilities such as $B(E2)$ and $B(M1)$. In the case of p-shell hypernuclei, the Doppler shift attenuation method can be used for $B(E2)$ measurements in the a few MeV energy range, and for $B(M1)$ measurements in the several hundred keV range. As described in Section 2, the recoil velocity of a hypernucleus is large for the (π^+, K^+) reaction ($\beta \sim 0.4/A$) due to the large momentum transfer, while it is small ($\beta < 0.2/A$) for the (K^-, π^-) reaction, particularly at very forward angles. In these measurements, the optimum combination of the recoil velocity and the target density must be selected so that the stopping time is compatible with the expected lifetime.

Transition rates for Λ spin-flip $M1$ transitions are comparable to the weak decay rate (of the order of $(100\ \text{ps})^{-1}$) when the transition energy is around 100 keV. In such a case, the upper member of the ground-state doublet undergoes weak decays with a sizable branching ratio. The "γ–weak coincidence method" has been proposed [107] for measuring transition probabilities for lifetimes of the order of 100 ps or longer. In this method, the lifetime is measured directly from the time distribution of the weak decay products (p and π^-). Here, coincidence measurements of weak decay products and γ transitions are necessary to distinguish between the weak decay from the excited state and that from the ground state.

In the direct reaction method, yields of γ rays are generally small because of the small cross sections for the production of particular hypernuclear states (of the order of μb/sr for the (π^+, K^+) reaction). The hypernuclear species and hypernuclear levels that we can study are limited due to selectivity of population in the reaction and available target nuclei.

5.4.2. Inclusive γ-ray measurement of hyperfragments

Another method for hypernuclear γ spectroscopy is the inclusive measurement of γ rays from hyperfragments produced by K^- beams, namely, (K^-, γ) measurements. In

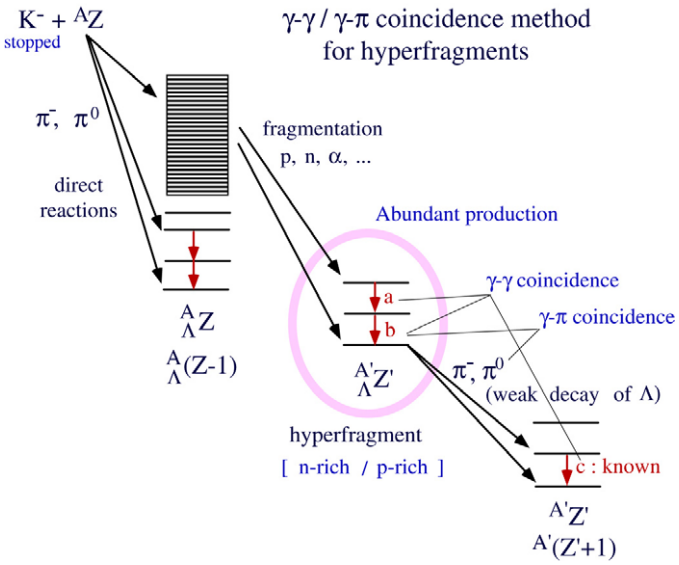

Fig. 44. Production of hyperfragments from stopped K^- reactions and their γ spectroscopy. Here, γ–γ and γ–π coincidence methods are useful for identifying hypernuclei. Taken from [105].

particular, it is known that hyperfragments are produced abundantly from stopped K^- absorption; the production rate for any hypernucleus is measured to be about 10% per stopped K^- for the light (C, N, O) target nuclei in emulsion and about 50% for the heavy (Ag, Br) target nuclei in emulsion [108]. In this method, various hypernuclear species including neutron-rich and proton-rich hypernuclei can be produced and their γ transitions can be observed as shown in Fig. 44, although the production rates of neutron- and proton-rich hypernuclei are much lower than others.

Since the production of hypernuclei is not tagged in this method, it suffers from backgrounds from normal nuclear γ rays and neutrons, and particularly from backgrounds due to fast-neutron induced γ rays from surrounding materials. In addition, a Doppler shift correction is impossible when the stopped K^- is used, since information on the recoil of produced hypernuclei cannot be obtained. Identification and assignment of hypernuclear γ rays are not straightforward, but they are possible by using the γ–γ coincidence with another transition in the cascade γ decay or with γ rays emitted in the daughter nuclei after weak decay [109]. One can also measure a coincidence with pions from weak decay [34, 35], as illustrated in Fig. 44. Target dependence of the γ-ray yield is also helpful for assigning the hypernuclear species (see Section 5.11).

This method was used in early experiments with NaI detectors, and even in the first γ-spectroscopy experiment [18], but only the $A = 4$ hypernuclear transitions were observed. Recently, it was revived with Hyperball (KEK E509), by taking advantage of the excellent resolution of Ge detectors, as described in Section 5.11.

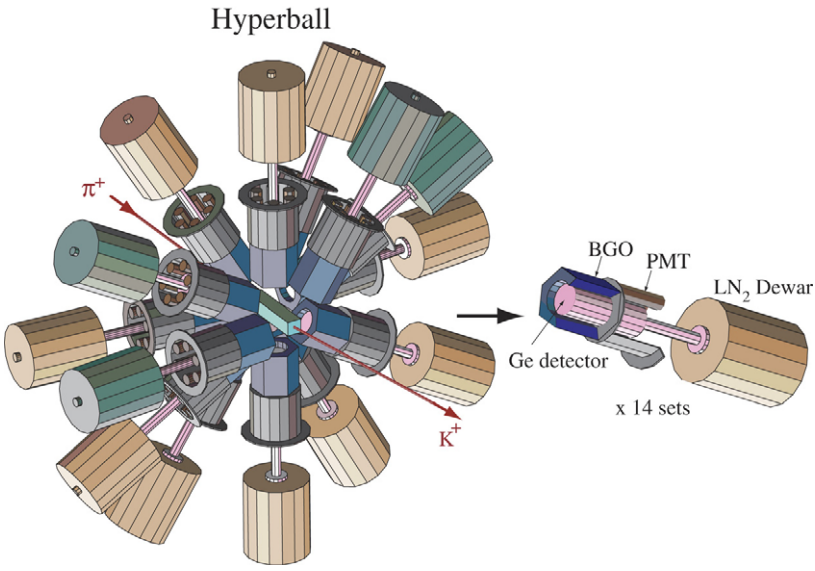

Fig. 45. Schematic view of Hyperball.

5.4.3. Detectors — Hyperball

Hyperball is a large-acceptance germanium (Ge) detector array dedicated to hypernuclear γ-ray spectroscopy. Details of Hyperball are described in Ref. [110,111]. Figs. 45 and 46 (right) show schematic views of Hyperball. It consists of fourteen n-type coaxial Ge detectors, each of which has a crystal of about 70 mmϕ $\times$ 70 mm and has a photo-peak efficiency of 60% relative to a $3''\phi \times 3''$ NaI detector. Each Ge detector is equipped with fast electronics, including low-gain transistor-reset preamplifiers and fast shaping amplifiers with gated integrators. They enabled operation of the Ge detectors in the presence of the severe radiation backgrounds in hypernuclear experiments using high-energy meson (K^- or π^+) beams. The most serious radiation is caused by high-momentum ($\sim$1 GeV/c) charged particles, such as beam particles that scattered in a thick ($\sim$10 g/cm^2) target or beam line components, and decay particles (pions or muons) from beams, penetrating a Ge detector and depositing a large ($\sim$50 MeV) amount of energy. Each Ge detector is located at a distance of 10–15 cm from the beam axis to the Ge crystal surface; the distance can be varied depending on experimental conditions. In a typical set-up at 15 cm, the Ge detectors cover a solid angle of about 15% of 4π sr in total and have a photo-peak efficiency of 2.5% at 1 MeV for a point source.

Each Ge detector is surrounded by six BGO (bismuth germanate) scintillation counters, used to suppress background events such as high-energy γ rays from π^0, high-energy charged particles penetrating the Ge detectors, and Compton scattering events. The use of the BGO counters is essential to detect the weak γ-ray signals from hypernuclei under these background conditions.

In the direct reaction method, data from all of the detectors in Hyperball are recorded by the (π^+, K^+) or (K^-, π^-) trigger provided by the magnetic spectrometer system.

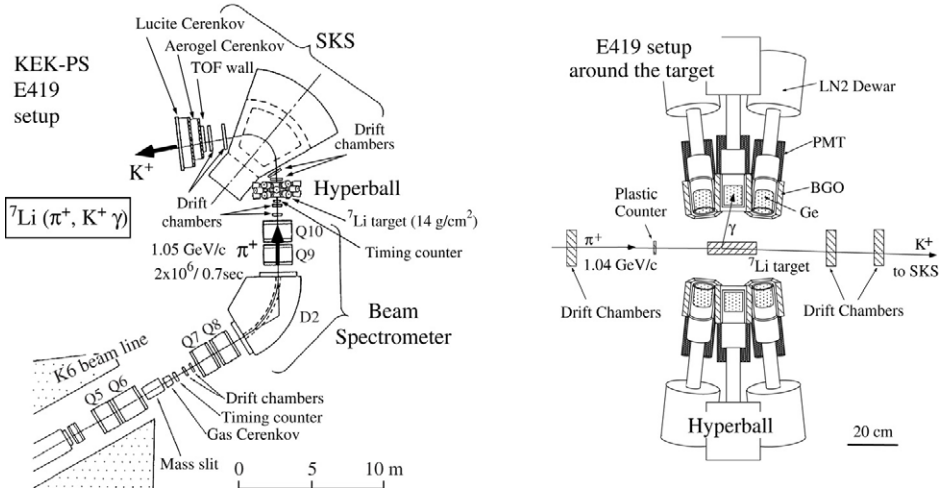

Fig. 46. The set-up for the γ-spectroscopy experiment of ${}^{7}_{\Lambda}$Li (KEK E419) using the K6 beam line and the SKS spectrometer (left). A side view of the region around the target surrounded by Hyperball is also shown (right).

However, in order to reduce the trigger rate, a coincident hit of any one of the Ge detectors is sometimes required as a second-level trigger. In inclusive experiments with stopped K^- beams, a hit of any one Ge detector in coincidence with the stopped K^- trigger is required.

In order to monitor the performance of the Ge detectors, a weak (1 kBq) ^{60}Co β–γ source embedded in a plastic scintillator is mounted behind each Ge detector. By using γ rays triggered by this scintillator's signal, the in-beam performance as regards electronics dead time, energy resolution, and energy shifts can be monitored for each Ge detector simultaneously with the data taking through the experiment.

In previous experiments, the energy calibration of the Ge detectors was made in the energy range of 0.1–1.8 MeV using standard sources such as ^{137}Cs, ^{60}Co, ^{88}Y, ^{123}Eu. Beam induced prompt γ rays from the target and surrounding materials contaminating the recorded data were also used for energy calibration and for checking the energy shift between beam-off and beam-on periods. In addition, self-triggered data from the Ge detectors were also taken (in E930('01)) so that γ rays from activities produced by the beam such as ^{24}Na(2754 keV) and ^{16}N(6129, 7115 keV) could also be used for calibration of the energy region above 2 MeV. In the ${}^{16}_{\Lambda}$O experiment in E930('01), the 6129 keV and 7115 keV ^{16}N γ rays and their single- and double-escape peaks at 5107, 5618, and 6604 keV were useful for energy calibration in the 6–7 MeV region.

In the experiments using the (π^+, K^+) reaction carried out at KEK (E419 and E518), the pion beam intensity acceptable by Hyperball before the dead time became too large and the energy resolution was degraded was close to the pion intensity (2–3×10^6/s) usually available at the K6 beam line. In our running condition with the pion beam intensity of 2×10^6/s and a 10–20 g/cm^2 thick target, the dead time of the Ge detectors was about 40%–50% and the detector resolution began to deteriorate with higher pion intensity. On the other hand, in the (K^-, π^-) experiments at BNL (E930('98) and ('01)), the dead time

of the Ge detectors was less than 10% with the maximum K^- beam intensity available at the AGS D6 beam line (2×10^5 K^-/spill at 0.93 GeV/c).

Radiation damage to the Ge detectors is a rather serious problem, particularly in (π^+, K^+) and stopped K^- reactions. It is caused by fast neutrons produced from pions at the target and surrounding material, as well as scattered pions making nuclear reactions in the Ge detectors. In the (π^+, K^+) experiment at KEK with a beam intensity of 2–3 $\times 10^6$ π^+ every cycle (4 s), a slight degradation of the resolution from radiation damage was observed after one month's run.

5.4.4. *Detectors — NaI detector array*

For γ rays with energies above several MeV, use of large-volume NaI detectors is effective because they have much larger photo-peak efficiencies than Ge detectors. Since the background level is lower for higher γ-ray energies, the worse energy resolution of NaI detectors is not as disadvantageous as in the case of low-energy γ rays. In the BNL experiments for ${}^{13}_{\Lambda}$C, searching for the ~11 MeV Λ inter-shell ($p_\Lambda \rightarrow s_\Lambda$) transitions, large-volume NaI detectors were used. In the first ${}^{13}_{\Lambda}$C experiment [37] two counters with large NaI crystals (20.3 cm$\phi \times$ 15.2 cm) were used. The second experiment [39] employed two arrays of 6 × 6 NaI detectors, each of which was 6.5 × 6.5 × 30 cm^3 and was located 10.5 cm from the target center. These arrays had a total efficiency of 4.5% for 11 MeV γ rays. The fine segmentation of the NaI array was effective in permitting operation under high counting rates.

5.5. *Identified hypernuclear γ rays*

Fig. 47 shows all the hypernuclear γ transitions observed and identified to date. The γ rays from ${}^{4}_{\Lambda}$H, ${}^{4}_{\Lambda}$He and ${}^{13}_{\Lambda}$C were observed only with NaI detectors. The $E2$ transitions in ${}^{7}_{\Lambda}$Li and ${}^{9}_{\Lambda}$Be were first observed with NaI detectors [36], and then with Hyperball. All the other γ rays were observed only with Hyperball.

Hyperball was constructed in 1998 and has been employed in several experiments as shown in Table 3. In 1998, two Hyperball experiments were carried out; KEK E419 for ${}^{7}_{\Lambda}$Li [26,38,109] and BNL E930('98) for ${}^{9}_{\Lambda}$Be [40]. These measurements were performed using the ^{7}Li$(\pi^+, K^+\gamma)$ and ^{9}Be$(K^-, \pi^-\gamma)$ reactions, respectively. In 2001, the second run of BNL E930 (E930('01)) investigated ${}^{16}_{\Lambda}$O and ${}^{15}_{\Lambda}$N using the ^{16}O$(K^-, \pi^-\gamma)$ reaction and ${}^{10}_{\Lambda}$B, ${}^{9}_{\Lambda}$Be, and ${}^{7}_{\Lambda}$Li using the ^{10}B$(K^-, \pi^-\gamma)$ reaction. In 2002, Hyperball was moved from BNL to KEK and two experiments were performed, E509 for hyperfragments with stopped K^- beams [43] and E518 for ${}^{11}_{\Lambda}$B using the ^{11}B$(\pi^+, K^+\gamma)$ reaction [44].

5.6. ${}^{7}_{\Lambda}$Li — *the best studied hypernucleus*

${}^{7}_{\Lambda}$Li is the hypernucleus that has been best studied using γ spectroscopy. Five γ transitions have been observed in ${}^{7}_{\Lambda}$Li and the complete level scheme for all the bound states (with energies and spins) has been determined as shown in Fig. 47(a). In addition, the $B(E2)$ value was also measured.

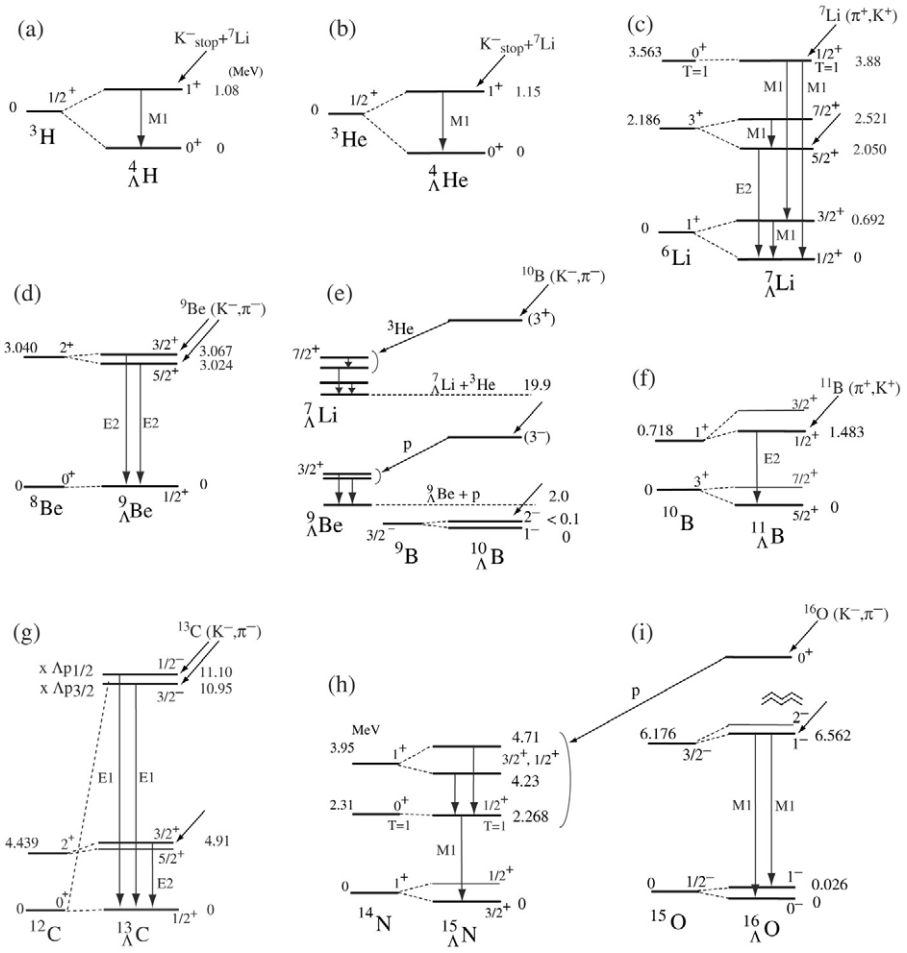

Fig. 47. All the hypernuclear γ transitions observed and identified to date for ${}^{4}_{\Lambda}$H [34], ${}^{4}_{\Lambda}$He [35], ${}^{7}_{\Lambda}$Li [36,26], ${}^{9}_{\Lambda}$Be [36,40], ${}^{10}_{\Lambda}$B [94,42], ${}^{11}_{\Lambda}$B [44], ${}^{15}_{\Lambda}$N [42], and ${}^{16}_{\Lambda}$O [41]. The level schemes of these hypernuclei with the energies (in MeV) and the assigned spins and parities are shown together with the reactions used to populate the excited states in γ spectroscopy experiments.

5.6.1. ^{7}Li$(\pi^+, K^+\gamma)$ ${}^{7}_{\Lambda}$Li *experiment (KEK E419)*

In the first experiment with Hyperball (KEK E419), the ${}^{7}_{\Lambda}$Li hypernucleus was studied at the 12 GeV PS in KEK.

The experimental set-up is depicted in Fig. 46. Bound states of ${}^{7}_{\Lambda}$Li were produced via the ^{7}Li(π^+, K^+) reaction with 1.05 GeV/c pions, employing the K6 beam line and the SKS spectrometer, and γ rays were detected with Hyperball installed surrounding the target. In this experiment, the large acceptance of the SKS spectrometer played an essential role in permitting the experiment to observe hypernuclear γ rays with a small yield.

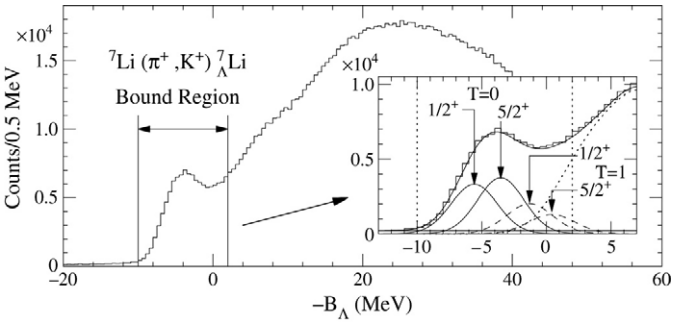

Fig. 48. The hypernuclear mass spectrum of ${}^{7}_{\Lambda}$Li (plotted versus the Λ binding energy, B_Λ) taken using the (π^+, K^+) reaction with a 25 cm thick ^{7}Li target. The "bound region" is defined as shown. The inset shows the decomposition of the states produced (see the text). Taken from Ref. [26].

The intensity of the π^+ beam was typically 1.8×10^6 per spill (0.7 s duration occurring every 3 s). The trajectory of each beam particle was measured with the K6 beam spectrometer. The beam pions hit a 25 cm thick 98%-enriched ^{7}Li target and outgoing K^+ mesons were identified and momentum analyzed by the SKS spectrometer. The target was irradiated with a total of 1.0×10^{12} pions over a one-month run. Detailed descriptions on the K6 beam line and the SKS spectrometer are available in Refs. [23,50].

Fig. 48 shows the excitation spectrum of ${}^{7}_{\Lambda}$Li plotted versus the Λ binding energy, B_Λ, obtained from the determination of the missing mass in the ^{7}Li(π^+, K^+) reaction. In the KEK E336 experiment for ^{7}Li(π^+, K^+), performed under the same conditions but with a thin ^{7}Li target (1.8 MeV FWHM resolution), the observed ${}^{7}_{\Lambda}$Li spectrum (Fig. 13) was decomposed into four peaks (#1–#4) for the $-B_\Lambda \leq 0$ region. The energies and relative intensities of these peaks agreed fairly well with theoretically calculated level energies and cross sections [58,100] for the four most strongly populated states, namely, $1/2^+$ ($T = 0$), $5/2^+$ ($T = 0$), $1/2^+$ ($T = 1$), and $5/2^+$ ($T = 1$) (see Fig. 50). (The notation "($T = 0$)" is omitted hereafter.) In the present spectrum, the energy resolution is worse due to energy loss effects in the thick target. By folding these four peaks with 4.2 MeV FWHM resolution, the present spectrum was reproduced well, as shown in Fig. 48 inset. The gate for the "bound region" was set at $-10 < -B_\Lambda < 2$ MeV as shown in the figure.

Fig. 49(a) is the γ-ray energy spectrum when the unbound region ($-B_\Lambda > 2$ MeV) of ${}^{7}_{\Lambda}$Li is selected. In this spectrum background γ rays and X rays are seen. On the other hand, Fig. 49(b) shows the γ-ray spectrum for the bound region, where more peaks appear at 429, 692 and at 2050 keV, and the peak at 478 keV is more prominent than in (a). The 429 and 478 keV peaks are interpreted as transitions in the daughter nuclei resulting from ${}^{7}_{\Lambda}$Li weak decay, ${}^{7}_{\Lambda}\mathrm{Li} \to \pi^- + {}^{7}\mathrm{Be}^*(429)$ and ${}^{7}_{\Lambda}\mathrm{Li} \to \pi^0 + {}^{7}\mathrm{Li}^*(478)$.

The peak at 2050 keV is attributed to the $E2(5/2^+ \to 1/2^+)$ transition in ${}^{7}_{\Lambda}$Li. This transition was previously observed at 2034 ± 23 keV using NaI detectors at BNL [36]. The peak has broad tails due to partial Doppler broadening, indicating that the lifetime of the γ-emitting excited state is of the same order as the stopping time (∼10 ps) of a

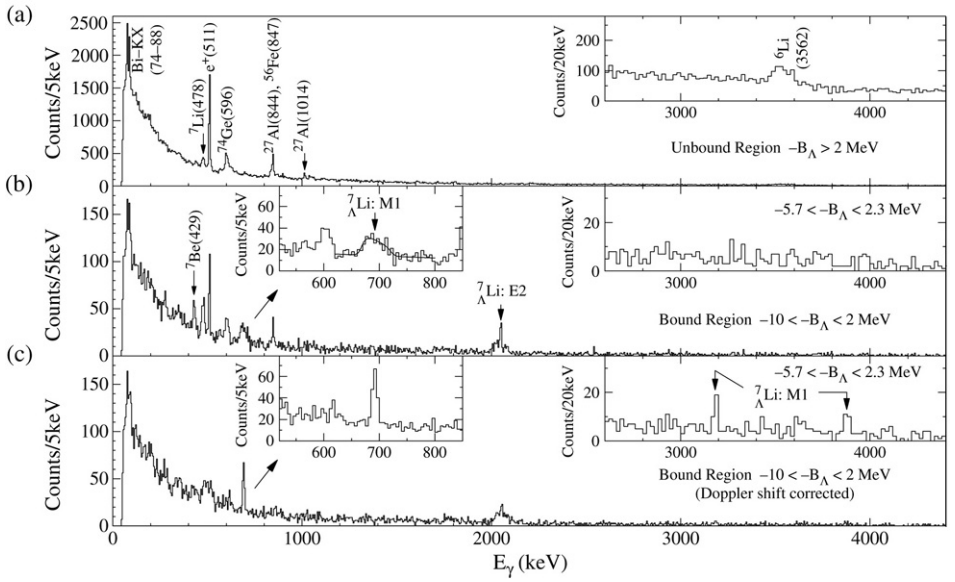

Fig. 49. Spectra of γ rays from the ^{7}Li(π^+, K^+) reaction for (a) the unbound region ($-B_\Lambda > 2$ MeV), and (b) the bound region ($-10 < -B_\Lambda < 2$ MeV) of $^{7}_{\Lambda}$Li. The two peaks at 692 and 2050 keV in (b) are assigned as $M1(3/2^+ \rightarrow 1/2^+)$ and $E2(5/2^+ \rightarrow 1/2^+)$ transitions of $^{7}_{\Lambda}$Li, respectively. The curve in the left inset in (b) shows a Doppler broadened peak shape simulated for γ-ray emission before the recoiling $^{7}_{\Lambda}$Li slows down. (c) is the same spectrum as (b) but the event-by-event Doppler shift correction was applied. In the right insets of (b) and (c), the bound region condition is changed to $-5.7 < -B_\Lambda < 2.3$ MeV. The two peaks observed in the right inset of (c) are assigned as $M1(1/2^+(T = 1) \rightarrow 3/2^+, 1/2^+)$ transitions. Taken from Ref. [26].

recoiling hypernucleus in the target. The inferred lifetime (of order 10 ps) is consistent with a transition rate for $E2$.

As shown in the left inset in Fig. 49(b), the shape of the 692 keV peak is well reproduced by a simulation (solid curve) in which the Doppler shift is calculated assuming that γ rays are emitted from $^{7}_{\Lambda}$Li promptly (i.e., before a significant slowing down occurs). Therefore, this transition is faster than 2 ps and assigned as an $M1$ transition in $^{7}_{\Lambda}$Li. After the event-by-event Doppler shift correction, the broad peak at 692 keV becomes sharp as shown in Fig. 49(c). This indicates that the γ ray is emitted from $^{7}_{\Lambda}$Li. The energy was determined as $691.7 \pm 0.6(\text{stat}) \pm 1.0(\text{syst})$ keV.

In the Doppler shift corrected spectrum (right inset in Fig. 49(c)), two peaks were also observed at $3877 \pm 5 \pm 7$ keV and at $3186 \pm 4 \pm 5$ keV. From their energies and the relative yields (∼1:1), they are assigned as $M1(1/2^+(T = 1) \rightarrow 3/2^+$ and $1/2^+)$ transitions (see Fig. 50). Their energy difference (691 ± 6 keV) coincides with the 692 keV peak energy. Therefore, the 692 keV transition is assigned as $M1(3/2^+ \rightarrow 1/2^+)$, but not as $M1(7/2^+ \rightarrow 5/2^+)$. This assignment is further supported by the relative γ-ray yields of these transitions [26].

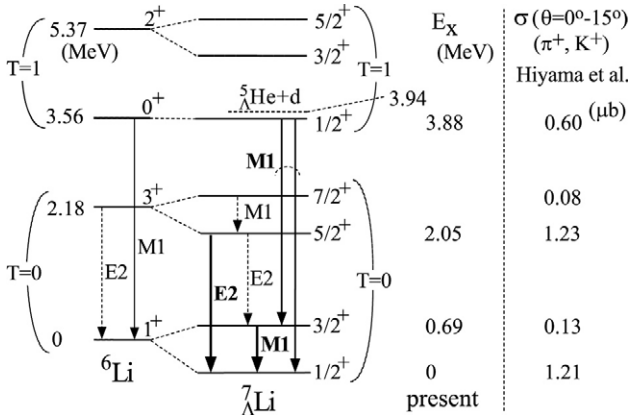

Fig. 50. Level scheme and γ transitions of ${}^{7}_{\Lambda}$Li obtained from the ^{7}Li$(\pi^+, K^+\gamma)$ experiment (KEK E419). Thick arrows show transitions observed, and "present" shows level energies measured in the experiment. Transitions from $1/2^+(T = 1)$ to the ground-state doublet members were observed with less statistical significance. $\sigma(\theta = 0°–15°)$ shows calculated production cross sections for the (π^+, K^+) reaction at 1.05 GeV/c and integrated for 0°–15° (∼SKS acceptance) [100]. Taken from Ref. [26].

5.6.2. *Spin-flip $M1(3/2^+ \to 1/2^+)$ transition and ΛN spin–spin interaction*

Since the ground state of the core nucleus ^{6}Li(1^+) has an almost pure $S = 1, L = 0$ configuration, the energy spacing of the ${}^{7}_{\Lambda}$Li ground-state doublet $(3/2^+, 1/2^+)$ is a good measure of the strength of the spin–spin interaction. Before the Hyperball experiments, the hypernuclear doublet spacing, which is sensitive to the spin–spin interaction strength, was measured only for the $A = 4$ hypernuclei (the $(1^+, 0^+)$ spacing for ${}^{4}_{\Lambda}$H and ${}^{4}_{\Lambda}$He). However, since this spacing is expected to contain a large effect of the three-body ΛNN force [102,103], measurement of the hypernuclear doublet spacing in p-shell hypernuclei, such as ${}^{7}_{\Lambda}$Li in particular, was long awaited. In the phenomenological approach [7,8] a shell model calculation predicted the spacing to be 610 keV [8] using a spin–spin interaction parameter of $\Delta \sim 0.5$ MeV, which was estimated from the 1.1 MeV $A = 4$ doublet spacing and the ground-state binding energies of various p-shell hypernuclei. Another shell model calculation by Fetisov et al. [99], in which the parameter of $\Delta = 0.3$ MeV was chosen to explain the ${}^{10}_{\Lambda}$B result [94] rather than the $A = 4$ doublet spacing, gave 440 keV.

The Hyperball experiment (KEK E419) measured the ground-state doublet spacing of ${}^{7}_{\Lambda}$Li to be 691.7 ± 0.6(stat) ± 1.0(syst) keV. Since the ${}^{7}_{\Lambda}$Li doublet spacing is given by $\frac{3}{2}\Delta$ in the LS coupling limit of $S = 1, L = 0$, the experimental result corresponds to $\Delta \sim 0.5$ MeV. In a recent shell model calculation by Millener [53], the spacing is written as

$$E(3/2^+) - E(1/2^+) = 1.444\Delta + 0.054S_\Lambda + 0.016S_N - 0.271T, \tag{17}$$

and the parameter Δ was determined as 0.48 MeV as described in Section 5.10. The value was modified later to $\Delta = 0.43$ MeV by Millener [101], who took into account the ΛN–ΣN coupling effect, which gives a +0.071 MeV contribution to the spacing (see Section 5.10).

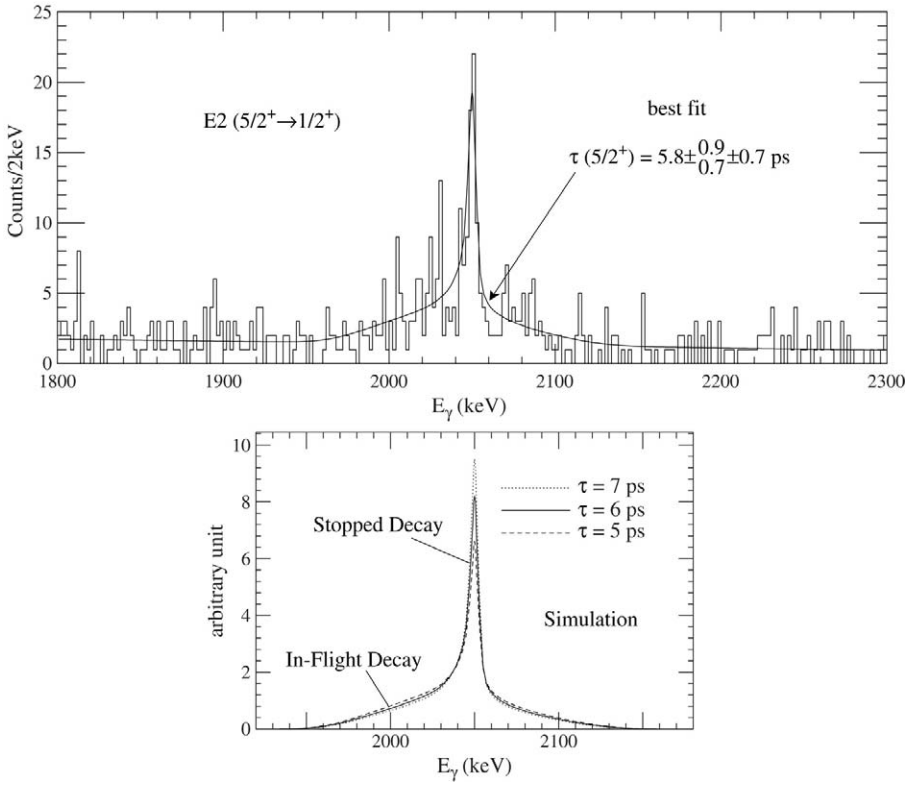

Fig. 51. ${}^{7}_{\Lambda}$Li γ-ray spectrum around the $E2(5/2^+ \rightarrow 1/2^+)$ peak at 2050 keV. The simulated peak shape is fitted to the spectrum to determine the experimental value of the lifetime: $5.8^{+0.9}_{-0.7}$(stat) $\pm$ 0.7(syst) ps. The simulated peak shapes for different lifetimes of the $5/2^+$ state are shown below.

Hiyama et al. [112] calculated the doublet spacing using an α–p–n–Λ cluster model and the Nijmegen model F interaction, in which the ΣN channel contribution is renormalized into ΛN interactions and the strength of the ΛN spin–spin interaction was adjusted to reproduce the 1.1 MeV $A = 4$ doublet spacing. They predicted a ${}^{7}_{\Lambda}$Li doublet spacing of 650 keV when the spin–orbit interaction is switched off. Thus, the experimental result on ${}^{7}_{\Lambda}$Li can be explained consistently with the $A = 4$ data.

The spin–spin interaction strength obtained from the ${}^{7}_{\Lambda}$Li$(3/2^+, 1/2^+)$ spacing gives a strong constraint to baryon–baryon interaction models as described in Section 5.10.

5.6.3. $B(E2)$ and the hypernuclear shrinking effect

Since the 2050 keV peak is partly broadened by Doppler shift as shown in Fig. 51 (top), the Doppler shift attenuation method can be applied to derive the lifetime of the $5/2^+$ state.

Fig. 51 (bottom) shows the simulated peak shape for various lifetimes. These curves were fitted to the experimental spectrum to obtain the lifetime as shown in Fig. 51 (top). The lifetime of the $5/2^+$ state was determined as $5.8^{+0.9}_{-0.7}$(stat) $\pm$ 0.7(syst) ps. This was

converted to a $B(E2)$ value of $3.6 \pm 0.5(\text{stat})^{+0.5}_{-0.4}(\text{syst})\ e^2\text{fm}^4$ using the branching ratio of $5/2^+ \to 1/2^+$ which is estimated to be $93.8^{+3.6}_{-0.8}\%$ [38]. This is the first measurement of a reduced transition probability in a hypernucleus.

This $B(E2)$ value is three times smaller than the $B(E2)$ of $10.9 \pm 0.9\ e^2\text{fm}^4$ for the corresponding transition in the core nucleus, $^6\text{Li}(3^+ \to 1^+)$. Now we turn to the size factor, which is defined as

$$S = \sqrt[4]{\frac{9}{7}\frac{B(E2;\ ^7_\Lambda\text{Li}(5/2^+ \to 1/2^+))}{B(E2;^6\text{Li}(3^+ \to 1^+))}}. \tag{18}$$

It will be unity if the ^{6}Li core in $^7_\Lambda$Li is the same as free ^{6}Li, but smaller than unity if the ^{6}Li core is contracted by the presence of the Λ hyperon. In a di-cluster model ($\alpha + d$ for ^{6}Li), S is proportional to the inter-cluster distance. The observed value is $S = 0.81 \pm 0.04$, which indicates a significant shrinkage of the ^{6}Li core in $^7_\Lambda$Li. A more detailed description is found in Ref. [38].

This shrinking effect was predicted by Motoba, Bandō, and Ikeda in 1983 [96] based on cluster model calculations to be a general property of light hypernuclei; inter-cluster distances of α–d, α–t, and α–α for $^7_\Lambda$Li, $^8_\Lambda$Li, and $^9_\Lambda$Be, respectively, were found to be contracted by about 20% in their calculations. According to a recent calculation with the α–p–n cluster model for ^{6}Li [100], which encouraged the $B(E2)$ measurement in $^7_\Lambda$Li, the measured $B(E2)$ reduction may be interpreted as contraction of the distance between the α cluster and the center of mass for p and n by $19 \pm 4\%$.

The phenomenon of nuclear shrinkage induced by a Λ hyperon has been experimentally confirmed. This is a good example of the "impurity effects" on nuclear structure that arise from the introduction of a Λ hyperon. It should be emphasized that effects of this type have become accessible experimentally as a consequence of the excellent resolution now achievable in γ spectroscopy.

5.6.4. Determination of the ground-state spin

Another important result on $^7_\Lambda$Li is the determination of its ground-state spin from the yield of the 429 keV ^{7}Be γ rays emitted after the weak decay of $^7_\Lambda\text{Li} \to {}^7\text{Be}^* + \pi^-$ [109]. When the bound-state region of $^7_\Lambda$Li is selected, the 429 keV γ-ray peak of ^{7}Be appears prominently, as shown in Fig. 49(b). From the yield of this γ ray, the branching ratio of the $^7_\Lambda$Li weak decay to ($^7\text{Be}^*(1/2)^-$, 429 keV) was obtained as $(6.0^{+1.3}_{-1.6}) \times 10^{-2}$. Because the non-spin-flip (parity-changing) amplitude is much larger than the spin-flip (parity-conserving) amplitude in the $\Lambda \to N\pi$ decay, the decay into $^7\text{Be}^*(1/2^-)$ occurs dominantly from the $1/2^+$ state of $^7_\Lambda$Li. The measured large branching ratio indicates that the weakly decaying ground state of $^7_\Lambda$Li has a spin of $1/2$ rather than $3/2$. Furthermore, the measured branching ratio agrees with the value calculated for spin $1/2((5.8 \pm 1.9) \times 10^{-2})$ but is an order of magnitude larger than the value calculated for spin $3/2((0.6 \pm 0.2) \times 10^{-2})$ [109].

5.6.5. $^7_\Lambda$Li γ rays from $^{10}\text{B}(K^-, \pi^-\gamma)$ (BNL E930('01))

More information on $^7_\Lambda$Li was obtained from $^{10}\text{B}(K^-, \pi^-\gamma)$ data taken in an experiment performed later at BNL (E930('01)). This experiment observed γ rays from

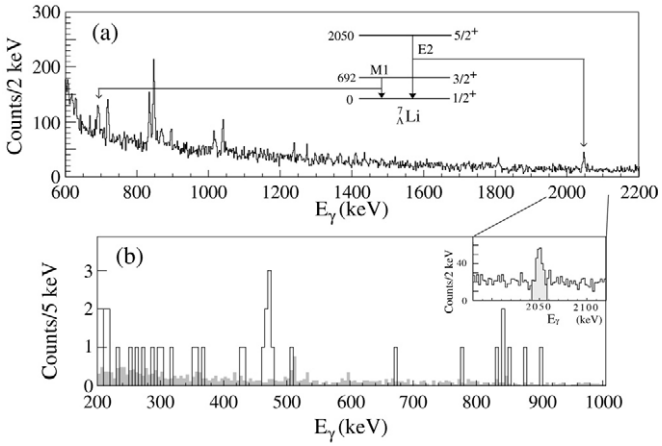

Fig. 52. (a) the γ-ray spectrum for the unbound region ($0 < -B_\Lambda < 40$ MeV) of ${}^{10}_{\Lambda}$B. Two γ-ray peaks from ${}^{7}_{\Lambda}$Li hyperfragments are observed. (b) the γ-ray spectrum in coincidence with the ${}^{7}_{\Lambda}$Li $E2(5/2^+ \rightarrow 1/2^+)$ γ-ray peak. This spectrum exhibits a significant peak at 471 keV. The shadowed histogram is a background spectrum obtained by gating a region above the $E2$ peak.

${}^{7}_{\Lambda}$Li produced as hyperfragments from highly excited states of ${}^{10}_{\Lambda}$B, presumably though the s-substitutional ${}^{10}_{\Lambda}$B (3^+, ~28 MeV excited) state decaying into ${}^{7}_{\Lambda}\mathrm{Li} + {}^{3}\mathrm{He}$ as shown in Fig. 47(e) [42,113]. The possibility of observing ${}^{7}_{\Lambda}$Li γ rays from ${}^{10}_{\Lambda}\mathrm{B}(3^+) \rightarrow {}^{7}_{\Lambda}\mathrm{Li} + {}^{3}\mathrm{He}$ decay was suggested in Ref. [98]. In the γ-ray spectrum with the unbound region of ${}^{10}_{\Lambda}$B ($0 < -B_\Lambda < 40$ MeV) selected (Fig. 52(a)), the $M1(3/2^+ \rightarrow 1/2^+)$ and $E2(5/2^+ \rightarrow 1/2^+)$ γ rays of ${}^{7}_{\Lambda}$Li were observed (see Fig. 47(c)). Then γ–γ coincidence was applied to the $E2$ γ ray; Fig. 52(b) is the spectrum of γ rays emitted in coincidence with the $E2$ γ-ray peak events (the shadowed region in the inset). A significant peak was observed at $470.8 \pm 1.9(\mathrm{stat}) \pm 0.6(\mathrm{syst})$ keV; it was assigned to the $M1(7/2^+ \rightarrow 5/2^+)$ transition (see Fig. 47(a)). The shadowed histogram in Fig. 52(b) is the background spectrum obtained by gating the region (2100–4000 keV) above the $E2$ peak. The $E2$ coincident spectrum is consistent with the background spectrum except for the 471 keV peak. This is the first successful application of the γ–γ coincidence method to hypernuclei.

The energy of the $(7/2^+, 5/2^+)$ spacing can be used as a consistency test for the spin-dependent interaction parameters. Because the core ${}^{6}\mathrm{Li}(3^+)$ has predominantly the $S = 1$, $L = 2$ configuration, the doublet $(7/2^+, 5/2^+)$ spacing is determined not only from the spin–spin interaction (Δ) but also from the Λ-spin-dependent spin–orbit interaction (S_Λ) and the tensor interaction (T) terms: $E(7/2^+) - E(5/2^+) = 1.29\Delta + 2.20S_\Lambda + 0.02S_N - 2.39T + \Lambda\Sigma$ [101]. By using the previously determined values of the parameters and the theoretically calculated $\Lambda\Sigma$ value (see Section 5.10) this equation gives 511 keV, close to the observed value [42]. A similar conclusion was also reached in Hiyama's cluster model calculation [112]. It predicted the spacing to be 80 keV when the spin–orbit interaction in the Nijmegen F model was assumed, and to be 560 keV when the spin–orbit interaction was switched off. Both calculations indicate that the spacing is explained consistently with the spin–spin interaction strength that reproduced the ${}^{7}_{\Lambda}\mathrm{Li}(3/2^+, 1/2^+)$ spacing and the

very small magnitude of the Λ-spin-dependent spin–orbit interaction strength determined from ${}^{9}_{\Lambda}$Be and ${}^{13}_{\Lambda}$C data (see the next section).

The change of the core level spacing (^{6}Li$(3^+, 1^+)$) in ${}^{7}_{\Lambda}$Li is a good measure of the nucleon-spin-dependent spin–orbit interaction strength (S_N). By taking the center of gravity for the $(7/2^+, 5/2^+)$ and $(3/2^+, 1/2^+)$ doublets, the level spacing between the two doublets was determined as 1858 keV. The value can be compared with the Millener shell model result [101] of

$$\overline{E(7/2^+, 5/2^+)} - \overline{E(3/2^+, 1/2^+)} = E({}^{6}\mathrm{Li}; 3^+) - E({}^{6}\mathrm{Li}; 1^+) - 0.05\Delta + 0.07S_\Lambda + 0.70S_N - 0.08T, \quad (19)$$

where $\overline{E(J_1, J_2)} = [(2J_1 + 1)E(J_1) + (2J_2 + 1)E(J_2)]/(2J_1 + 2J_2 + 2)$ denotes the center of gravity energy for the doublet (J_1, J_2). From this equation, S_N was determined as -0.43 MeV almost independently of the other three parameters [113].

5.7. ${}^{9}_{\Lambda}$Be *and* ${}^{13}_{\Lambda}$C — ΛN *spin–orbit interaction*

Investigation of the ΛN spin–orbit interaction is particularly important, because it is expected to provide clues to the understanding of the origin of the nuclear spin–orbit interaction, which is not well understood today. As described in Sections 3.3.3 and 3.4, some hypernuclear data suggest a very small spin–orbit splitting of Λ single-particle states, while other data suggest a much larger one. Thus, high-resolution data for specific hypernuclei such as ${}^{9}_{\Lambda}$Be and ${}^{13}_{\Lambda}$C, which provide the size of the Λ spin–orbit splitting and hence allow us to extract definite information on the ΛN spin–orbit interaction, have been of great interest.

5.7.1. ^{9}Be$(K^-, \pi^-\gamma)$ ${}^{9}_{\Lambda}$Be *experiment (BNL E930('98))*

In the case of ${}^{9}_{\Lambda}$Be, the energy spacing of the $(5/2^+, 3/2^+)$ doublet is mainly governed by the Λ-spin-dependent ΛN spin–orbit interaction (S_Λ) because the core ^{8}Be(2^+) state has an $L = 2$ configuration.

A γ-ray spectroscopy experiment for ${}^{9}_{\Lambda}$Be (BNL E930('98)) was carried out using the high-intensity, high-purity kaon beam available on the D6 beam line of the BNL-AGS [40]. Details of this experiment are described in Ref. [40]. ${}^{9}_{\Lambda}$Be hypernuclei were produced using the (K^-, π^-) reaction on ^{9}Be target at $p_{K^-} = 0.93$ GeV/c, and γ rays emitted from the hypernuclei were measured with Hyperball. The set-up of the experiment is shown in Fig. 53. It is almost identical to the previous experiments on the D6 beam line [114,39]. A beam line spectrometer (not shown in Fig. 53) and a dipole magnetic spectrometer with a large acceptance analyzed momenta of K^- and π^-, respectively, from which the mass spectrum of ${}^{9}_{\Lambda}$Be was obtained with a resolution of $\sim$15 MeV (FWHM). An 18.5 g/cm^2 ^{9}Be target was irradiated with a total of 1.9×10^{10} K^-. A severe γ-ray background due to π^0's from K^- decay in flight was effectively suppressed by the BGO counters.

Fig. 54 shows the γ-ray spectrum when the bound-state region ($-21 < -B_\Lambda < 4$ MeV) in the ${}^{9}_{\Lambda}$Be mass spectrum was selected and an event-by-event Doppler shift correction was applied. The structure observed at around 3.05 MeV in the spectrum without the Doppler shift correction (Fig. 3 in Ref. [40]) changed into two prominent peaks as shown in Fig. 54 when the Doppler shift correction was made [42]. The expected

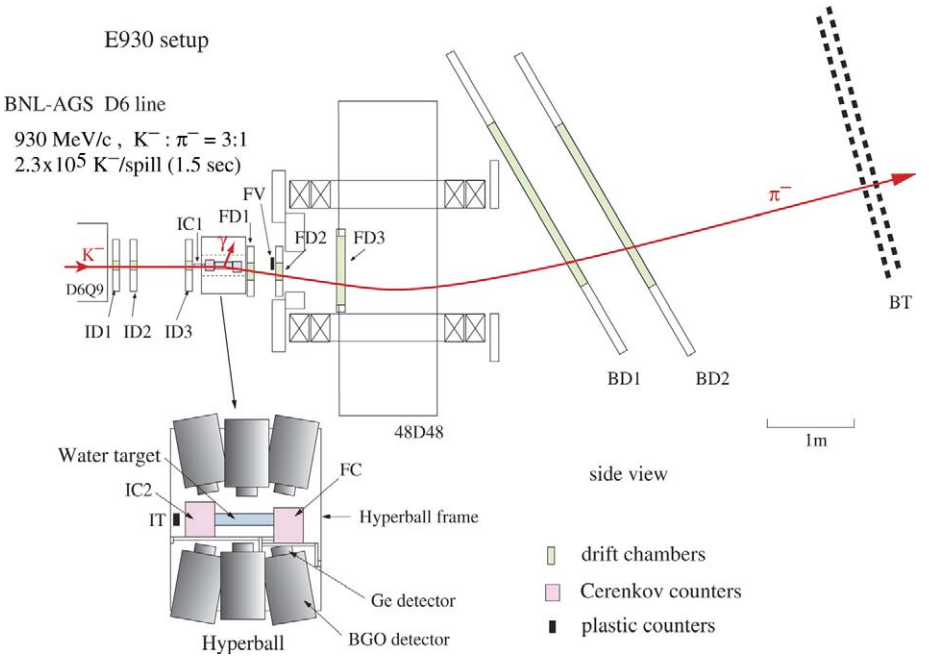

Fig. 53. The set-up of the hypernuclear γ spectroscopy experiment (E930) at the BNL-AGS. The beam spectrometer located upstream of the target is not shown.

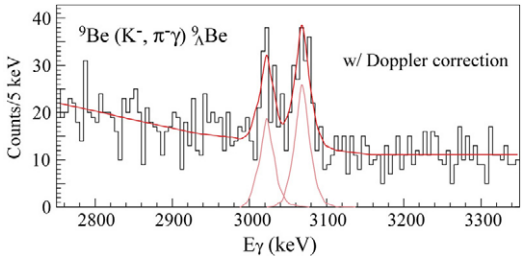

Fig. 54. The measured γ-ray spectrum of ${}^{9}_{\Lambda}$Be after Doppler shift correction [42]. The twin-peak structure was well fitted with a simulated peak shape for the Doppler shift correction for a short lifetime of $\tau < 0.1$ ps. The two peaks are assigned as the $E2(5/2^+, 3/2^+ \rightarrow 1/2^+)$ transitions.

peak shapes in the Doppler shift corrected spectrum were calculated by a simulation for various lifetimes of the excited state, taking into account inaccuracies in the Doppler shift correction. The observed peaks were well fitted to with the peak shape simulated for a short (<0.1 ps) lifetime. The peak energies were obtained as $3024 \pm 3 \pm 1$ and $3067 \pm 3 \pm 1$ keV. The peaks are assigned as the $E2(5/2^+ \rightarrow 1/2^+$ and $3/2^+ \rightarrow 1/2^+)$ transitions in ${}^{9}_{\Lambda}$Be (see Fig. 47(b)). The $(3/2^+, 5/2^+)$ doublet has a spacing of only 43 ± 5 keV. This is a typical example of hypernuclear fine structure.

5.7.2. ${}^{9}_{\Lambda}$Be γ rays from ^{10}B$(K^-,\pi^-\gamma)$ (BNL E930('01))

In the ^{9}Be$(K^-,\pi^-\gamma)\,{}^{9}_{\Lambda}$Be experiment, the spins of ${}^{9}_{\Lambda}$Be cannot be assigned because the production cross sections for the $5/2^+$ and $3/2^+$ states are almost equal. Later, the spin assignments were made successfully with the ^{10}B$(K^-,\pi^-\gamma)$ data taken in E930('01) [42]. In this experiment, the same ${}^{9}_{\Lambda}$Be γ rays were observed when the region of the excitation energy slightly higher than the ${}^{10}_{\Lambda}$B bound-state region was selected. The observed intensity of the upper energy peak (3067 keV) is larger than that of the lower peak. Considering the calculated production cross sections for ${}^{10}_{\Lambda}$B excited states and their predicted ${}^{10}_{\Lambda}\mathrm{B} \to {}^{9}_{\Lambda}\mathrm{Be} + p$ decay branching ratios [115,116], the production rate for the ${}^{9}_{\Lambda}$Be$(3/2^+)$ state is expected to be much larger than that for the ${}^{9}_{\Lambda}$Be$(5/2^+)$ state. Comparing this prediction with the data, the $3/2^+$ state is found to be the upper member of the doublet. This result determines the sign of the Λ-spin-dependent spin–orbit interaction parameter S_Λ to be negative, as described in the next paragraph. This sign is consistent with that given by the ${}^{13}_{\Lambda}$C data, as described below.

5.7.3. Λ-spin-dependent spin–orbit interaction from ${}^{9}_{\Lambda}$Be

According to a shell model calculation [101], the spacing is given by

$$E(3/2^+) - E(5/2^+) = -0.037\Delta - 2.464S_\Lambda + 0.003S_N + 0.994T + \Lambda\Sigma, \qquad (20)$$

where the ΛN–ΣN coupling effect (see Section 5.10) is estimated to be $\Lambda\Sigma = -0.008$ MeV. It is to be noted that the spacing is mainly determined by the S_Λ term but with a considerable contribution from the tensor term T. Since T was obtained as 0.03 MeV from the ${}^{16}_{\Lambda}$O data as described in Section 5.8, the observed ${}^{9}_{\Lambda}$Be spacing gives a Λ-spin-dependent spin–orbit strength with the negative sign and a very small magnitude, $S_\Lambda = -0.01$ MeV (see Section 5.10). It is found that both S_Λ and T terms additively produce spacing with almost equal contributions due to a very small magnitude of S_Λ. Implications of the result for S_Λ are discussed later, in Section 5.10.

5.7.4. ${}^{13}_{\Lambda}$C and Λ spin–orbit splitting (BNL E929)

The spin–orbit splitting of Λ single-particle states in hypernuclei is another good measure of the Λ-spin-dependent spin–orbit interaction. A BNL experiment (E929) was performed to investigate the spin–orbit splitting between $(p_{1/2})_\Lambda$ and $(p_{3/2})_\Lambda$ orbits in ${}^{13}_{\Lambda}$C by separately detecting the Λ inter-shell transition of $(p_{1/2})_\Lambda \to (s_{1/2})_\Lambda$ and $(p_{3/2})_\Lambda \to (s_{1/2})_\Lambda$ around 11 MeV (see Fig. 47(g)) [39].

The experiment was carried out at the AGS D6 beam line in 1998 prior to the ${}^{9}_{\Lambda}$Be run of E930, employing a large-volume NaI array that provided a much larger efficiency for 11 MeV γ rays than Hyperball. With the exception of the γ-ray detectors used, the experiment was almost identical to the ${}^{9}_{\Lambda}$Be experiment with Hyperball described above.

Bound states of ${}^{13}_{\Lambda}$C were populated using the 0.93 GeV/c ^{13}C(K^-,π^-) reaction. The K^- beam was incident on an active target made of a benzene liquid scintillator in which the carbon was 99%-enriched ^{13}C. The active target detected the energy deposited by hypernuclear weak decay; this provided a clean trigger free from K^- decay events. The ${}^{13}_{\Lambda}$C$(1/2^-)$ $[{}^{12}\mathrm{C}(0^+) \otimes (p_{1/2})_\Lambda]$ state, which is a substitutional $(\Delta L = 0)$ state in the (K^-,π^-) reaction, is populated at very forward angles ($\sim 4^\circ$), while the ${}^{13}_{\Lambda}$C$(3/2^-)$

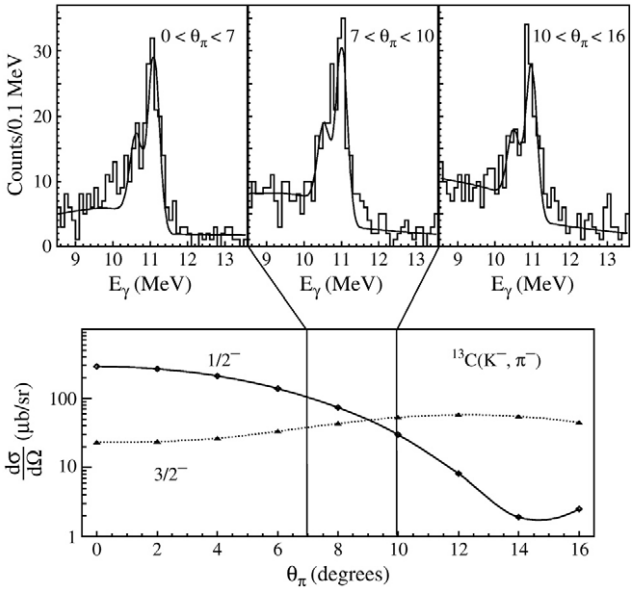

Fig. 55. The $^{13}_{\Lambda}$C γ-ray spectrum in the ^{13}C$(K^-, \pi^-\gamma)$ reaction for three different ranges of the π^- scattered angles. Differential cross sections of $1/2^-$ and $3/2^-$ states calculated by Motoba are shown also. Taken from Ref. [39].

$[^{12}\mathrm{C}(0^+) \otimes (p_{3/2})_\Lambda]$ state requires $\Delta L = 2$ and is populated at backward ($\theta \sim 13°$) angles. Using a magnetic spectrometer with a large angular acceptance (0°–16°), the $1/2^-$ and $3/2^-$ states were produced simultaneously without changing the spectrometer angle.

Fig. 55 shows the γ-ray spectra for three ranges of the π^- scattered angles θ_π ($0 < \theta_\pi < 7°$, $7° < \theta_\pi < 10°$ and $10° < \theta_\pi < 16°$) together with the calculated cross sections of the $1/2^-$ and $3/2^-$ states of $^{13}_{\Lambda}$C as a function of θ_π. It was found that the energy of the observed peak at 11 MeV shifts slightly as a function of θ_π. Combining this information with the calculated cross sections, the $E(1/2^-) - E(3/2^-)$ splitting was determined as $152 \pm 54 \pm 36$ keV as shown in Fig. 47(g). It is 20–30 times smaller than the $p_{1/2}$–$p_{3/2}$ spin–orbit splitting of ~5 MeV for nucleons.

In the Millener shell model calculation [53], the $^{13}_{\Lambda}$C splitting was estimated to be 107 keV from the strength of the Λ-spin-dependent spin–orbit interaction for the $p_N s_\Lambda$ wavefunction of $S_\Lambda = -0.013$ MeV. This indicates that the $^{9}_{\Lambda}$Be and $^{13}_{\Lambda}$C data consistently give a very small magnitude and negative sign for the Λ-spin-dependent spin–orbit interaction strength. It should also be noted that the tensor interaction makes a large contribution to both of the $^{13}_{\Lambda}$C and $^{9}_{\Lambda}$Be spacings, but with opposite signs.

5.8. $^{16}_{\Lambda}$O *and* $^{15}_{\Lambda}$N — *ΛN tensor interaction*

The ΛN tensor interaction can be investigated using measurements of the energy spacings of the ground-state doublets in $p_{1/2}$-shell hypernuclei such as $^{16}_{\Lambda}$O and $^{15}_{\Lambda}$N because these spacings have a large contribution from T [8]. Since one-pion exchange,

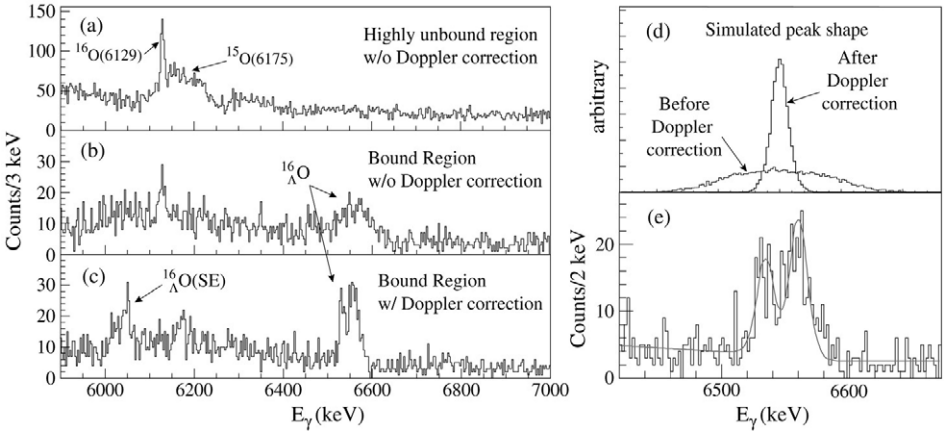

Fig. 56. $^{16}_{\Lambda}$O γ-ray spectra measured in the ^{16}O(K^-, π^-) reaction at the BNL-AGS (E930('01)). (a) Highly unbound region ($-B_\Lambda > 50$ MeV) is selected and the Doppler shift correction is not applied. (b) Bound-state region ($-17 < -B_\Lambda < 3$ MeV) is selected and the Doppler shift correction is not applied. A bump structure is observed around 6.55 MeV. (c) Spectrum (b) with a Doppler shift correction. A bump in (b) has turned into a twin-peak structure, which is ascribed to γ rays from $^{16}_{\Lambda}$O. (d) Simulated peak shapes for a fast γ transition before and after the Doppler shift correction. (e) The structure around 6.55 MeV in the $^{16}_{\Lambda}$O γ-ray spectrum (c) was fitted with two peaks of the simulated peak shape after the Doppler shift correction was applied.

which results in a large tensor interaction between nucleons, is forbidden between a Λ hyperon and a nucleon, the ΛN tensor interaction is naively expected to be small. However, kaon exchange and two-pion exchange through the ΛN–ΣN coupling are expected to make a significant contribution. It is interesting to examine whether the ΛN tensor interaction can be explained by meson-exchange models of baryon–baryon interactions.

5.8.1. $^{16}_{\Lambda}$O and the ΛN tensor interaction (BNL E930('01))

In 2001, $^{16}_{\Lambda}$O and $^{15}_{\Lambda}$N were studied with Hyperball using the ^{16}O(K^-, π^-) reaction (BNL E930('01)). See Ref. [41] for details. The set-up is almost identical to that of the previous $^{9}_{\Lambda}$Be experiment. Fig. 56 shows the γ-ray spectrum of $^{16}_{\Lambda}$O. When the bound-state region of $^{16}_{\Lambda}$O is selected, the γ-ray spectrum exhibits a broad bump at 6.55 MeV as shown in Fig. 56(b), while it is not seen in the spectrum for the highly unbound region (Fig. 56(a)). The bump becomes sharp peaks after event-by-event Doppler shift correction as shown in Fig. 56(c). In this reaction, only the 6 MeV-excited 1^- state and the 1^- state in the ground-state doublet are expected to be populated in the $^{16}_{\Lambda}$O bound states. Therefore, the observed 6.55 MeV peaks are attributed to the $M1(1^-_2 \rightarrow 1^-_1, 0^-)$ transitions of $^{16}_{\Lambda}$O. The width of the bump before the Doppler shift correction is consistent with the fully Doppler broadened peak width (Fig. 56(d)) which is expected for fast γ-ray emissions before the recoiling hypernucleus slows down. As shown in Fig. 56(e), the peaks in the Doppler corrected spectrum are fitted well with the simulated peak shape for fast transitions (Fig. 56(d)). This is also consistent with the expected short lifetime for a 6 MeV $M1$ transition ($\sim 10^{-15}$ s).

The γ-ray energies obtained from the fitting were: $6534.3 \pm 1.2(\text{stat}) \pm 1.7(\text{syst})$ keV and $6560.4 \pm 1.1(\text{stat}) \pm 1.7(\text{syst})$ keV. The spacing of the ground-state doublet was determined as $26.1 \pm 1.4(\text{stat}) \pm 0.6(\text{syst})$ keV. The excitation energy of the 1^-_2 state was found to be

6561.7 keV after the nuclear recoil correction was applied. Since the branching ratio of the $1_2^- \to 1_1^-$ to the $1_2^- \to 0^-$ decay is 1:2 in the weak-coupling limit between the Λ hyperon and the core, the γ-ray yield ratio of the two peaks gives the spin assignment of the doublet members as shown in Fig. 47(i).

With a shell model calculation by Millener, the spacing is described as [101]

$$E(1^-) - E(0^-) = -0.382\Delta + 1.378S_\Lambda - 0.004S_N + 7.850T - 0.014\ \text{MeV}. \quad (21)$$

where the constant term includes a Λ–Σ coupling effect of -30 keV and a small 1^- mixing effect of 16 keV. Using the other spin-dependent parameters determined from the ${}^{7}_{\Lambda}$Li and ${}^{9}_{\Lambda}$Be data, the value of T is derived as 0.03 MeV. It is found that the very small doublet spacing results from the cancellation of the contributions from the spin–spin interaction and the tensor interaction.

5.8.2. ${}^{15}_{\Lambda}$N γ *rays from* ^{16}O$(K^-, \pi^-\gamma)$ *(BNL E930('01))*

In the E930('01) experiment with an ^{16}O target, γ rays attributed to ${}^{15}_{\Lambda}$N transitions were also observed. The 11 MeV-excited $[(p_{1/2})_n^{-1}(p_{1/2})_\Lambda]_{0^+}$ state and the 17 MeV-excited $[(p_{3/2})_n^{-1}(p_{3/2})_\Lambda]_{0^+}$ state of ${}^{16}_{\Lambda}$O, which are substitutional states having large cross sections in the (K^-, π^-) reaction, are expected to decay to excited states of ${}^{15}_{\Lambda}$N by proton emission with sizable branching ratios, which is followed by emission of ${}^{15}_{\Lambda}$N γ rays [97].

When the region for these excited states is selected in the ${}^{16}_{\Lambda}$O mass spectrum, three γ rays were observed at around 1960, 2268, and 2442 keV. Since the 2268 keV peak is not Doppler broadened, it is assigned as the $1/2^+(T = 1) \to 3/2^+$ transition (see Fig. 47(h)), because the core transition of ^{14}N$(0^+(T = 1) \to 1_1^+(\text{g.s.}))$ is slow (68 fs lifetime). On the other hand, the two Doppler broadened γ rays of 1960 and 2442 keV are assigned as the transitions of $1/2_2^+ \to 1/2^+(T = 1)$ and $3/2_2^+ \to 1/2^+(T = 1)$, because the core transition of ^{14}N$(1_2^+ \to 0^+(T = 1))$ is fast (5 fs lifetime). Here, the spin ordering of the doublet $(3/2_2^+, 1/2_2^+)$ cannot be determined experimentally but the positive Δ value strongly suggests the $3/2_2^+$ state is the upper member of the doublet. Unfortunately, the $1/2^+(T = 1) \to 1/2^+$ transition was not observed, presumably because it has a small branching ratio, and so the ground-state doublet spacing could not be determined [42,116].

5.9. ${}^{10}_{\Lambda}$B *and* ${}^{11}_{\Lambda}$B *— consistency problems*

5.9.1. ${}^{10}_{\Lambda}$B *(BNL E930('01))*

The main purpose of the ^{10}B target run in E930('01) was to measure the energy spacing of the ${}^{10}_{\Lambda}$B ground-state doublet $(2^-, 1^-)$ by observing the spin-flip $M1$ transition $(2^- \to 1^-)$. Since the cross section of the 2^- state is considerable in the (K^-, π^-) reaction, the $M1$ transition can be observed if the level spacing is as large as predicted ($\sim$200 keV). On the other hand, if the spacing is smaller than $\sim$100 keV, the γ transition is overcome by weak decay. This transition was searched for but not observed in an old BNL experiment with Ge detectors [94]. This experiment set a limit for the level spacing as $E(2^-) - E(1^-) < 80$ keV, which is inconsistent with the value of $\Delta = 0.43$ MeV obtained from the ${}^{7}_{\Lambda}$Li$(3/2^+, 1/2^+)$ spacing. Therefore, more experimental studies on the ${}^{10}_{\Lambda}$B$(2^-, 1^-)$ spacing are of great importance.

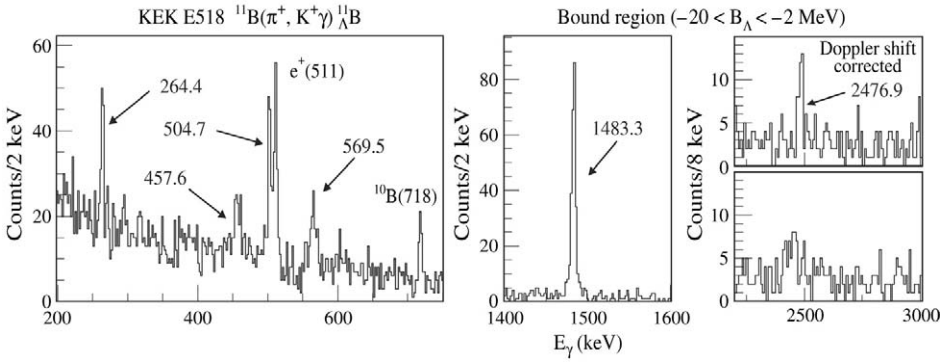

Fig. 57. The $^{11}_{\Lambda}$B γ-ray spectrum measured in the ^{11}B(π^+, K^+) reaction at KEK (E518). The bound-state region ($-20 < -B_\Lambda < -2$ MeV) in the $^{11}_{\Lambda}$B mass spectrum was selected. Six γ transitions at 264, 458, 505, 570, 1483, and 2477 keV were identified as γ rays from $^{11}_{\Lambda}$B. The 2477 keV peak was observed only in the Doppler shift corrected spectrum.

In the E930 experiment, a 99%-enriched ^{10}B target was irradiated with a K^- beam using the same set-up as the ^{16}O target run. In the $^{10}_{\Lambda}$B γ-ray spectrum with the bound-state region of $^{10}_{\Lambda}$B selected, no peak was observed in the energy range from 100 to 1 MeV. This result also implies that the 2^- state is higher than the 1^- state by 100 keV or less, or that the ordering of the spins in the doublet is reversed, although another experiment with higher sensitivity is necessary to completely confirm this result.

A recent calculation by Millener gives [101]

$$E(2^-) - E(1^-) = 0.579\Delta + 1.413S_\Lambda + 0.013S_N - 1.073T + \Lambda\Sigma, \tag{22}$$

where the ΛN–ΣN coupling effect is $\Lambda\Sigma = -0.015$ MeV. The experimental result of $E(2^-) - E(1^-) < 100$ keV gives $\Delta < 0.30$ MeV, which is in contradiction with the value of $\Delta = 0.48$ MeV (or 0.43 MeV obtained with the ΛN–ΣN coupling effect as shown in Section 5.10). This result suggests that further theoretical and experimental studies are necessary, particularly for the ΛN–ΣN coupling effect as investigated in Ref. [101].

5.9.2. $^{11}_{\Lambda}$B (KEK E518)

Structure of $^{11}_{\Lambda}$B was recently studied with Hyperball in the ^{11}B(π^+, $K^+\gamma$) $^{11}_{\Lambda}$B reaction at 1.05 GeV/c at the KEK-PS K6 beam line [44].

One of the purposes of this experiment was a consistency test of the ΛN spin-dependent interaction parameters that were determined from the $^{7}_{\Lambda}$Li, $^{9}_{\Lambda}$Be, and $^{16}_{\Lambda}$O experiments with Hyperball. The other purpose was to measure the transition probability $B(M1)$ of the Λ spin-flip $M1$ transition $^{11}_{\Lambda}$B($3/2^+ \rightarrow 1/2^+$) and to extract information on the magnetic moment of a Λ hyperon inside a nucleus as described in Section 5.3.

The experimental set-up was almost identical to that used in E419 [26,38]. The mass spectrum of $^{11}_{\Lambda}$B was measured with the K6 and SKS spectrometers, and γ rays were detected with Hyperball located around a 98.8%-enriched ^{11}B target (6–10 cm thick). The total irradiation was $1.6 \times 10^{12}\pi^+$ in one month.

Fig. 57 is the observed γ-ray spectrum for the bound-state region ($-20 < -B_\Lambda < -2$ MeV) in the ${}^{11}_{\Lambda}$B mass spectrum. By comparing it with the γ-ray spectrum for the highly unbound region ($20 < -B_\Lambda < 40$ MeV), six γ transitions were identified as coming from the bound-state region of ${}^{11}_{\Lambda}$B. They had energies of: $263.6 \pm 0.5 \pm 1.1$ keV, $457.6 \pm 1.2 \pm 1.1$ keV, $504.7 \pm 1.0 \pm 1.1$ keV, $569.5 \pm 0.5 \pm 1.1$ keV, $1483.3 \pm 0.2 \pm 0.7$ keV, and $2476.9 \pm 2.1 \pm 1.2$ keV. The 2479 keV peak was observed after the Doppler shift correction, while all of the other peaks were observed before the Doppler shift correction was made.

The 1483 keV γ transition was found to have a lifetime longer than 10 ps from the Doppler unbroadened peak width, and hence suggested to be an $E2$ transition. This transition was naively assigned to an $E2$ core transition corresponding to the 718 keV $E2(1^+ \to 3^+(\text{g.s.}))$ transition in ^{10}B (lifetime of 0.7 ns), most probably to the $E2(1/2^+ \to 5/2^+)$ transition [44]. In addition, the 1483 keV γ ray had the largest yield of all the observed ${}^{11}_{\Lambda}$B γ rays. According to the Millener shell model calculation [101, 115], the $E2(1/2^+ \to 5/2^+)$ transition has the largest yield and is the only transition with a lifetime longer than 10 ps. Therefore, this 1482 keV γ ray was identified as ${}^{11}_{\Lambda}\text{B}(1/2^+ \to 5/2^+)$. In Millener's calculation, the spacing is described as

$$E(1/2^+) - E(5/2^+) = 0.243\Delta - 1.090S_N + 1.234S_\Lambda - 1.627T + \Lambda\Sigma \qquad (23)$$

with $\Lambda\Sigma = 0.004$ MeV. Replacing the spin-dependent interaction parameters with the values obtained from the ${}^{7}_{\Lambda}$Li, ${}^{9}_{\Lambda}$Be and ${}^{16}_{\Lambda}$O levels (Eq. (24)), the spacing is estimated to be 1020 keV. This is significantly lower than the experimental value. If the inconsistency is ascribed to the value of S_N, we need $S_N = -0.9$ MeV, which is inconsistent with a broad variety of other hypernuclear data, such as the core excitation energies in ${}^{7}_{\Lambda}\text{Li}(E(7/2^+, 5/2^+) - E(3/2^+, 1/2^+))$, in ${}^{13}_{\Lambda}\text{C}(E(3/2^+) - E(1/2^+))$, and in ${}^{16}_{\Lambda}\text{O}\,(E(1_2^-) - E(1^-, 0^-))$. It is conjectured that the wavefunction of the core nucleus used in the shell model calculation must be examined.

Assignment of the other γ rays was difficult because of limited statistics and the small Ge detector efficiency in the present experiment which did not allow a γ–γ coincidence.

5.10. Discussion on ΛN spin-dependent interactions

5.10.1. Determination of the spin-dependent interaction strengths

Table 18 lists the results of the shell model calculations by Millener and the experimental data for the four hypernuclear level spacings that were used to determine the parameter values. From these four data sets, all of the ΛN spin-dependent interaction parameters have been determined as

$$\Delta = 0.48 \text{ MeV}, S_\Lambda = -0.01 \text{ MeV}, S_N = -0.43 \text{ MeV}, T = 0.03 \text{ MeV}. \qquad (24)$$

Although each parameter value was originally assumed to be constant through the whole p-shell nuclei, they may be slightly different as a function of the mass number because of a difference in the Λ wavefunction. This effect was estimated to be about $\pm 10\%$ [53]. Eq. (24) shows the values for ${}^{7}_{\Lambda}$Li.

Recently, Millener estimated the ΛN–ΣN coupling effect for a Λ (Σ) hyperon in the s orbit and nucleons in the p orbit [101], assuming the ΛN–ΣN coupling force based on the

Table 18
Energies of the four hypernuclear level spacings that are described in terms of the spin-dependent ΛN interaction parameters obtained by Millener's shell model calculations [101]

Hypernuclear levels		Shell model calculation by Millener	$\Lambda\Sigma$ (MeV)	Exp. (MeV)
${}^{7}_{\Lambda}$Li	$E(3/2^+) - E(1/2^+)$	$1.444\Delta + 0.054S_\Lambda + 0.016S_N - 0.271T$	+0.071	0.692
${}^{7}_{\Lambda}$Li	$\overline{E(7/2^+, 5/2^+)}$	$-0.05\Delta + 0.07S_\Lambda + 0.70S_N - 0.08T$		1.858
	$-\overline{E(3/2^+, 1/2^+)}$[a]	$+\Delta E_{\rm core}$[b]		
${}^{9}_{\Lambda}$Be	$E(3/2^+) - E(5/2^+)$	$-0.037\Delta - 2.464S_\Lambda + 0.003S_N + 0.994T$	−0.008	0.043
${}^{16}_{\Lambda}$O	$E(1^-) - E(0^-)$	$-0.382\Delta + 1.378S_\Lambda - 0.004S_N + 7.850T$	−0.014[c]	0.026

Experimental energies obtained by the Hyperball experiments are also shown. The effect of the Λ–Σ coupling estimated by Millener is listed as $\Lambda\Sigma$.

[a] $\overline{E(J_1, J_2)} = [(2J_1 + 1)E(J_1) + (2J_2 + 1)E(J_2)]/(2J_1 + 2J_2 + 2)$ denotes the center of gravity energy for the doublet (J_1, J_2).

[b] $\Delta E_{\rm core} = E({}^{6}{\rm Li}; 3^+) - E({}^{6}{\rm Li}; 1^+) = 2.186$ MeV.

[c] A small 1^- mixing effect of 0.016 MeV is added to a Λ–Σ coupling effect of −0.030 MeV.

NSC97f interaction, which reproduces the s-shell hypernuclear level energies well [103]. This Λ–Σ coupling effect was found to be small for the p-shell hypernuclear levels as shown in Table 18. The parameters in Eq. (24) were derived without considering the Λ–Σ coupling effect, but when taking this effect into account, only the parameter Δ needs to be slightly modified (from 0.48 to 0.43 MeV) and the others are almost unchanged.

5.10.2. Spin–spin interaction

Let us compare these parameter values with theoretical predictions by various versions (ND, NF, NSC89, NSC97, etc.) of the Nijmegen meson-exchange interaction models through G-matrix calculation [88]. The Nijmegen models cannot predict the spin–spin interaction; the NSC97 interaction was modified into various versions (NSC97a–f) so as to give different strengths of the spin–spin interaction. The experimental value of Δ is between the values for NSC97e and NSC97f. This result is consistent with the conclusion given by comparison between few-body calculations and experimental data for s-shell hypernuclei [103].

5.10.3. Spin–orbit interaction

It is found that the ΛN spin–orbit interaction cannot be explained by meson-exchange models. In terms of S_Λ and S_N, the Nijmegen meson-exchange model interactions give $-0.18 < S_\Lambda < -0.13$ MeV and $-0.29 < S_N < -0.26$ MeV, values that are inconsistent with the experimental values in Eq. (24). This conclusion is also derived from the cluster model calculations of Hiyama et al. [117], which predicted a spacing of 80–200 keV for ${}^{9}_{\Lambda}$Be$(3/2^+, 5/2^+)$ and 0.39–0.96 MeV for ${}^{13}_{\Lambda}$C$(1/2^-, 3/2^-)$ using several versions of the Nijmegen potential. In both cases, the meson-exchange models predict level spacings several times larger than the observed value.

The very small value of $|S_\Lambda|$ and the large value of $|S_N|$ indicate that the symmetric LS force ($\propto \boldsymbol{l}_{\Lambda N}(\boldsymbol{s}_\Lambda + \boldsymbol{s}_N)$) and the antisymmetric LS force ($\propto \boldsymbol{l}_{\Lambda N}(\boldsymbol{s}_\Lambda - \boldsymbol{s}_N)$) between a Λ hyperon and a nucleon have comparably large magnitudes but opposite signs, and

they almost cancel in S_Λ. This situation is consistent with a quark model prediction, where the Λ-spin-dependent ΛN spin–orbit interaction has a very small magnitude due to the cancellation of the symmetric and antisymmetric LS forces [118]. Actually, Hiyama suggested [117] that the quark model based LS force can reproduce the observed small splittings in ${}^{9}_{\Lambda}$Be and ${}^{13}_{\Lambda}$C. However, a recent calculation by Fujiwara with the quark model based LS force together with meson-exchange forces cannot reproduce the small spacing of ${}^{9}_{\Lambda}$Be [119]. More theoretical studies are necessary to understand the origin of the spin–orbit force.

5.10.4. Tensor interaction

In contrast, the meson-exchange picture seems to work well for the ΛN tensor interaction. The Nijmegen interactions predict a value $0.018 < T < 0.054$ MeV, which is in broad agreement with the experimental value. Moreover, considering ambiguities in the other parameters, the experimental value of T is rather accurately determined as 0.024–0.030 MeV [116]. It provides a constraint on the meson-exchange models.

5.10.5. Consistency test

The parameter set shown in Eq. (24) can also explain most of the other data for p-shell hypernuclei obtained in recent γ-spectroscopy experiments. As already discussed in Section 5.6, the ${}^{7}_{\Lambda}\mathrm{Li}(7/2^+, 5/2^+)$ spacing (Fig. 47(c)) is reproduced well with the Δ, S_Λ and T values in Eq. (24). The ${}^{16}_{\Lambda}\mathrm{O}(1^-_2, 1^-_1)$ (Fig. 47(i)) and ${}^{13}_{\Lambda}\mathrm{C}(3/2^+, 1/2^+)$ (Fig. 47(g)) spacings, which are essentially core excitation energies determined by S_N, are also explained by the value of $S_N \sim -0.4$ MeV [53,115,116].

Among all the level energies in Fig. 47, the ${}^{10}_{\Lambda}\mathrm{B}(2^-, 1^-)$ and the ${}^{11}_{\Lambda}\mathrm{B}(1/2^+, 5/2^+)$ spacings cannot be consistently explained by the parameter set. This indicates that further experimental and theoretical efforts are necessary to completely understand the ΛN interaction and hypernuclear structure. In particular, the ΛN–ΣN coupling effect in hypernuclei, which is estimated at present assuming the NSC97f interaction, must be investigated further.

5.11. Inclusive γ spectroscopy of hyperfragments

As described in Section 5.4, inclusive γ-ray measurements of hyperfragments in the stopped K^- absorption reaction, which is known to produce various hyperfragments with large production yields, are expected to be an effective method for studying γ rays from various hypernuclei.

In 2002, an experiment using this method was attempted with Hyperball at the KEK-PS (E509) (see Ref. [43] for details). A 650 MeV/c K^- beam from the K5 beam line was degraded and then stopped on several light targets (^{7}Li, ^{9}Be, ^{10}B, ^{11}B, and ^{12}C). Hyperball, which was installed around the target, measured γ rays using the $(K^-_{\mathrm{stopped}}, \gamma)$ trigger. The following criteria were used to search for candidates of hypernuclear γ rays: (1) The γ-ray energy does not agree with any of the known γ rays in all the normal nuclei with a mass number lighter than the target mass number. (2) The γ-ray timing is prompt, being faster than that of background γ rays from fast-neutron induced reactions. (3) The yield of the γ ray has a target dependence. In particular, if the unknown γ ray is observed in the target

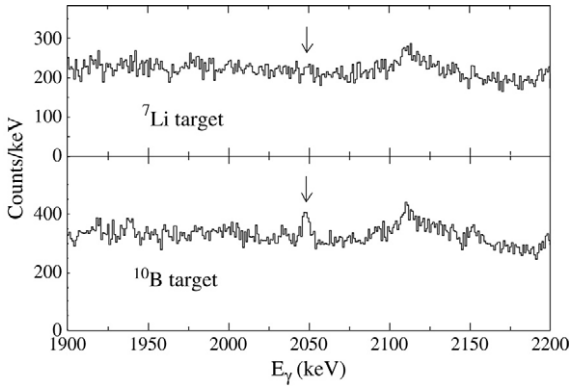

Fig. 58. Spectra of γ rays in the $(K^-_{\rm stop}, \gamma)$ reaction on ^{7}Li and ^{10}B targets. The 2050 keV γ ray from $^7_\Lambda$Li is abundantly observed in the ^{10}B target spectrum.

with the mass number A and heavier than A but never observed in the targets lighter than A, it is a candidate for a hypernuclear γ ray from a hyperfragment with a mass number smaller than A.

In this experiment, two γ-ray peaks that satisfied these criteria were found at 2049.4 ± 0.6 keV and 1302.9 ± 0.6 keV. The 2049 keV γ ray was observed in the ^{10}B, ^{11}B, and ^{12}C target spectra (see Fig. 58). From its energy, it is attributed to the $^7_\Lambda$Li$(5/2^+ \to 1/2^+)$ transition at 2050 keV (Fig. 47(c)). The yield of this γ ray for the ^{10}B target is very large (500 counts in 3.5 days' beam time), suggesting the effectiveness of this method. The production rate of the $^7_\Lambda$Li$(5/2^+)$ state is derived as $0.075 \pm 0.016\%$ per stopped K^- on ^{10}B target.

The 1303 keV γ ray was observed in the ^{9}B, ^{10}B, and ^{11}C target spectra. It is a candidate for being an unknown hypernuclear γ ray, presumably from an $A = 8$ hyperfragment.

This method would be powerful with a larger Ge detector array, where the use of the γ–γ coincidence technique would allow both efficient detection of hypernuclear γ rays and their assignments.

5.12. Future plans

Further experiments on hypernuclear γ-ray spectroscopy are planned at the KEK-PS and the BNL-AGS, and will be a major program at the 50 GeV high-intensity proton synchrotron facility, J-PARC.

The series of Hyperball experiments have clarified each strength of the spin-dependent terms in the ΛN interaction. However, the existence of some hypernuclear data that cannot be explained consistently with the other data suggests more experimental information is necessary. One of the most important hypernuclei to study is $^{12}_\Lambda$C, because the ground-state doublet of $^{12}_\Lambda$C$(2^-, 1^-)$ has a structure similar to $^{10}_\Lambda$B$(2^-, 1^-)$, but the effect of the Λ–Σ coupling on the doublet spacing is expected to be opposite to that in $^{10}_\Lambda$B at least in the context of calculations using NSC97f interaction [115]. Thus, $^{12}_\Lambda$C data could solve the inconsistency problem of $^{10}_\Lambda$B. An experiment for $^{12}_\Lambda$C hypernucleus is planned at

KEK [120] with Hyperball2, an upgraded version of Hyperball having twice the efficiency of Hyperball. In the ${}^{12}_{\Lambda}$C experiment, it may be also possible to measure the $B(M1)$ for the Λ spin-flip transition between the ground-state doublet members ($7/2^+ \rightarrow 5/2^+$) of ${}^{11}_{\Lambda}$B, where the ${}^{11}_{\Lambda}$B($7/2^+$) state is produced by proton emission from the p_Λ states of ${}^{12}_{\Lambda}$C.

After 2007, intense and pure K^- beams from the 50 GeV proton synchrotron at J-PARC will be available; a program of high-precision γ-ray spectroscopy of Λ hypernuclei is planned as one of the laboratory's main projects on strangeness nuclear physics. The proposed experiments are listed below, and details are described in Ref. [121].

(1) Complete study of light ($A < 30$) Λ hypernuclei with the (K^-, π^-) reaction: (1-a) Survey experiment for all possible target nuclei. (1-b) Detailed study with measurements of angular correlation, γ-ray polarization, $B(E2)$, etc. for several important hypernuclei.
(2) Systematic study of medium and heavy Λ hypernuclei with the (K^-, π^-) reaction.
(3) Study of hyperfragments including neutron-rich hypernuclei with in-flight or stopped K^- beams.
(4) Study of neutron-rich and mirror hypernuclei with the (K^-, π^0) reaction.
(5) $B(M1)$ measurements with the (K^-, π^-) and (π^+, K^+) reactions using the Doppler shift attenuation method.
(6) $B(M1)$ measurements using the γ–weak coincidence method.
(7) Spectroscopy of Ξ^-–atomic X rays and double Λ hypernuclei using the (K^-, K^+) reaction.

In many of these experiments, the (K^-, π) reaction at both of 1.1 and 0.8 GeV/c will be used. The 1.1 GeV/c (K^-, π^-) reaction has a large spin-flip amplitude, while the 0.8 GeV/c (K^-, π^-) reaction has no spin-flip amplitude. Therefore, comparison of these two γ-ray spectra, together with the γ–γ coincidence method, will greatly strengthen our ability to determine the level scheme of the hypernuclei produced.

The initial program will include a systematic study of p- and sd-shell hypernuclei with all available targets with $A < 30$. For some important hypernuclei such as ${}^{12}_{\Lambda}$C, ${}^{20}_{\Lambda}$Ne, and ${}^{28}_{\Lambda}$Si, extensive data will be taken to measure the angular correlations between γ and π^-, γ-ray polarizations, and the $B(E2)$ values. These data will allow the assignments of the spin parity of the observed states and will provide information on hypernuclear sizes.

The second phase of the program will be the study of medium and heavy hypernuclei, where the most interesting data is expected to be the inter-shell $E1(p_\Lambda \rightarrow s_\Lambda)$ transitions, which provide information on the p-wave ΛN interaction. In order to study neutron-rich hypernuclei, mirror hypernuclei, and other hypernuclei that cannot be produced by the (K^-, π^-) reaction, it is planned to use the (K^-, π^0) reaction as well as hyperfragment production from in-flight or stopped K^- beams. In neutron-rich nuclei, the introduction of a Λ hyperon is expected to induce a drastic change of structure, which can be investigated by $B(E2)$ measurements.

The systematic study of the Λ spin-flip $B(M1)$ for a wide mass range of hypernuclei is another important subject. Spin-flip states of the doublets are produced by the (K^-, π^-) reaction at 1.1 GeV/c, and $B(M1)$ values will be measured using the Doppler shift attenuation method and the γ–weak coincidence method (see Section 5.4.1). By use

of the (K^-, K^+) reaction, Ξ^--atomic X rays for various atomic numbers will be studied to investigate the ΞN interaction. One of the ultimate goals at J-PARC is the γ spectroscopy of double Λ hypernuclei by the (K^-, K^+) reaction, which will provide detailed information on the $\Lambda\Lambda$ interaction and is expected to reveal larger shrinking effects induced by the presence of two Λ hyperons.

In these experiments at J-PARC, Ge detectors will suffer from much more radiation due to the high beam intensity. In the present Hyperball, the beam (pion + kaon) intensity is limited to 3×10^6 particle/s by the readout electronics of the Ge detectors (with the detectors located 15 cm from the target). R&D studies are in progress, aimed at developing a faster detector system that will allow us to increase the limit by a factor of 5 or more so that the full K^- beam at J-PARC can be accepted. Construction of "Hyperball-J", a new, larger Ge detector array using a faster readout method combined with faster background suppression counters, is proposed for J-PARC experiments.

6. Prospects of Λ hypernuclear spectroscopy

Several experimental programs on Λ hypernuclear spectroscopy are running and others are planned currently.

At JLab, the second-generation $(e, e'K^+)$ spectroscopy study for a wide variety of Λ hypernuclei is in progress, as described in Section 4.3, using the recently constructed high-resolution kaon spectrometer (HKS) in Hall C. It will achieve a high resolution (0.3–0.4 MeV FWHM), about 60 times higher hypernuclear yield rates, significantly suppressing backgrounds compared with the previous $(e, e'K^+)$ experiment in Hall C [27]. The first experiment with the new spectrometer system is planned in 2005 for ^{12}C, ^{28}Si and other targets. These will be followed by spectroscopic studies of various light to medium-heavy hypernuclei. In Hall A at JLab, another experiment has been also running using the High-Resolution Spectrometer (HRS) pair and a septum magnet to investigate the spectroscopy of light hypernuclei with a comparable resolution [122]. In Mainz, the electron accelerator upgraded to 1.5 GeV, MAMI-C, will be used for $(e, e'K^+)$ spectroscopy with the KAOS spectrometer in the near future [123].

At the DAΦNE facility, the FINUDA experiment has started Λ hypernuclear spectroscopy by the $(K^-_{\rm stop}, \pi^-)$ reaction [124], using low-momentum K^-'s which are emitted in the decay of ϕ mesons produced in e^-e^+ collisions. Since the K^- is monochromatic and has momentum of only 127 MeV/c, a thin target ($\sim$0.3 g/cm^2 $^{12}_{\Lambda}$C) can stop all the K^-'s. Consequently the hypernuclear mass resolution, which is usually limited by energy loss of π^- in a thick target in this reaction, can be improved to sub-MeV FWHM. With an improved luminosity, the study of neutron-rich hypernuclei by the $(K^-_{\rm stop}, \pi^+)$ reaction and γ-ray spectroscopy will be also possible [125].

The KEK-PS, which has played a leading role in the (π^+, K^+) spectroscopy and γ spectroscopy of Λ hypernuclei, will be succeeded by the 50 GeV high-intensity proton synchrotron under construction at J-PARC in Tokai, Japan. At J-PARC, high-precision hypernuclear γ spectroscopy is one of the main nuclear physics programs in the first stage (see Ref. [121] for details). Various hypernuclei in a wide mass number range (from $A = 4$ to 208) will be studied mainly using the (K^-, π^-) reaction. Intense K^- beams and the

further upgraded Hyperball will allow us to explore subjects now beyond reach, such as making a systematic study of the spin-flip $B(M1)$ transitions for various hypernuclei, a study of impurity effects including neutron-rich hypernuclei. γ spectroscopy of double Λ hypernuclei is also planned [121]. The program of (π^+, K^+) reaction spectroscopy with the SKS spectrometer will be extended to the (K^-, K^+) reaction, permitting spectroscopic study of Ξ hypernuclei with the upgraded SKS; this program will also provide information on the ΞN interaction [121]. Another plan at J-PARC is the high-resolution (π^+, K^+) reaction using its high-resolution GeV pion beam line, which is under design to have a momentum dispersive focal plane at the target (similar to what was used for the EPICS spectrometer at LAMPF). (π^+, K^+) spectroscopy with high resolution ($\sim$0.3 MeV FWHM) can be conducted without the need to track beam particles [126]. This high-resolution pion beam line will be used not only for the study of Λ hypernuclei using the (π^+, K^+) reaction but also for the study of neutron-rich hypernuclei and Coulomb-assisted bound states of Σ hypernuclei by the (π^-, K^+) reaction [127]. These experiments by the hadronic reactions will be complimentary to those to be carried out using the $(e, e'K^+)$ reaction at the electron accelerator facilities.

At GSI, the new accelerator facility will also have a substantial program of hypernuclear physics. An experiment of γ-ray spectroscopy of double Λ hypernuclei produced by an antiproton beam via $\Xi\overline{\Xi}$ production is proposed [123].

All these programs of hypernuclear physics form synergetic efforts for the investigation of strangeness nuclear physics.

7. Summary

Recent progress has demonstrated the power of hypernuclear reaction spectroscopy and γ-ray spectroscopy. We have learned that hypernuclear spectroscopy is indispensable for the quantitative investigation of the Λ hypernuclear structure and the ΛN interaction.

(π^+, K^+) reaction spectroscopy with the SKS spectrometer established the value of hypernuclear spectroscopy. Thanks to the good resolution (1.5–2 MeV FWHM) and the high detection efficiency, good-quality spectra were obtained for a wide range of excitation energies and a wide mass region of Λ hypernuclei ($^{7}_{\Lambda}$Li, $^{9}_{\Lambda}$Be, $^{10}_{\Lambda}$B, $^{12}_{\Lambda}$C, $^{13}_{\Lambda}$C, $^{16}_{\Lambda}$O, $^{28}_{\Lambda}$Si, $^{51}_{\Lambda}$V, $^{89}_{\Lambda}$Y, $^{139}_{\Lambda}$La, $^{208}_{\Lambda}$Pb).

In the p-shell region, high-statistics excitation spectra were measured using the (π^+, K^+) reaction and compared with recent DWIA calculations based on advanced phenomenological ΛN interactions and shell model wavefunctions. For $^{12}_{\Lambda}$C, $^{13}_{\Lambda}$C and $^{16}_{\Lambda}$O, both the excitation function and the angular distributions of the kaons were measured and compared with the DWIA calculations. The general features of the excitation spectra were well reproduced by the calculations. Core excited states of $^{12}_{\Lambda}$C, which were observed for the first time in the high-quality (π^+, K^+) spectrum, provided new information on hypernuclear structure and a good testing ground for further investigation of both hypernuclear structure and ΛN interactions. Genuine hypernuclear states were clearly observed in $^{9}_{\Lambda}$Be and interpreted using cluster models and shell models. The spin–orbit splitting of a Λ hyperon was found to be very small from the $^{16}_{\Lambda}$O spectrum, consistent with the recent hypernuclear γ-ray data. For heavy Λ hypernuclei, the spectral structure

was discussed taking into account various neutron hole excitations of the core nucleus. The hypernuclear mass dependence of Λ binding energies was derived for each single-particle orbit in a wide mass range from light Λ hypernuclei in the p-shell region to heavy hypernuclei (up to $^{208}_{\Lambda}$Pb). It revealed that, to first order, a Λ hyperon keeps its identity as a baryon even in the deeply bound states of heavy Λ hypernuclei. Information on the properties of the Λ nuclear potential was also obtained.

Λ hypernuclear spectroscopy using the $(e, e'K^+)$ reaction has great potential for the quantitative investigation of strangeness nuclear physics in the $S = -1$ sector. The JLab E89-009 experiment was the first that succeeded in measuring a $^{12}_{\Lambda}$B spectrum by means of the $(e, e'K^+)$ reaction with sub-MeV resolution. The measured spectrum was reasonably well described by a DWIA calculation, and demonstrated the feasibility of $(e, e'K^+)$ reaction spectroscopy. Based on a thorough examination of data obtained during the E89-009 experiment, a new experiment (E01-011), which intends to extend precision spectroscopy beyond the p-shell region and to reveal behavior of a Λ hyperon in a nuclear medium, was proposed. The experiment starts data taking in 2005. A high-resolution kaon spectrometer (HKS), which has a large solid angle, has been installed in JLab Hall C. The new experimental configuration based on the new "tilt method" with the HKS spectrometer provides an opportunity for measuring high-quality hypernuclear mass spectra with significantly better resolution and with statistics comparable to (π^+, K^+) reaction spectroscopy.

Hypernuclear γ-ray spectroscopy with the Ge detector array Hyperball, which is capable of detecting γ rays with a few keV resolution in an environment with a very high count rate, has recently demonstrated that "precision spectroscopy" is now available for hypernuclei. Bound states in various p-shell hypernuclei (such as $^{7}_{\Lambda}$Li, $^{9}_{\Lambda}$Be, $^{10}_{\Lambda}$B, $^{11}_{\Lambda}$B, $^{15}_{\Lambda}$N and $^{16}_{\Lambda}$O) have been investigated and the ΛN spin-dependent interactions have been studied from their level structure. In particular, the strengths of the spin–spin force, the Λ-spin-dependent spin–orbit force, the N-spin-dependent spin–orbit force and the tensor force in the ΛN effective interaction were successfully determined from the $^{7}_{\Lambda}$Li$(3/2^+, 1/2^+)$, $^{9}_{\Lambda}$Be$(3/2^+, 5/2^+)$, $^{7}_{\Lambda}$Li$(7/2^+, 5/2^+, 3/2^+, 1/2^+)$ and $^{16}_{\Lambda}$O$(1^-, 0^-)$ spacings, respectively. The hypernuclear shrinking effect was confirmed experimentally from the $B(E2)$ value in $^{7}_{\Lambda}$Li measured by the Doppler attenuation method. In addition, the spin–orbit splitting was observed in $^{13}_{\Lambda}$C by detecting the $\Lambda p_{1/2}$, $p_{3/2} \rightarrow s_{1/2}$ inter-shell transitions with an array of NaI detectors. The very small magnitude of the Λ-spin-dependent spin–orbit force was thus confirmed with the $^{13}_{\Lambda}$C and $^{9}_{\Lambda}$Be data. Further upgrading of the Ge detector system that has much higher detection efficiency is under way. With this improvement it should be possible to obtain crucial information, particularly on the spin-dependent ΛN interaction.

Major new facilities for hypernuclear spectroscopy are nearing completion at DAΦNE FINUDA, MAMI-C, GSI PANDA and J-PARC 50 GeV in addition to the JLab hypernuclear facility. These facilities will be the "home ground" for the next generation of hypernuclear spectroscopy. With these experimental facilities and opportunities, we foresee a bright future for the spectroscopy of Λ hypernuclei and beyond, which will offer key data on the hadronic matter with a strangeness degree of freedom.

Acknowledgements

The experiments with the SKS spectrometer were carried out under the KEK-PS SKS collaboration and those by the $(e, e'K^+)$ reaction under JLab E89-009 and E01-011 collaboration. A series of γ-ray spectroscopy experiments were conducted under Hyperball collaboration. The authors deeply thank the collaborators for their efforts and useful discussions, in particular, Profs. S. Homma, S. Kato, T. Nagae, H. Noumi, T. Takahashi, T. Fukuda, E. Hungerford, L. Tang, J. Reinhold, S.N. Nakamura, K. Imai, T. Kishimoto, M. May, S.H. Zhou and Drs. T. Hasegawa, Y. Fujii, T. Endo, H. Hotchi, T. Miyoshi, S. Ajimura, K. Tanida, H. Akikawa, R.E. Chrien, M. Ukai and Y. Miura. We are also grateful to Prof. T. Yamazaki as the director of Institute for Nuclear Study (INS), University of Tokyo, and Prof. K. Nakai as the head of the office of KEK experiment planning and program coordination for their support at the earlier stage of this research program. Discussions on the theoretical aspects of Λ hypernuclear spectroscopy with Profs. T. Motoba, K. Itonaga, E. Hiyama and Drs. D.J. Millener, M. Sotona and P. Bydzovski were also indispensable to the present work. We are very grateful to Prof. L. Cardman for a critical reading of the manuscript. The program is partly supported by the Specially Promoted Program (12002001), Creative Research Program (16GS0201), Scientific Research on Priority Areas (08239102) and Basic Research (09304028, 09554007, 11440070, 15204014) of Grant-in-Aid from the MEXT, Japan and US–Japan Collaborative Research Program of Japan Society for the Promotion of Science.

References

[1] B. Povh, Prog. Part. Nucl. Phys. 18 (1987) 183.
[2] R. Chrien, C. Dover, Ann. Rev. Nucl. Part. Sci. 39 (1989) 113.
[3] H. Bandō, T. Motoba, J. Žofka, Intermat. J. Modern Phys. 21 (1990) 4021.
[4] M.M. Nagels et al., Phys. Rev. D 15 (1977) 2547; Phys. Rev. D 20 (1979) 1633;
P.M. Maessen et al., Phys. Rev. C 40 (1989) 2226;
Th.A. Rijken, V.G.J. Stokes, Y. Yamamoto, Phys. Rev. C 59 (1999) 21.
[5] B. Holzenkamp et al., Nuclear Phys. A 500 (1989) 458;
K. Holinde, Nuclear Phys. A 547 (1992) 245c.
[6] Y. Yamamoto et al., Progr. Theoret. Phys. Suppl. 118 (1994) 361.
[7] R.H. Dalitz, A. Gal, Ann. Phys. 116 (1978) 167.
[8] D.J. Millener, A. Gal, C.B. Dover, R.H. Dalitz, Phys. Rev. C 31 (1985) 499.
[9] M. Danysz, J. Pniewski, Phil. Mag. 44 (1953) 348.
[10] M.A. Faessler et al., Phys. Lett. B 46 (1973) 468.
[11] W. Brückner et al., Phys. Lett. B 55 (1975) 107.
[12] W. Brückner et al., Phys. Lett. B 62 (1976) 481.
[13] W. Brückner et al., Phys. Lett. B 79 (1978) 157.
[14] R. Bertini et al., Phys. Lett. B 83 (1979) 306.
[15] R. Bertini et al., Nuclear Phys. A 360 (1981) 315;
R. Bertini et al., Nuclear Phys. A 368 (1981) 365.
[16] R.E. Chrien et al., Phys. Lett. B 89 (1979) 31.
[17] M. May et al., Phys. Rev. Lett. 47 (1981) 1106.
[18] A. Bamberger et al., Phys. Lett. B 36 (1971) 412; Nuclear Phys. B 60 (1973) 1.
[19] C. Milner et al., Phys. Rev. Lett. 54 (1985) 1237.
[20] P.H. Pile et al., Phys. Rev. Lett. 66 (1991) 2585.

[21] M. Akei et al., Nuclear Phys. A 534 (1991) 478.
[22] T. Hasegawa et al., Phys. Rev. Lett. 74 (1995) 224.
[23] T. Hasegawa et al., Phys. Rev. C 53 (1996) 1210.
[24] O. Hashimoto et al., Nuclear Phys. A 639 (1998) 93c.
[25] H. Hotchi et al., Phys. Rev. C 64 (2001) 044302.
[26] H. Tamura et al., Phys. Rev. Lett. 84 (2000) 5963.
[27] T. Miyoshi et al., Phys. Rev. Lett. 90 (2003) 232502.
[28] H. Bandō, T. Motoba, Y. Yamamoto, Phys. Rev. C 31 (1985) 265.
[29] A. Likar, M. Rosina, B. Povh, Z. Phys. A 324 (1986) 35.
[30] H. Tamura et al., Progr. Theoret. Phys. Suppl. 117 (1994) 1.
[31] M. Ahmed et al., Phys. Rev. C 68 (2003) 064004.
[32] F. Dohrmann et al., Phys. Rev. Lett. 93 (2004) 242501.
[33] P.K. Saha et al., Phys. Rev. Lett. 94 (2005) 052502.
[34] M. Bedjidian et al., Phys. Lett. B 62 (1976) 467.
[35] M. Bedjidian et al., Phys. Lett. B 83 (1979) 252.
[36] M. May et al., Phys. Rev. Lett. 51 (1983) 2085.
[37] M. May et al., Phys. Rev. Lett. 78 (1997) 4343.
[38] K. Tanida et al., Phys. Rev. Lett. 86 (2001) 1982.
[39] S. Ajimura et al., Phys. Rev. Lett. 86 (2001) 4255;
H. Kohri et al., Phys. Rev. C 65 (2002) 034607.
[40] H. Akikawa et al., Phys. Rev. Lett. 88 (2002) 082501.
[41] M. Ukai et al., Phys. Rev. Lett. 93 (2004) 232501.
[42] H. Tamura, Nuclear Phys. A 754 (2005) 58c.
[43] K. Tanida et al., Nuclear Phys. A 721 (2003) 999c;
K. Miwa et al., Nuclear Phys. A 754 (2005) 80c.
[44] Y. Miura et al., Nuclear Phys. A 754 (2005) 75c;
Y. Miura, Ph.D. Thesis, Tohoku University, 2005.
[45] C.B. Dover, L. Ludeking, G.E. Walker, Phys. Rev. C 22 (1980) 2073.
[46] H. Bandō, Nuclear Phys. A 450 (1986) 217c.
[47] T. Motoba, H. Bandō, R. Wünsch, J. Žofka, Phys. Rev. C 38 (1988) 1322.
[48] H. Thiessen et al., BNL-AGS proposal E758 (1980).
[49] O. Hashimoto et al., Il Nuovo Cimento 102 (1989) 679.
[50] T. Fukuda et al., Nuclear Instrum. Methods A 361 (1995) 485.
[51] P. Dluzewski et al., Nuclear Phys. A 484 (1988) 520;
D.H. Davis, Nuclear Phys. A 547 (1992) 369c.
[52] K. Itonaga, T. Motoba, O. Richter, M. Sotona, Phys. Rev. C 49 (1994) 1045.
[53] D.J. Millener, Nuclear Phys. A 691 (2001) 93c.
[54] K. Itonaga, Private communication, 2001.
[55] T. Motoba, Nuclear Phys. A 639 (1998) 135c.
[56] A. Gal, Nuclear Phys. A 670 (2000) 229c.
[57] E. Hiyama, M. Kamimura, K. Miyazaki, T. Motoba, Phys. Rev. C 59 (1999) 2351.
[58] O. Richter, M. Sotona, J. Žofka, Phys. Rev. C 43 (1991) 2753.
[59] E. Hiyama, M. Kamimura, T. Motoba, T. Yamada, Y. Yamamoto, Phys. Rev. C 53 (1996) 2075.
[60] R.H. Dalitz, A. Gal, Phys. Rev. Lett. 36 (1976) 362.
[61] E.H. Auerbach et al., Ann. Phys. 148 (1983) 381.
[62] T. Yamada, K. Ikeda, T. Motoba, H. Bandō, Phys. Rev. C 38 (1988) 854.
[63] M. Juric et al., Phys. Rev. B 52 (1973) 1.
[64] T. Motoba, Y. Yamamoto, Nuclear Phys. A 585 (1995) 29c.
[65] K. Itonaga, T. Motoba, H. Bandō, Progr. Theoret. Phys. 84 (1990) 291.
[66] A. Bouyssy, Phys. Lett. B 84 (1979) 41;
A. Bouyssy, Phys. Lett. B 91 (1979) 15.
[67] R.H. Dalitz et al., Nuclear Phys. A 625 (1997) 71.
[68] D.H. Davis, Private communication, 1997.

[69] H. Bandō, T. Motoba, J. Žofka, in: T. Yamazaki, K. Nakai, K. Nagamine (Eds.), Perspectives of Meson Science, North Holland, 1991, p. 571.
[70] T. Motoba, Private communication, 2003.
[71] D.J. Millener, C.B. Dover, A. Gal, Phys. Rev. C 38 (2001) 2700.
[72] Y. Yamamoto, H. Bandō, J. Žofka, Progr. Theoret. Phys. 80 (1988) 757.
[73] D.E. Lanskoy, Y. Yamamoto, Phys. Rev. C 55 (1997) 2330.
[74] C.B. Dover, Proc. Int. Symp. on Medium Energy Physics, Beijing, World Scientific, Singapore, 1987, p. 257.
[75] H. Yamazaki et al., Phys. Rev. C 52 (1995) 1157.
[76] K. Maeda, H. Tamura, S.N. Nakamura, O. Hashimoto (Eds.), Proc. Int. Symp. on Electrophotoproduction of strangeness on nucleons and nuclei, SENDAI03, 16–18 June, Sendai, World Scientific, 2003.
[77] T. Mizutani, C. Feyard, G.-H. Lamot, B. Saghai, Phys. Rev. C 58 (1998) 75.
[78] T. Mart, C. Bennhold, Phys. Rev. C 61 (2000) 012201.
[79] T. Takahashi et al., Nuclear Phys. A 721 (2003) 991c.
[80] G. Niculescu et al., Phys. Rev. Lett. 81 (1998) 1805;
R.M. Mohring et al., Phys. Rev. C 67 (2003) 055205.
[81] K. Maeda, H. Tamura, S.N. Nakamura, O. Hashimoto (Eds.), Proc. Int. Symp. on Electrophotoproduction of strangeness on nucleons and nuclei, SENDAI03, 16–18 June, Sendai, World Scientific, 2003, p. 221.
[82] M.Q. Tran et al., SAPHIR Collaboration, Phys. Lett. B 455 (1998) 20.
[83] M. Sotona, S. Furullani, Progr. Theoret. Phys. Suppl. 117 (1994) 151.
[84] T. Motoba, M. Sotona, K. Itonaga, Progr. Theoret. Phys. Suppl. 117 (1994) 123.
[85] M. Sotona, Private communication, 1998.
[86] T. Miyoshi et al., Nucl. Instrum. Methods A 496 (2003) 362.
[87] T. Motoba, Private communication, 2004.
[88] D.J. Millener, in: L. Tang, O. Hashimoto (Eds), Proc. JLab Workshop on Hypernuclear Physics with Electromagnetic Probes, HYPJLAB99, 2–4 December, Hampton, USA, 1999, p. 79.
[89] T. Motoba, in: J. Adams et al. (Eds.), Proc. 8th Mesons and Light Nuclei, in: AIP Conference series, vol. 603, 2001, p. 125 and private communication.
[90] JLab proposal E01-011, Spokespersons O. Hashimoto, L. Tang, J. Reinhold, S.N. Nakamura, 2001.
[91] JLab proposal E99-003, Spokesperson A. Margarian, L. Tang, 1999.
[92] JLab proposal E94-107, Spokesperson S. Frullani, F. Garibaldi, J. LeRose, P. Markowitz, T. Saito, 1994.
[93] J.C. Herrera et al., Phys. Rev. Lett. 40 (1978) 158.
[94] R.E. Chrien et al., Phys. Rev. C 41 (1990) 1062.
[95] R.H. Dalitz, A. Gal, J. Phys. G 4 (1978) 889.
[96] T. Motoba, H. Bandō, K. Ikeda, Progr. Theoret. Phys. 70 (1983) 189.
[97] A. Gal, Phys. Rev. C 28 (1983) 2186.
[98] L. Majling et al., Z. Phys. A 337 (1990) 337.
[99] V.N. Fetisov, L. Majling, J. Žofka, R.A. Eramzhyan, Z. Phys. A 339 (1991) 399.
[100] E. Hiyama, M. Kamimura, K. Miyazaki, T. Motoba, Phys. Rev. C 59 (1999) 2351.
[101] D.J. Millener, Nuclear Phys. A 754 (2005) 48c.
[102] B.F. Gibson, D.R. Lehman, Phys. Rev. C 37 (1988) 679.
[103] Y. Akaishi et al., Phys. Rev. Lett. 84 (2000) 3539.
[104] A.R. Bodmar, Q.N. Usmani, Phys. Rev. C 31 (1985) 1400.
[105] H. Tamura, Eur. Phys. J. A 13 (2002) 181.
[106] T. Sakuda, H. Bandō, Progr. Theoret. Phys. 78 (1987) 1317.
[107] H. Tamura, Nuclear Phys. A 691 (2001) 86c.
[108] M. Csejthey-Barth, G. Schorochoff, P.M. Van Binst, Nuclear Phys. B 14 (1969) 330.
[109] J. Sasao et al., Phys. Lett. B 579 (2004) 258.
[110] K. Tanida, Ph.D. Thesis, University of Tokyo, 2000.
[111] H. Tamura et al., Nucl. Instrum. Methods (in preparation).
[112] E. Hiyama, M. Kamimura, T. Motoba, T. Yamada, Y. Yamamoto, Nuclear Phys. A 639 (1998) 173c.
[113] M. Ukai et al., Phys. Rev. C 73 (2006) 012501(R).
[114] P. Khaustov et al., Phys. Rev. C 61 (2000) 054603.
[115] D.J. Millener, Private communication.

[116] M. Ukai, Ph.D. Thesis, Tohoku University, 2004.
[117] E. Hiyama, M. Kamimura, T. Motoba, T. Yamada, Y. Yamamoto, Phys. Rev. Lett. 85 (2000) 270.
[118] O. Morimatsu, S. Ohta, K. Shimizu, K. Yazaki, Nuclear Phys. A 420 (1984) 573.
[119] Y. Fujiwara, M. Kohno, K. Miyagawa, Y. Suzuki, Phys. Rev. C 70 (2004) 047002.
[120] KEK-PS proposal E566, Spokesperson H. Tamura, 2004.
[121] K. Imai et al., Letter of Intent for Nuclear and Particle Physics Experiments at the J-PARC (L06), The J-PARC Project Office, KEK, J-PARC 03-6, 2003, p. 77.
[122] F. Garibaldi, Eur. Phys. J. A 24 (s1) (2005) 91.
[123] J. Pochodzalla, Nuclear Phys. A 754 (2005) 430c.
[124] M. Agnello et al., Nuclear Phys. A 754 (2005) 399c.
[125] T. Bressani, E. Botta, A. Feliciello, V. Paticchio, Nuclear Phys. A 754 (2005) 410c.
[126] H. Noumi, Nuclear Phys. A 638 (1998) 121c.
[127] H. Noumi et al., Letter of Intent for Nuclear and Particle Physics Experiments at the J-PARC (L08), The J-PARC Project Office, KEK, J-PARC 03-6, 2003, p. 77;
T. Fukuda et al., Letter of Intent for Nuclear and Particle Physics Experiments at the J-PARC (L09), The J-PARC Project Office, KEK, J-PARC 03-6, 2003, p. 185.